Modeling Rett syndrome with Patient-specific Induced Pluripotent Stem Cells

By

Emily Suzannah Cunningham Williams

A dissertation submitted in partial fulfillment of
the requirements for the degree of

Degree of Doctor of Philosophy
(Genetics)

at the

UNIVERSTY OF WISCONSIN-MADISON

2013

Date of final oral examination: 8/19/13

This dissertation is approved by the following members of the Final Oral Committee:
Qiang Chang, Associate Professor, Genetics
Barry Ganetzky, Professor, Genetics
Akihiro Ikeda, Associate Professor, Genetics
Albee Messing, Professor, Comparative Biosciences
Su-Chun Zhang, Professor, Neuroscience

Acknowledgements

I would like to acknowledge and express my sincere thanks to those who have guided and supported me through my graduate school experience at the University of Wisconsin-Madison. First, to my advisor, Qiang Chang, who believed that I could achieve a rather risky project and has been a source of leadership and direction. I would also like to express my gratitude to the collaborative research community at the Waisman Center. Numerous individuals in this community have provided their technical expertise, scientific insight, and the kind use of instruments and reagents. I would also like to extend a special thanks to Gene Ananiev, who introduced me to many of the techniques utilized throughout my thesis project and who has been a source of collaboration and support.

I would like to acknowledge my husband who has been my strongest supporter, providing both love and understanding through trying times. I would also like to thank my family who instilled in me a deep desire to achieve through commitment and self-discipline.

Finally, to the families who donated the tissues utilized in this thesis, it is my hope that your gift to the RTT research community will be exponentially rewarded in the future.

Dedication

Dedicated to the families affected by Autism spectrum disorders, may you be blessed with love, perseverance and hope.

Abstract

Rett syndrome (RTT) is one of the leading causes of intellectual disability in girls. Mutations in the X-linked methyl-CpG-binding protein 2 (*MECP2*) gene have been identified as the cause of RTT. Mouse and patient-derived induced pluripotent stem cell (iPSC) model systems have been developed to better understand the molecular roles of MeCP2/MECP2 and gain insight on the disease pathophysiology. Recently, there has been an interest in the determining the glial component of RTT pathology. To model the non-cell autonomous glial component in RTT pathology in a human-based system, we have developed a patient-derived RTT astrocyte/neuron co-culture system. We have validated a detrimental non-cell autonomous effect of RTT astrocytes, and by utilizing three different RTT mutational lines, have determined that this effect is consistent and is mediated in part by astrocyte secreted factors. We have also gone on to test the efficacy of neurotrophic factors in ameliorating this glial effect and have found insulin-like growth factor 1 (IGF-1) and its tripeptide cleavage product, Glycine-Proline-Glutamate (GPE), to increase the somal area and to promote neurite outgrowth in GABAergic interneurons.

Table of Contents

Acknowledgements…….....i

Dedication…….……ii

Abstract……...……...……...…...iii

Table of Contents…….…...iv

List of Figures and Tables…….……...v-vi

Abbreviations……....vii-viii

Introduction: Background and Significance……..…1-68

Chapter I: Isogenic Pairs of Wild Type and Mutant Induced Pluripotent Stem Cell (iPSC) Lines from Rett Syndrome Patients as *In Vitro* Disease Model……..69-102

Chapter II: Mutant astrocytes differentiated from Rett syndrome patients-specific iPSCs have adverse effects on wild type neurons……103-156

Chapter III: Future Directions……..……157-168

List of Figures and Tables

Table I. RTT iPSC lines currently available to the RTT research community…….49

Chapter I Figure 1. RTT mutations used in this study……88

Chapter I Figure 2. RTT iPSCs are bona fide induced pluripotent stem cells……..89

Chapter I Figure 3. The *Androgen Receptor* assay…….90-91

Chapter I Figure 4. RTT iPSCs exhibit a nonrandom, skewed pattern of XCI that remains constant through differentiation……92-93

Chapter I Figure 5. Clonal and allele-specific expression of *XIST* SNPs and *MECP2* in female human iPSC lines and their differentiation products…..94-95

Chapter I Figure 6. Directed neuronal differentiation of iPSC/hESCs…….96

Chapter I Figure 7. Isogenic pairs of wild type and mutant RTT iPSC lines can be differentiated into post mitotic neurons……97

Chapter I Figure 8. Phenotypic characterization of R294X isogenic pair neurons…….98

Chapter I Table 1. Summary of XCI status screening and allele-specific expression of *MECP2* in multiple RTT iPSC lines……99

Chapter II Figure 1. XCI status of isogenic RTT iPSC pairs used in this study……130-131

Chapter II Figure 2. Differentiation of isogenic RTT iPSC lines into GFAP+ astrocytes……..132-133

Chapter II Figure 3. Expression of cell type markers in glial differentiation……134

Chapter II Figure 4. Maintenance of the isogenic status in astroglial progenitors differentiated from isogenic RTT iPSC lines……135-136

Chapter II Figure 5. WT astrocytes express detectable levels of MECP2 protein……..137

Chapter II Figure 6. Schematic of experimental design and representative images of wild type mouse hippocampal neurons co-cultured on wild type and mutant RTT astrocytes……..…138-139

Chapter II Figure 7. Morphological and functional defects of wild type mouse hippocampal neurons co-cultured on mutant RTT astrocytes……..140-141

Chapter II Figure 8. Schematic of experimental design, representative images and effect of wild type human forebrain neurons co-cultured on wild type and mutant RTT astrocytes……..142-143

Chapter II Figure 9. Schematic of experimental design and representative images of wild type mouse hippocampal neurons cultured in medium conditioned by wild type and mutant RTT astrocytes….144-145

Chapter II Figure 10. Morphological defects of wild type mouse hippocampal neurons cultured in medium conditioned by mutant RTT astrocytes……..146

Chapter II Figure 11. Schematic of experimental design and representative images of WT and MT RTT GABAergic interneurons co-cultured on WT and MT RTT astrocytes and effects of IGF-1/GPE treatment…….147-148

Chapter II Figure 12. Morphological effects of WT and MT RTT GABAergic interneurons (IN) co-cultured with WT and MT RTT astrocytes (AS) and the effects of IGF-1/GPE treatment……...…149-150

Chapter II Figure 13. Neurons and astrocytes differentiated from RTT iPSCs express the IGF-1 receptor (IGF-1R)……..151

Chapter II Table 1. Between-subjects effects from the two-way ANOVA analysis of neuronal morphological measures in the RTT interneuron/astrocyte co-culture with no treatment……..152

Chapter II Table 2. Between-subjects effects from the three-way ANOVA analysis of neuronal morphological measures in the RTT interneuron/astrocyte co-culture treated with IGF-1/GPE……153

Chapter III Figure 1. RTT iPSC-derived astroglial progenitors differentiate into astrocytes *in vivo*…….……166

Abbreviations

7,8-DHF - 7,8-dihydroxyflavone
ACM - Astrocyte conditioned media
AD - Alzheimer's disease
ADNF - Activity-dependent neurotrophic factor
ALS - Amyotrophic lateral sclerosis
ANOVA – Analysis of variance
AP - Astroglial progenitor
AQP4 - Aquaporin 4
AS – Astrocyte
Aß - ß-amyloid protein
AxD - Alexander Disease
BBB - Blood brain barrier
BDNF - Brain-derived neurotrophic factor
Car - Carbonic anhydrase
CDKL5 - Cyclin-dependent kinase like 5
CS-PG - Chondroitin-6-sulfate proteoglycan
cMYC - Myc proto-oncogene protein
CNS - Central nervous system
CNTF - Ciliary neurotrophic factor
CN - Cytotactin/tenascin
DM - Dextromethorphan
DS - Down syndrome
EAAT1 - Excitatory amino acid transporter 1 (GLAST)
EAAT2 - Excitatory amino acid transporter 2 (GLT-1)
EB - Embryoid body
ECM - Extracellular matrix
EGF - Epidermal growth factor
eIF2B - Eukaryotic initiation factor 2B
FDA - Food & Drug Administration
FGF2 - Fibroblast growth factor 2
***FMR1* - Fragile X mental retardation 1 gene**
***FOXG1* - Forkhead box G1**
FXS - Fragile X
GABA - Gamma-aminobutyric acid
GDNF - Glial cell line-derived neurotrophic factor
GFAP - Glial fibrillary acidic protein
GLUT1 - Glucose transporter 1
Gpc4/6- glypican 4/6
GPE - Glycine-Proline-Glutamine ((1-3)IGF-1)
HD - Huntington's disease
HDAC - Histone deacetylases
hESC - Human embryonic stem cell
***htt* - Huntingtin gene**
IGF-1 - Insulin-like growth factor 1

IGFBPs - IGF binding proteins (1-6)
IGF-1R- Insulin-like growth factor 1 receptor
IL – Interleukin
IN – Interneuron
iPSC - Induced pluripotent stem cell
kb – Kilobase
KLF4 - Kruppel-like factor 4
MAP2 - Microtubule-associated protein 2
MBD - Methyl-CpG-binding domain
MECP2 - Methyl-CpG-binding protein 2
mEPSCs - Miniature excitatory postsynaptic currents
MT – Mutant
NcoR - Nuclear receptor corepressor
NE - Neuroepithelia
NFIX- Nuclear factor 1 X-type
NGF - Nerve growth factor
NLS - Nuclear localization signal
NMDA - N-methyl-D-aspartate
NP-C - Niemann-Pick type C
NS - Neurosphere
OCT - Octamer-binding transcription factor 4
PD - Parkinson's disease
PGE2 - Prostaglandin E2
RTT - Rett syndrome
SOD1 - Superoxide dismutase 1
SOX2 - Sex determining region Y-box 2
TCA - Tricarboxylic acid
TG - Transgenic (mouse)
TGFß – Transforming growth factor ß
TNFα - Tumor necrosis factor-α
TRD - Transcriptional repression domain
TSP-1 - Thrombospondin 1
UPR - Unfolded protein response
UTR - Untranslated region
VEGT - Vascular endothelial growth factor
VWM - Vanishing white matter leukodystrophy
WT - Wildtype
XCI - X-chromosone inactivation
***Xist* - X-inactive specific transcript**

Introduction

Background and Significance

I) Rett syndrome

Clinical diagnosis

Rett syndrome (RTT) is an autism spectrum disorder that affects an estimated 1 in 10,000-15,000 girls (Hagberg, 2002). RTT patients appear normal during fetal and postnatal development. Then in early childhood, the disease progression initiates rapidly, proceeding through a defined pattern of stages. The exact timing of each stage varies from patient to patient. Stagnation of development marks the first stage of the disease progression, with a noticeable lack of head growth. This acquired microcephaly is often one of the first indications for a RTT diagnosis. Developmental stagnation is followed by an increase in the clinical severity within the rapid regression stage. During this stage, a hallmark hand stereopathy presents in the form of hand wringing. This particular aspect of the disorder was the basis of the first documented RTT cases in the German literature by the disorder's namesake, Andreas Rett, in 1966 (Chahrour and Zoghbi 2007) and consequently brought RTT syndrome to international recognition almost 20 years later by Hagberg (Hagberg *et al*. 1983). Loss of purposeful control of the trunk also occurs, either affecting gait or leading to a complete loss of mobility (Hagberg 2002). Additional symptoms also present in some RTT patients include the following: respiratory and heart beat dysrhythmia, sleep abnormalities, seizures, growth delays, and scoliosis (Hagberg, 2002). A striking stationary stage then follows the rapid regression stage, with symptoms stabilizing for unknown reasons. There is an increased incidence of sudden death due to autonomic dysfunction in individuals of this stage during their adolescent years (Kerr *et al*., 1997). RTT patients who survive into the fourth or fifth decade require comprehensive daily assistance due to late motor skill deterioration. RTT patients have

impaired expressive and receptive language development. Such features make intellectual tests difficult to administer and historically, patients have been characterized as intellectually disabled. New testing platforms are being employed to assay patients' nonverbal cognitive abilities (Djukic and McDermott, 2012) in hopes of developing supportive therapies to improve patients' quality of life. Currently, there is no cure for RTT.

Pathophysiology

Due to the delayed, postnatal onset of symptoms in RTT, neurodegeneration might be suspected. Yet post-mortem studies point to a neurodevelopmental disease course (Neul and Zoghbi 2004). Demyelination and gliosis are not present and there is little evidence of neural atrophy or loss that would be indicative of neurodegeneration (Jellinger *et al*., 1988; Reiss *et al*., 1993). Acquired microencephaly affects the brain globally with retention of normal gross structure. On the cellular level, neurons appear to be the most affected cell type. In the cerebral cortex, hypothalamus and hippocampus, neurons are smaller and more densely packed, with a reduction in the size and complexity of dendritic arbors (Bauman *et al*., 1995a; Bauman *et al*., 1995b; Armstrong *et al*., 1995; Armstrong et al., 1998). These features are suspected be to the main cause of microencephaly. On the subcellular level, dendritic spines are reduced and display malformed, dysgenic features in the pyramidal neurons of the frontal cortex (Belichenko *et al*., 1994; Jellinger *et al*., 1998) and the hippocampal CA1 region (Chapleau *et al*., 2009). Spine dysgenesis is one of the most consistent anatomical features of intellectual disability and is present in the following disorders: Down, Angelman, Fragile X, Fetal

alcohol, Williams and Rubinstein-Taybi syndromes (Marin-Padilla 1972; Purpura 1974; Irwin *et al*., 2000; Ferrer and Galofre 1987; Williams *et al*., 1980; Pogacar *et al*., 1973). Such surprising morphological commonality despite different causes in each disorder highlights the common pathways controlling cognitive function. Thus, elucidating the pathways involved in a monogenic disorder like RTT could, in turn, lead to a better understanding of the molecular mechanisms underlying neurodevelopmental disorders.

II) MECP2 as causative locus

Linkage analysis

Due to the over-representation of RTT in females, the disorder was first hypothesized to be X-linked dominant with the potential of lethality in males (Hagberg *et al*., 1983; Amir *et al*., 1999; Sirianni *et al*., 1998). Because RTT is sporadic in >99% of the reported cases, locating the causative locus through linkage mapping proved difficult (Calfa *et al*., 2011). Advancement occurred in 1990-92, when an aunt-niece pair and half-sister pair were used to perform exclusion mapping and the chromosome region Xq28 was identified (Anvret *et al*., 1990; Archidiancon *et al*., 1991; Ellison *et al*., 1992). This region is gene-rich and due to the spectrum of phenotypes seen in patients, there was no obvious candidate (Xiang *et al*., 1998). Systematic screening approaches were utilized and led to the identification of the *Methyl-CpG-binding protein 2* (*MECP2)* gene as the causative locus (Amir *et a*l., 1999). To date, *MECP2* mutations are found to be responsible for over 95% RTT cases.

Once the causative locus was identified, it became evident that individuals without *MECP2* mutations had been previously misdiagnosed due to displaying certain phenotypes that overlapped with classical RTT. This in turn led to the classification of two other disorders. While classical RTT is caused by mutations in the *MECP2* gene, congenital and atypical Rett-like phenotypes are linked to mutations in the *forkhead box G1* (*FOXG1)* (Van der Aa *et al*., 2011; Kortum *et al*., 2011, Le Guen *et al*., 2011) and *cyclin-dependent kinase like 5* (*CDKL5*) (Weaving *et al*., 2004, Scala *et al*., 2005) genes respectively. In addition to the lack of *MECP2* mutation, these two disorders have a congenital rather than postnatal onset. Patients with *CDKL5* mutations experience infantile spasms, while patients with *FOXG1* mutations have a marked early malformation of the corpus callosum (Kortum *et al*., 2011). As noted previously, there are no gross changes in brain structure in classical RTT.

The *MECP2* gene

Structure and expression

The *MECP2* locus spans 76 kb on Xq28 in a region that is conserved between human and mouse (Quaderi *et al*.,1994). The human *MECP2* gene has four exons with an unusually long 8.5 kb 3'-untranslated region (UTR) (Reichwald *et al*., 2000). In mammals, *Mecp2* is expressed at embryonic and adult stages, with three different transcripts varying in length (1.8, ~7.5 and ~10 kb) due to differential usage of the polyadenylation signals in the 3'UTR (Singh *et al*., 2008). The long and short transcripts are expressed throughout the body, displaying spatiotemporal variation in expression (D'Esposito *et al*., 1996; Reichwald et al. 2000; Coy *et al*., 1999; Shahbazian *et al*.,

2002). In the mammalian nervous system, *Mecp2* transcript levels are high during embryogenesis, with a dip at postnatal timepoints that rise again in adulthood (Shahbazian *et al*., 2002; Akbarian *et al*., 2001). The level of *Mecp2* expression needs to be tightly regulated. In human, loss of MECP2 function leads to RTT; while overexpression of *MECP2* caused by duplication of the part of the X chromosome including *MECP2* leads to MECP2 duplication syndromes (Esch *et al*., 2005). In mouse, a one-fold decrease or increase in *Mecp2* expression level can lead to Rett-like phenotypes (Guy *et al*., 2001; Chen *et al*., 2001; Pelka *et al*., 2006; Collins *et al*., 2004).

The MECP2 protein

Isoforms and expression

The *MECP2* gene encodes the MECP2 protein, which has two isoforms due to alternative splicing, MECP2A (MeCP2ß in rodent) and MECP2B (MeCP2α in rodent). MECP2A is 486 amino acids long encoded by exons 2, 3 and 4 while MECP2B is 498 amino acids long encoded by exons 1,3 and 4 (Mnatzakanian et al., 2004; Kriaucionis and Bird, 2004; Weaving et al., 2005). In addition to the regulation of splice sites in different tissues, it appears that MeCP2/MECP2 translation is post-transcriptionally regulated as there is no direct correlation in RNA and protein levels (Shahbazian et al., 2002). The two isoforms are expressed in different tissues, with MECP2B predominantly expressed in the brain and MECP2A expression more abundant in placenta, liver and skeletal muscle. Recent studies have postulated MECP2A to be essential for placental development (Itoh et al., 2012), while MECP2B is more directly correlated with RTT pathology (Mnatzakanian et al., 2004; Kriaucionis and Bird, 2004). In the nervous

system, the timing of upregulated MeCP2 protein expression is correlated with the pattern of development and maturation of different brain regions and cell types, with the highest levels of expression in post-mitotic neurons (Kishi *et al*., 2004). While expression levels are highest in neurons, other cell types of the nervous system have recently been verified to express MeCP2 including astrocytes, microglia and oligodendrocytes (Maezawa *et al*., 2009; Ballas *et al*., 2009, Maezawa *et al*., 2010).

MECP2 functional domains

The functional domains of MeCP2 are responsible for various components of the protein's activities. The domains allow for recognition of gene target sites, differential binding of protein co-factors and cellular localization. In mammals, MeCP2 has four important domains: the methyl-CpG-binding domain (MBD) at residues 78-163, the transcriptional repression domain (TRD) at residues 205-310, the nuclear localization signal (NLS) at residues 255-271 and the C-terminal region (Nan *et al*., 1993; Nan *et al*., 1996; Nan *et al*., 1997; Chandler *et al*., 1999). With its specialized MBD, MeCP2 is able to bind methylated DNA. The affinity and specificity of this binding is partially dependent on the presence of an A/T run of 4 or more base pairs adjacent to a methyl-CpG (Klose *et al*., 2005). With the TRD, MeCP2 has been shown to physically associate with core repression complex members Sin3A and histone deacetylases HDAC1 and HDAC2, and most recently, with the NcoR complex (Nuclear receptor corepressor) (Jones *et al*., 1998; Lyst *et al*., 2013; Ebert *et al*., 2013). The association between MeCP2 and core repression complex members leads to a repressive chromatin environment (Nan *et al*., 1997; Bird and Wolffe, 1999). The NLS allows for MeCP2 to be transported across

the nuclear envelope and gain entry into the nucleus, where the bulk of its activities are performed. Finally, the C-terminal region from residues 295-486 facilitates MeCP2's binding to the nucleosome core (Nan *et al.,* 1996; Chandler *et al.,* 1999). A recent study has identified another potentially important domain in the C-terminal region of MeCP2, an AT-hook domain (Baker *et al.,* 2013). This domain might be important for regulating chromatin structure.

Because of its preferential binding to methylated DNA and association with a known repressor complex, MeCP2 was first described as a transcriptional silencer. Upon further examination in mouse models, it was determined that MeCP2 is also able to activate gene transcription through association with the transcriptional activator cAMP responsive element binding protein 1 (CREB1) at activated gene promoters (Chahrour *et al.,* 2008). MeCP2 has also been shown to have a role in splicing regulation through its interaction with RNA-binding protein Y box-binding protein 1 (Young *et al.,* 2005). From these seminal works and others that have built upon them, the multi-faceted roles of MeCP2 in different molecular contexts are coming into focus, providing clues into the potential mechanisms underlying RTT pathophysiology.

Causative mutations

Mode of causative mutations

MECP2 mutations are usually *de novo* in origin, arising in the paternal germline (Girard *et al.,* 2001). Due to this *de novo* nature, the majority of female patients are heterozygous, having one wild type and one mutant *MECP2* allele. Rare cases of RTT hemizygous males occur due to maternal transmission or maternal germline mosiacism

(Mari *et al*., 2004). RTT XY males, having only the mutant *MECP2* copy, often have a severe presentation of symptoms that prove incompatible with continued postnatal survival. An extremely rare case of a male 47, XXY Klinefelter RTT male has also been reported (Schwartzman *et al*., 2001). In this case, the extra X chromosome resulted from a non-disjunction in the paternal first meiotic division in conjunction with a *de novo* *MECP2* mutation (Schwartzman *et al*., 1999).

Effect of XCI in disease presentation

MECP2 is a locus on the X chromosome that undergoes random X chromosome inactivation (XCI), resulting in females with mosaicism for mutant and wild type alleles. A mosiac pattern of XCI throughout the body may be one component that leads to differential disease severity from patient to patient. For patients with the same mutation, there is a potential for certain individuals to have a more favorable pattern of XCI, with an over-representation of the wild type allele expressed within the nervous system (Amir *et al*., 2000).

Type and severity of mutations

To date, over 600 unique RTT mutations including missense, nonsense, deletions or insertions and complex rearrangements have been identified (RettBase; http://mecp2.chw.edu.au/). These mutations span the entire MECP2 protein, of which eight common point mutations (R106W, R133C, T158M, R168X, R255X, R270X, R294X, R306C) account for more than 65% of classic RTT cases (Calfa *et al*., 2011). Another 15-18% of RTT cases are due to deletions, either involving one or more exons or

localizing to the C-terminus (Calfa *et al*., 2011). The genetic screening strategy to locate causative RTT mutations first starts with a screen of exons 3 and 4, utilizing denaturing HPLC (high performance liquid chromatography) followed by sequencing (Williamson and Christodoulou 2006). Second, if no mutation is identified in this region, then further screening of exons 1 and 2 follows. Third, if no pathogenic mutations are found in the screen of exons 1-4, assays for large deletions/insertions including Southern analysis or MLPA (multiplex ligation probe amplification) can be performed. There are commercial MLPA kits specifically developed for *MECP2*, one of which is produced by MCR-Holland. Fourth, if no deletions or insertions are identified in *MECP2*, screening for *CDKL5* mutations would be initiated, especially if the patient experienced seizures in the first 6 months of life. In addition, screening for *FOXG1* mutations would also be recommended.

Due to the vast number of unique mutations and random XCI, there is no clear genotype-phenotype correlation for many specific mutations. But when certain categories of mutations are compared, it is clear that certain mutational types and locations cause more severe symptoms than others. The most complete study of genotype-phenotype correlations to date was able to draw a parallel between different types of RTT mutations and markers of clinical severity (mobility, hand use, and language) (Neul *et al*., 2008). Specific mutations (R133C, R294X, C-terminal truncations) were shown to be less severe than other mutations (large deletions and R168X). Patients with the R168X mutation were shown to be on the most severe end of the clinical spectrum. This mutation leads to a truncation close to the MBD, resulting in complete loss of the TRD (Obata *et al*., 2000). In work performed in *Xenopus* embryos, it appears that this particular mutation causes a

dominant negative phenotype in which MECP2 fails to dissociate from gene promoters when given the appropriate cues (Neul *et al*., 2004). Individuals with C-terminal truncations had limited purposeful hand use but were more likely to be ambulatory and acquire/retain language skills (Neul *et al*., 2008). Lastly, individuals with the R306C mutation, which is located in the TRD of MECP2, appeared to have the mildest features of the common mutations with adverse effects mostly in language abilities (Neul *et al*., 2008).

To understand the effects of particular MECP2 mutations, different mouse models that carry either point mutations or deletions in *Mecp2* have been engineered for *in vivo* and *in vitro* analysis (please refer to the following section). Additionally, induced pluripotent stem cells (iPSCs) have been derived from RTT patients with different causative mutations, including both common and rare types.

III) Experimental models for studying Rett syndrome

Mouse models

Given the high degree of MECP2/MeCP2 protein conservation in humans and mice and the tractability of genetic engineering in mice, different RTT mouse models have been engineered to study MeCP2 function *in vivo*. The most widely used mouse models are *Mecp2*$^{tm1.1Bird}$, *Mecp2*$^{tm1.1Jae}$ and *Mecp2*^{tm1Pplt}. These mice were engineered to express a functionally null *Mecp2* gene product by different approaches (Guy *et al*., 2001; Chen *et al*., 2001; Pelka *et al*., 2006). *Mecp2*$^{tm1.1Bird}$ is an exon 3-4 deletion resulting in complete absence of transcript and protein; *Mecp2*$^{tm1.1Jae}$ is an exon 3 deletion loss-of-function allele that generates a truncated product; *Mecp2*^{tm1Pplt} is a deletion of the MBD

resulting in a non-functional null *Mecp2* allele. These models are regarded as similar to the large deletions found in ~10% of RTT cases. The predominantly used male germline nulls represent the most severe end of the RTT spectrum. Male mice display behavioral phenotypes reminiscent of autistic features, exhibit hindlimb clasping reminiscent of the stereotypic hand movements observed in RTT patients and show hallmark cellular brain pathology (Guy *et al*., 2001; Chen *et al*., 2001; Pelka *et al*., 2006). No characteristic stage of regression is present in these mice; their life span is greatly reduced with few males living longer than 12-14 weeks (Katz *et al*., 2012). Death is often sudden in these mice. This may parallel the high incidence of sudden death in RTT patients during the adolescent years.

Other models have been engineered with C-terminal truncations or single-nucleotide mutations that are homologous to those common in RTT (A140V: *Mecp2*$^{tm1.1Vnar}$; T158A: *Mecp2*$^{tm1.1Joez}$; R168X: *Mecp2*$^{tm1.1Coyle}$; R270X: transgenic *Mecp2*R270X; G273X: transgenic *Mecp2*G273X; R306C: *Mecp2*^{R306C}, 308-C-terminal truncation: *Mecp2*^{tm1Hzo}) (Katz *et al*., 2012; Baker *et al*., 2013, Lyst *et al*., 2013). These models recapitulate certain hallmark phenotypes of the disorder and have been utilized to study behavioral and molecular aspects of the disorder.

- A140V

Mecp2$^{tm1.1Vnar}$ is a knockin missense A140V mutation (Jentarra *et al*., 2010) and does not display a reduction in survival. Pathology is present at the cellular level, with increased cell packing density in the cerebrum and reduced dendritic complexity in layer II/III of the somatosensory cortex.

- T158A

Mecp2$^{tm1.1Joez}$ is a knockin missense T158A mutation (Goffin *et al*., 2012). Male mice exhibit hindlimb clasping at 5 weeks with behavioral phenotypes manifesting at 9 weeks. Roughly 50% of males die by 16 weeks. Tremor is seen occasionally in males (Katz *et al*., 2012).

- R168X

Mecp2$^{tm1.1Coyle}$ is a knockin nonsense R168X mutation that models the common human R168X mutation (Lawson-Yuen *et al*., 2007). This mutation results in the truncation of the protein within the critical MBD. Phenotypic severity is similar to the germline null *Mecp2*. R168X male mice display tremor and hindlimb clasping at day 40-60 with survival length not greater than 100 days.

- R270X/ R273X

The *Mecp2*R270X is a model for the common R270X truncation mutation while the *Mecp2*R273X is a model for a very uncommon truncation mutation (Baker *et al*., 2013). The *Mecp2*R270X transgenic mice exhibit phenotypic severity in a time course comparable to the *Mecp2* null while the *Mecp2*G273X transgenic mice display more moderate phenotypes with a later onset (Baker *et al*., 2013). Huda Zogbi's group compared the *Mecp2*R270X and *Mecp2*R270X mouse models and determined that a conserved AT-hook domain is disrupted in MeCP2-R270X, leading to the loss of MeCP2's function in modification of chromatin structure (Baker *et al*., 2013).

- R306C

Recently, a *Mecp2*^{R306C} knockin mouse model has been generated and characterized by Adrian Bird's lab. Male mice exhibit phenotypes beginning at 6 weeks of age, including hindlimb clasping, mobility deficits, and a reduced lifespan (Lyst *et al*., 2013). This

model has been used to characterize a putative NCOR/SMRT co-repressor binding domain within MECP2, which is regulated by neuronal activity (Lyst *et al*., 2013, Ebert *et al*., 2013).

- 308-C-terminal truncation

The *Mecp2*^{tm1Hzo} line has a terminal truncation occurring at codon 308, retaining the TRD (Shahbazian *et al*., 2002). Male mice show tremor phenotypes at 6 weeks, diminished activity at 5 months, and a lifespan shortened to 15 months.

Expanding upon mouse models

Using RTT mouse models, several studies have shown that the disease progression can be slowed down via manipulating pathways deregulated by the loss of MeCP2 functions (Chang *et al*., 2006; Gemelli *et al*., 2006; Luikenhuis *et al*., 2004; Roux *et al*., 2007; Tropea *et al*., 2009; Zanella *et al*., 2008), or reversed via reactivating the expression of MeCP2 (Guy *et al*., 2007). Consequently, clinical trials have been initiated in human RTT patients to test the safety and efficacy of these potential drugs as revealed by the mouse studies, which clearly demonstrates the power of using mouse models to study the molecular mechanism of RTT. However, these mouse models still have their limitations in mimicking human RTT mutations and in drug screening. For instance, the most widely studied RTT mouse models are loss-of-function alleles that either lacks the whole gene or harbors large deletions (Chen *et al*., 2001; Guy *et al*., 2001; Shahbazian *et al*., 2002). These alleles are inherently different from the missense point mutations in the human RTT patients, and may not truly model the abnormal function of the missense mutant proteins. In addition, these loss-of-function alleles cannot be used to test drug

candidates that enhance reading through the nonsense mutations. Finally, 92% of new drugs that pass preclinical tests, including tests on animals, fail to reach the market either because of safety or efficacy failures (*US FDA: Report on Challenge and Opportunity on the Critical Path to New Medical Products, March 2004*). This highlights the significant differences in the underlying biology between humans and common research animals. Therefore there is a need for establishing cell culture-based human models whenever possible for studying disease mechanisms to validate and expand the knowledge learned using research animal models.

Patient-specific induced pluripotent stem cells

Patient-derived induced pluripotent stem cells (iPSCs) have huge potential in translational medicine, allowing *in vitro* disease modeling, drug screening and individualized cellular therapy. iPSCs cells, like human embryonic stem cells, are pluripotent cells that have the potential to differentiate into any cell type of the body if given the appropriate cues. By different methods, two independent groups reported the initial reprogramming of human somatic tissues into iPSCs (Takahashi *et al*., 2007; Yu *et al*., 2007). The Yamanaka group performed reprogramming mediated by retroviral transfer of the stem cell factors *OCT4, SOX2, KLF4* and *c-MYC* (Takahashi *et al*., 2007) while the Thomson group used lentiviral mediated transfer of *OCT4, SOX2, NANOG*, and *LIN28* (Yu *et al*., 2007). Following the initial reports of this groundbreaking technology, the number of patient-derived iPSC lines has risen exponentially. In tandem, guided differentiation protocols were developed to specify patient-derived iPSCs into the cell types affected in a particular disorder. These guided differentiation protocols draw upon a

wealth of knowledge gained in studying human embryonic stem cells and human embryonic development. Their utilization in a patient iPSC-based system allows testing of not only cell-based morphological and functional phenotypes of a particular disorder, but also the molecular and biochemical pathways underlying these pathologies, all within a human system. Thus, with a patient-iPSC based system, there is great power to not only validate past findings from mouse models, but also to generate novel insights in human disorders.

Rett induced pluripotent stem cells

- Generation of lines

Several groups, including ours, have reported the generation of iPSC lines from RTT patient somatic cells (Ananiev *et al*., 2011; Hotta *et al*., 2009; Marchetto *et al*., 2010; Cheung *et al*., 2011; Kim *et al*., 2011; Pomp *et al*., 2011). The common R106W, R133C, T158M, R168X, R255X, R270X, R294X, and R306C RTT mutations were of special interest in the derivation of RTT iPSCs due to their power to model a large percentage of RTT cases. As discussed previously, there is no clear genotype phenotype correlation present in RTT individuals, thus *in vitro* modeling allows for a reductionist approach which may advance our understanding of the molecular and biochemical effects of specific RTT mutations in specific cell types. To date, RTT iPSC lines for the common T158M, R294X, and R306C mutations have been generated by our lab and others (Ananiev *et al*., 2011; Marchetto *et al*., 2010; Cheung *et al*., 2011; Kim *et al*., 2011; Pomp *et al*., 2011). The T158M iPSC lines were generated by our group, and the Muotri, Ellis, Park, and Colman groups (Ananiev *et al*., 2011; Marchetto *et al*., 2010; Cheung *et*

al., 2011; Kim *et al*., 2011; Pomp *et al*., 2011) and were derived from the same Coriell Cell Bank fibroblast GM17880 line. The R294X iPSC lines generated by our group were derived from a fresh RTT patient skin biopsy rather than a banked fibroblast line (Ananiev *et al*., 2011). The R306C iPSC lines were reported by our group, the Muotri, Ellis, and Park groups (Ananiev *et al*., 2011; Marchetto *et al*., 2010; Cheung *et al*., 2011; Kim *et al*., 2011) and were derived from the same Coriell Cell Bank fibroblast GM11270 line. Additionally, other RTT iPSC lines have been derived from RTT patients with less common RTT mutations (Ananiev *et al*., 2011; Marchetto *et al*., 2010; Cheung *et al*., 2011; Kim *et al*., 2011; Pomp *et al*., 2011). Please refer to **Table 1** for a detailed description of RTT iPSC lines currently available to the RTT research community.

- XCI analysis of RTT iPSCs

There have been inconsistencies in reports of RTT-iPSCs' XCI status (Ananiev *et al*., 2011; Hotta *et al*., 2009; Marchetto *et al*., 2010; Cheung *et al*., 2011; Kim *et al*., 2011; Pomp *et al*., 2011 and listed in **Table 1**). James Ellis and colleagues have proposed a classification system for the XCI status of iPSCs to aid the research community (Cheung *et al*., 2012). In this classification system, iPSCs that have two active X's (Xa), as indicated by the lack of *XIST* RNA and H3K27me3 marks, are termed pre-XCI iPSCs. Upon differentiation, these pre- XCI hPSCs initiate random XCI, leading to biallelic expression of X-linked genes. Post-XCI iPSCs carry an inactive X (Xi), as indicated by *XIST* RNA and H3K27me3. Pure populations of post-XCI iPSCs retain a skewed non-random XCI pattern when differentiated, resulting in monoallelic expression of X-linked genes. Post-XCI iPSCs allow for the comparison of isogenic paired lines generated from

the same RTT patient. In our study, all of the female RTT iPSC lines assayed (23 total) exhibited a post-XCI status (Ananiev *et al*., 2011). These results are consistent with the original discovery of nonrandom XCI in female human iPSC lines and with the findings in the Ellis and Coleman groups (Tchieu *et al*., 2010; Cheung *et al*., 2011; Pomp *et al*., 2011).

The Muotri and Park groups reported a mix of Pre and Post XCI in their RTT iPSC lines (Marchetto *et al*., 2010; Kim *et al*., 2011). The pre-XCI RTT-hiPSCs reported by the Park group lacked H3K27me3 marks and expressed *MECP2* at twice the levels of wild type male hESCs (Kim *et al*., 2011). Likewise, the undifferentiated pre-XCI RTT-hiPSCs reported by the Muotri group lacked *XIST* RNA, H3K27me3, and expressed *MECP2* in a biallelic manner (Marchetto *et al*., 2010). When differentiated, the pre-XCI RTT-iPSCs in Muotri's group were shown to initiate XCI and exhibit mosaic expression of wild type and mutant *MECP2*. These results are in conflict with the apparent non-random skewed *Androgen Receptor* XCI assay data presented for neurons derived from these pre-XCI iPSC lines (Marchetto *et al*., 2010). As a whole, these data remain difficult to compare and interpret. Going into the future, careful analysis of the XCI status and the resulting allelic expression of *MECP2* by multiple independent assays will have to be determined independently for each RTT iPSC line and its differentiated derivatives.

- Differentiation and phenotypic characterization: RTT disease modeling

Our group and several others have gone on to differentiate RTT patient iPSCs into neurons and have performed analyses for characteristic RTT pathology (Ananiev *et al*., 2011; Marchetto *et al*., 2010; Cheung *et al*., 2011; Kim *et al*., 2011). Interestingly, the

Park group reported a defect in neuronal differentiation in their RTT iPSCs (Kim *et al*., 2011). At face value, this conflicts with several other reports including ours, thus necessitating further investigation (Bauman *et al*., 1995; Chen *et al*., 2001; Kishi and Macklis, 2004; Marchetto *et al*., 2010; Ananiev *et al*., 2011). The post-XCI RTT iPSC lines in the Ellis group and ours were shown to retain XCI status and allelic *MECP2* expression upon differentiation, allowing for comparison between mutant and isogenic wildtype control neurons (Ananiev *et al*., 2011; Cheung *et al*., 2011).

All three groups reported one common finding, which was a reduction in the soma size of RTT iPSC-derived mutant neurons (Ananiev *et al*., 2011; Marchetto *et al*., 2010; Cheung *et al*., 2011). This represents the first documentation of a hallmark RTT phenotype in a patient-specific *in vitro* system. It is important to note that the reduction in neuron soma size was present when we and other labs used different methods for derivation and differentiation in addition to testing several different *MECP2* mutations (Chang: R294X; Muorti: unspecified; Ellis: Exon 3-4 deletion). Due to the robustness of this phenotype, soma size of RTT neurons could potentially be utilized as a read-out in large-scale drug screens. The Muorti group has noted additional RTT phenotypes in their system, the more conclusive of which was a lentiviral overexpression of MECP2 rescuing the VGLUT1 puncta deficit in glutamatergic neurons, providing evidence that loss of MECP2 function lead to the phenotype (Marchetto *et al*., 2010).

IV) Elucidation of RTT disease mechanism

The search for MeCP2 target genes

Identification of transcripts affected by MECP2/MeCP2 dysfunction can provide

tangible clues into the disease mechanism of RTT. Many of the first studies aimed at determining MECP2/MeCP2 target genes were heavily influenced on the notion that, as a global transcriptional repressor, loss of MeCP2 function would lead to a large number of upregulated transcripts (Samaco and Neul 2011). Thus, the initial target gene studies were genome-wide transcription profiles in nature (Colantuoni *et al*., 2001; Tudor *et al*., 2002; Nuber *et al*., 2005). Given the understanding at that time, the subtle transcriptional alterations reported were surprising. These studies used material from patient postmortem tissues and, in the case of RTT mouse models, whole brain lysates. Certain groups reasoned the heterogeneous nature of the samples used in previous expression profiling experiments had limited the sensitivity of detection. Thus, MeCP2 dysfunction may be specific to particular brain regions or cell types (Jordan *et al*., 2007). A subsequent study went on to test this hypothesis by profiling specific brain regions in two widely used RTT mouse models (*Mecp2*$^{tm1.1Jae/y}$ and *Mecp2*$^{tm1.1Bird/y}$) and identified substantial expression changes in the cerebellum (Smrt *et al*., 2007). A second study (Chahrour *et al*., 2008) performed transcriptional profiling in the hypothalamus, comparing the *Mecp2*$^{tm1.1Bird/y}$ and MeCP2-TG mouse models (loss- and gain-of-function MeCP2, respectively) to wild type mice and focusing on loci of differential effect between loss- and gain-of-function MeCP2 models. With this approach, transcription of many genes was found to be altered: ~400 repressed targets and ~2000 activated targets. After Huda Zoghbi's group reported that MeCP2 could also activate gene transcription, a paradigm shift occurred in the RTT field that lead to the further characterization of MeCP2's multi-faceted roles (Chahrour *et al*., 2008). It is the current understanding that MeCP2 regulation of different target genes can occur within the context of specific cell types, at particular points of the life cycle,

and in response to neuronal activity. One such gene, *BDNF*, is differentially regulated in such a manner.

Example target gene: BDNF (brain-derived neurotrophic factor)

The *BDNF* gene has multiple differentially regulated promoters. The human gene has an estimated nine functional promoters (Pruunsild *et al*., 2007). Within the mammalian brain, *BDNF* displays a remarkable overlap with MeCP2's spatiotemporal expression patterns (Pruunsild *et al*., 2007; Shahbazian *et al*., 2002). *BDNF*/BDNF is highly expressed in neurons during post-natal development, with the highest levels of the BDNF protein present in the postnatal period in the hippocampal, amygdala, cerebral cortex, and hypothalamal brain regions (Pruunsild *et al*., 2007). BDNF is a member of the neurotrophin family of proteins (Cunha *et al*., 2010). It has been the most extensively characterized neurotrophin and shown to be critical for neuronal development, synaptic maturation, and plasticity (Murer *et al*., 2001; Cunha *et al*., 2010; Greenberg *et al*., 2009; Reichardt, 2006).

MeCP2 has been shown to regulate *Bdnf* transcription by different pathways, one of which displays context-dependent activation (Chen *et al*., 2003; Abuhatzira *et al*., 2007). In the absence of stimulation, MeCP2 was shown to directly bind the BDNF promoter III in rat (promoter IV in mouse) and repress its transcription (Chen *et al*., 2003). When stimulated, depolarization triggers a calcium-dependent phosphorylation of MeCP2 at serine 421 (S421), leading to its release from the *Bdnf* promoter and allowing transcription (Chen *et al*., 2003; Zhou *et al*., 2006). This activity-dependent phosophorylation at S421 was shown to regulate features of neural maturation, namely

dendritic patterning and spine morphogenesis *in vitro* (Zhou *et al*., 2006). *Mecp2* null mice show a reduction in BDNF levels, which may underlie some RTT phenotypes. Along these lines, as was shown in the *in vivo* context, conditional deletion of *Bdnf* in postmitotic neurons mirrors RTT phenotypes including hindlimb clasping, reduced brain weight, and reduced neuronal cell size (Chang *et al*., 2006). When *Bdnf* is deleted specifically in the forebrain of a *Mecp2*$^{-/Y}$ null, mice experience an earlier onset of locomoter dysfunction and a reduced lifespan. Conversely, when BDNF is overexpressed in the *Mecp2*$^{-/Y}$ mice, there is an improvement in locomoter function and lifespan.

The REST/co-REST complex has also been shown to repress *Bdnf* transcription by binding upstream of the MeCP2 binding site (Abuhatzira *et al*., 2007). A recent study has suggested that the low levels of BDNF observed in the *Mecp2* null mice may be due to dis-inhibition of the REST/Co-REST complex, as REST/Co-REST levels are increased in the *Mecp2* null (Abuhatzira *et al*., 2007). These results demonstrate that MeCP2 regulation of BDNF is necessary for proper neurological function and that therapeutic intervention targeting BDNF or BDNF signaling may provide improvement of RTT symptoms (Johnson *et al*., 2012).

Cellular mechanisms

Many *Mecp2* mouse models have been designed to utilize the Cre recombinase (Cre)/loxP system, allowing for inducible temporal and spatial control on manipulating *Mecp2*. Early studies sought to determine at what point in development *Mecp2* deficiency exerts pathological effects. Brain-specific deletion of *Mecp2* by Nestin-Cre (expressed at embryonic day 12) resulted in gait, posture, breathing and cellular pathology similar to

those observed in human RTT patients and germline *Mecp2* null, indicating RTT is primarily caused by the loss of MECP2 in the central nervous system (CNS) (Chen *et al*., 2001). When *Mecp2* is specifically deleted in postnatal excitatory neurons by Cam kinaseII-Cre, the onset of phenotypes is later and reduced in severity, as compared to the germline null (Chen *et al*., 2001). This later onset of more mild features suggests that these neurons may not be the only cell type affected by MeCP2 dysfunction, and that MeCP2 may play an important function in late embryonic development. In addition, studies in neural precursor cultures show that MeCP2 dysfunction does not alter cell fate decisions, but rather affects neuronal cells after exit from the cell cycle (Kishi *et al*., 2004).

- Cell autonomous component

Subsequent studies with neuron-specific or regional-*Mecp2*-deletions went on to reproduce certain aspects of RTT pathology, suggesting that specific features are associated with dysfunction in discrete neuronal populations (Gemelli *et al*., 2006; Fyffe *et al*., 2008; Samaco *et al*., 2009; Adachi *et al*., 2009, Chao *et al*., 2010). These studies demonstrate MeCP2 is critical for the normal function of neurons (Chao *et al*., 2010). To study the cell autonomy of RTT-like phenotypes, physical chimeras were made by transplanting either *Mecp2*-null or wild type immature cortical neurons into wild type mouse cortices. It was shown that *Mecp2* null neurons retain characteristic dendritic arborization defects in a manner independent of recipient environment (Kishi and Macklis, 2010).

- Non-cell autonomous component

In addition to a cell autonomous component of MeCP2 dysfunction, there are several lines of evidence for non-cell autonomous component in RTT pathology. In the neuronal transplant studies referred to above, it was also shown that wild type neurons develop dendritic deficits when transplanted into *Mecp2* null animals (Kishi and Macklis, 2010). Along the same lines, $Mecp2^{+/-}$ female animals have decreased dendritic arborization in both the mutant and wild type MeCP2-expressing neurons when compared to wild type animals (Belichenko *et al*., 2009). Non-cell autonomous mechanisms have been shown to affect MeCP2 protein levels. In the $Mecp2^{-/+}$ mouse and human RTT brains, the MeCP2+ cells show lower MeCP2 expression than those in $Mecp2^{+/+}$ tissues (Samaco *et al*., 2004). Additionally, although there is evidence for a cell-autonomous role of MeCP2 in the regulation of tyrosine hydroxylase (TH), which is expressed in dopaminergic neurons, wild type MeCP2-expressing neurons in $Mecp2^{-/+}$ mice have decreased levels of TH compared to wild type animals (Taneja *et al*., 2009). While these non-cell autonomous characteristics may be due in part to the interaction with other neurons, there has been recent interest in the interplay between neurons and glia in RTT pathology (Ballas *et al*., 2009; Maezawa *et al*., 2009; Lioy *et al*., 2011).

V) Glial contribution to RTT pathogenesis

- Historical studies of glia

Glia was first described in the mid 1800's by Rudolf Virchow as a "substance… which lies between the proper nervous parts, holds them together and gives the whole its form" (Virchow, 1858). This 'nervenkitt' or nerve-cement, which he termed 'neuroglia';

lead to the first postulated role of glia as the structural cells of the brain. A subset of these cells with a star-like morphology were later called astrocytes (Lenhossek 1891). With advances in staining techniques, Golgi and Santiago Ramón y Cajal were able to provide the first detailed morphological descriptions of the most numerous cell type of the brain (Golgi, 1873; Golgi, 1894; Ramón y Cajal, 1913). Relatively recent evidence gathered in the past three decades, indicates that astrocytes have diverse interconnected roles within the nervous system. The direct roles that astrocytes have been implicated to play upon neuronal function, morphology and viability will be discussed.

- Dynamic coupling

Through coupling synaptic activity with the uptake and metabolism of energy substrates, astrocytes have integral roles in the dynamic homeostasis of brain function (Tsacopoulos and Magistretti 1996). The coupling functions of astrocytes are displayed by the structure of different specialized processes that can 1) surround blood vessels or 2) ensheath the synapse of neurons. A single astrocyte can extend multiple processes to blood vessels (McCaslin *et al*., 2011) in addition to forming contacts with up to 600 neuronal dendrites (Halassa *et al*., 2007), creating an exclusive "territory" covering up to 100,000 synapses (Bushong *et al*., 2002). This allows astrocytes to act as single-cell moderators between the locus of neuronal activity (neurons) and the energy supply entry point (the circulatory system). Astrocytes have been shown to couple both blood supply to the brain and the bioavailability of energy sources to neurons and oligodendrocytes in an activity-dependent manner. The regulation of blood flow to the brain is modulated at the local level by astrocyte end-feet surrounding blood vessels. Astrocytes sense

vasoactive byproducts of neuronal activity and mediate vasodilation to active brain regions (Takano *et al*., 2006). Studies have shown prostaglandin E2 (PGE2) is a key vasodilator released by astrocytes (Iadecola and Nedergaard 2007). In tandem, astrocytes are able to couple synaptic activity with the uptake and metabolism of energy substrates to match neuronal demand with supply. Endfeet express surface proteins, such as the glucose transporter GLUT1, that allow for uptake of energy substrates from the endothelium (Kacem *et al.,* 1998). Following uptake, astrocytes can directly transport glucose to neurons or act as a reservoir for energy by the conversion of glucose into glycogen, depending upon the neural context (Stobart and Anderson 2013). During the course of a glutamatergic action potential, a presynaptic neuron releases glutamate into the extracellular space of the synapse, leading to the depolarization of a postsynaptic neuron (Tsacopoulos and Magistretti 1996). Glutamate released in the synaptic cleft is taken up by astrocytes through the excitatory amino acid transporters GLAST and GLT-1. This passage of glutamate through GLAST and GLT-1 is directly coupled to the activity of Na,K-ATPase (Rose *et al*., 2009). Activation of Na+/K+-ATPase stimulates glycolytic lactate production, providing an efficient means to couple neural activity with astrocytic energy production (Pellerin and Magistretti, 1994).

- Neurotransmitter clearance and synaptic transmission

Through their contacts with neurons, astrocytes are poised to manage extracellular levels of neurotransmitters at the synaptic cleft following neural transmission. In addition to removing the neurotransmitter glutamate from the synaptic cleft, astrocytes have also been shown to clear gamma-aminobutyric acid (GABA), norepinephrine, dopamine,

serotonin and acetylcholine (Kimelberg 1995). Once cleared, these neurotransmitters can then be converted into metabolites for alternative functions or modified and secreted harmlessly. The mechanism of astrocytic clearance of glutamate and its downstream effects has been well described (De Keyser *et al*., 2008). Once glutamate enters an astrocyte, it may be used as a substrate for oxidative metabolism (described above), converted to alpha-ketoglutarate to replenish the tricarboxylic acid (TCA) cycle, or recycled for neurotransmission (De Keyser *et al*., 2008). This recycling of glutamate for neurotransmission is called the glutamate-glutamine cycle. The glutamate-glutamine cycle is vital for excitatory transmission, as neurons cannot perform *de novo* synthesis of glutamate and high levels of extracellular glutamate leads to excitotoxicity. The astrocyte-specific enzyme glutamine synthase converts glutamate into glutamine (Martinez-Hernandez *et al*., 1977). After conversion, glutamine is then shuttled from astrocytes to neurons, where phosphate-activated glutaminase (PAG) allows conversion back into glutamate for neurotransmission. As the major excitatory neurotransmitter, glutamate production is controlled at multiple levels, with check-points at DNA transcription, mRNA splicing and degradation, protein synthesis and targeting, amino acid transport activity and the activities of associated ion channels (Danbold 2001). The activities of the astrocyte-specific excitatory amino acid transporters GLAST and GLT-1 are the only major mechanism for removal of glutamate from the extracellular fluid (De Keyser *et al*., 2008). This fine-tuned of control of glutamate is necessary as high levels of extracellular glutamate leads to sustained intracellular Ca^{2+} in neurons, which initiates an excitotoxic cell death cascade (Doble 1999). As such, antiglutamate drugs are being tested on neurodegenerative pathologies with a suspected excitotoxicity component

including inflammation, acute ischemic stroke, ALS, Parkinson's disease and Huntington's disease (Doble 1999).

- Growth and maturation of neurons

The process of elaborating and refining the processes that compose an individual astrocyte's "territory" continues into postnatal development, coinciding with a period of active synaptic refinement (Freeman *et al*., 2010). During this time, glutamate receptors (mGluRs) and the EAAT1/2 transporters (GLAST AND GLT-1) are expressed in astrocytes, indicating that astrocytes are primed at early stages to be responsive to neural activity (Regan et al., 2007; Schools and Kimelberg, 1999). *In vitro* studies have shown that different types of neurons make a greater number of functionally mature synapses when co-cultured or cultured in the conditioned media of astrocytes, indicating molecules secreted by astrocytes promote the formation of synapses (Pfrieger and Barres 1997; Ullian *et al*., 2001; Ullian *et al*., 2004). Initially, it was shown that the matricellular thrombospondins (TSP's) and the TSP receptor are highly expressed in astrocytes and their expression acts as a permissive switch that times CNS synaptogenesis (Christopherson *et al*., 2005). Additionally through *in vivo* studies, other molecules and pathways have implicated in astrocyte-induced synaptogenesis such as cholesterol, integrins, ephrins, and Hevin/Sparc (Pfrieger 2009). This is by no means a complete list, as additional factors and the actions of their corresponding signaling pathways are likely necessary for synaptic functionality and maintenance. For example, biochemical fractionation of astrocyte-conditioned medium was used to identify glypican 4 (Gpc4)

and glypican 6 (Gpc6) as integral in the induction of postsynaptic function of structural synapses (Allen *et al*., 2012).

Multiple studies have found that mutant astrocytes variably modify dendritic outgrowth of hippocampal neurons in culture, though as of date, the deficient factors involved have not clearly defined (Ballas *et al*., 2009; Jacobs and Doering 2010). Astrocytes have been shown to promote neurite growth by mechanisms involving membrane-bound proteins. Using a co-culture system consisting of rat astrocyte and chick retinal cell, the neurite inducing effects of the astrocyte membrane bound proteins N-cadherin and integrin ß1 upon neurons were demonstrated (Neugebauer *et al*., 1988). In a follow-up study utilizing genetic deletion of N-cadherin, this Ca^{2+}-dependent cell adhesion molecule was shown to directly affect neurite outgrowth (Ferguson and Scherer, 2012). In addition, TSPs, which have been shown to influence synapse formation, have also been shown to promote neurite outgrowth in some developmental contexts (Arber and Caroni *et al*., 1995).

Conversely, reactive astrocytes have been shown to inhibit neurite outgrowth *in vitro*. Using explant cultures McKeon *et al*., demonstrated the inability of the adult glial scar tissue to support neurite outgrowth was correlated with the expression of the extracellular matrix (ECM) molecules chondroitin-6-sulfate proteoglycan (CS-PG) and cytotactin/tenascin (CT) (1991). Thus, these astrocytic factors may be involved in limiting the growth of regenerating axons in the CNS after injury or in limiting the growth of neurites in diseased states (McKeon *et al*., 1991).

- *Regulation and secretion of neurotrophic factors and cytokines*

Astrocytes have been shown to produce a wide range of neurotrophic factors and cytokines that have a direct impact on neuronal morphology, function and viability (Allaman *et al*., 2011). The specific neurotrophic factors produced by astrocytes include NGF (nerve growth factor), BDNF (brain derived neurotrophic factor), CNTF (ciliary neurotrophic factor), GDNF (glial cell line-derived neurotrophic factor), IGF-1 (insulin-like growth factor-1), FGF-2 (fibroblast growth factor-2), VEGF (vascular endothelial growth factor) and ADNF (activity-dependent neurotrophic factor). Additionally, astrocytes secrete the anti-inflammatory cytokines interleukin (IL)-6 and TGF-ß, which have been implicated in neuroprotection (Liberto *et al*., 2004). IL-6 and TGF-ß's effects are counter-balanced with the pro-inflammatory cytokines (IL)-1β and tumor necrosis factor-α (TNFα), which have been shown to promote neurotoxicity (Liberto *et al*., 2004).

Astrocytes in disease

Due to their wide range of roles in the nervous system, astrocytes may play significant roles in neurological disease states. The variety of neurotropic factors secreted by astrocytes can play a neuroprotective role while dysfunction in astrocytic homeostatic mechanisms can lead to increased levels of known neurotoxic substrates with widespread effects. This is evident as a number of studies have implicated astrocytes in disorders of both neurodegenerative and neurodevelopmental origins. Neurodegenerative disorders with a glial component include Alexander Disease, Aceruloplasminemia, Amyotrophic lateral sclerosis, Alzheimer's disease, Huntington's disease, Neuromyelitis optica, Niemann-Pick type C disease, Parkinson disease and Vanishing white matter leukodystrophy. Neurodevelopmental disorders with a glial component include Fragile X,

Down syndrome, and with increasing evidence from our group and others, Rett syndrome. In the future, further characterization of each disorder is necessary to determine whether astrocytes play a primary role in pathogenesis or mediate secondary effects in diseased states. Below is a summary of the studies implicating a glial component in specific neurodegenerative and neurodevelopmental disorders.

- Alexander Disease

Alexander disease (AxD) is a neurodegenerative genetic disorder that directly targets astrocytes. Missense mutations in the *GFAP* gene have been shown to lead to an astrocyte-specific gain of function disease progression (Li *et al*., 2002, Messing *et al*., 2012). In AxD, oligodendrocyte and neuronal cells become dysfunctional as astrocytes, in a state of cellular stress, display alterations in morphology and in function. Damaged neuronal cells signal to astrocytes in a positive feedback loop, leading to both an increase of GFAP expression and a decrease of its degradation (Messing 2012). As a result, AxD astrocytes become hypertrophied and further accumulate stress protein inclusions, called Rosenthal fibers. Mechanistic studies using AxD mouse models have demonstrated that neuronal dysfunction could be due to either the loss of AxD astrocyte's homeostatic roles or a gain of detrimental effect. AxD astrocytes have reduced levels of the GLT-1 glutamate transporter. Dysfunction in the glutamate-glutamine cycle may also contribute to excitotoxicity for neurons, as has been demonstrated *in vitro* (Tian *et al*., 2012). Moreover, as it has been demonstrated *in vivo*, GFAP accumulation produces a toxic effect (Messing *et al*., 1998). Thus, there is a possibility that both the loss of supportive functions and the gain of detrimental functions are involved in the disease etiology

(Messing *et al*., 2012).

- Aceruloplasminemia

Aceruloplasminemia is an inherited disorder of iron metabolism. It is caused by loss-of-function mutations in the *ceruloplasmin* gene that encodes the ceruloplasmin ferroxidase (Harris *et al*., 1995). Ceruloplasmin is expressed primarily in hepatocytes and in astrocytes, affecting the distribution of tissue iron and through the oxidation of ferrous iron to ferric iron, protecting against reactive oxygen species (Miyajima 2003). As iron accumulates in the brain and visceral organs, patients display neurodegeneration of the retina and basal ganglia in conjunction with diabetes mellitus (Miyajima 2003). Within the nervous system, astrocytes are dysfunctional, displaying a globular structure characteristic of iron accumulation.

- Amyotrophic lateral sclerosis

Amyotrophic lateral sclerosis (ALS) is a neurodegenerative disorder leading to progressive paralysis and muscle atrophy (Rao *et al*., 2003). In the disease pathology, there is selective motor neuron degeneration in the cortex, brainstem and spinal cord accompanied by reactive gliosis (Strong 2003). Though multiple genes have been linked to ALS, the *SOD1* gene has been the most widely studied (Cleveland and Rothstein, 2001). Characterization of the *SOD1* rodent models has shown a complex interplay of dysfunctional non-cell autonomous interactions between motoneurons and multiple cell types including oligodendrocytes, Schwann cells, astrocytes and microglia (Ilieva *et al*., 2009). ALS/SOD1 mutant astrocytes show morphological and functional changes

including the formation of aggregated neurofilaments containing SOD1 protein and reduced expression of GLT-1 due to RNA mis-splicing (Barbeito *et al*., 2004). Both oxidative damage propagated by astrocytes and the disruption of astrocytes' roles in the glutamate-glutamine cycle have been implicated in the loss of motor neurons (Barbeito *et al*., 2004).

- Alzheimer's disease

The age-related progressive neurodegenerative disorder Alzheimer's disease (AD), is the most common cause of dementia. Pathological features include the formation of senile plaques, neurofibrillary plaques and tangles and loss of cholinergic and cholinoceptive neurons in the frontal cortex and hippocampus accompanied by the presence of activated macrophages and reactive astrocytes (Markiewicz and Lukomska 2006). Senile plaques are formed by extracellular deposits of ß-amyloid protein (Aß), which is a known activator of the astrocyte inflammation response (Holroyd and Shepherd 2001). In conjunction with the neurotoxic effects of Aß itself, Aß-activated astrocytes produce inflammatory cytokines, chemokines, thromboxanes, coagulation factors, proteases and reactive oxygen species that may lead to neuronal damage (Johnstone *et al*., 1999). Further damage may also be inflicted upon neuronal cells when microglia are attracted by the chemokines produced by activated astrocytes (Tuppo and Arias 2005).

- Huntington's disease

Huntington's disease (HD) is a neurodegenerative disorder caused by a CAG

repeat expansion in the *huntingtin* (*htt*) gene (Huntington's Disease Collaborative Research Group, 1993). In the striatum and cortex, neural cell death is accompanied by gliosis (Davies and Ramsden, 2001). While the role of glia in the disease progression is not well understood, work in a transgenic mouse model has shown that expression of mutant *htt* selectively in astrocytes affects the disease progression and recapitulates disease phenotypes, possibly by dysfunction of the glutamate-glutamine cycle as GLT-1 levels are reduced in mt *htt* astrocytes (Bradford *et al*., 2009).

- Niemann-Pick type C disease

Niemann-Pick type C (NP-C) disease is a lipid storage disorder leading to progressive deterioration of nervous system function. This autosomal recessive disorder is due to mutations in the *NPC1* gene (a small number of cases are due to *NPC2* mutations), leading to inactivation of the NPC1 protein (Park *et al*., 2003). NPC1 localizes to astrocytic processes near nerve terminals; these sites are the first to show signs of degeneration (Patel *et al*., 1999). The NP-C mouse model shows impairment in neurite growth and has significantly elevated levels of cholesterol within mitochondria membranes. A defect in cholesterol trafficking leads to the reduction of the mitochondrial membrane potential, the activity of ATP synthase and subsequent reduction in levels of ATP produced (Yu *et al*., 2005). Since exogenous ATP rescues the neurite outgrowth phenotype, astrocyte-mediated ATP signaling may play a role in the disease pathology (Yu *et al*., 2005).

- Neuromyelitis optica

Neuromyelitis optica is a demyelinating inflammatory disease that affects the optic nerve and spinal cord causing loss of vision and spinal cord function. A unique serum autoantibody IgG from patient has been shown to bind the astrocyte specific water channel aquaporin 4 (AQP4) (Lennon *et al*., 2005). AQP4 is expressed in astrocyte end feet at points interacting with blood vessels. Treatment of astrocyte cultures with IgG leads to the decrease of AQP4, the excitatory amino acid transporter GLT-1, and the activity of glutamine synthetase, an astrocyte specific enzyme that converts glutamate into glutamine (Marignier *et al*., 2010). As a result of reduced glutamine synthetase activity, glutamate levels rise and induce toxicity towards oligodendrocytes (Marignier *et al*., 2010).

- Parkinson disease

Parkinson's disease (PD) is a movement disorder characterized by selective loss of dopaminergic neurons in the substantia nigra. Mitochondrial dysfunction, oxidative stress, altered protein handling and neuroinflammation have been implicated in the disease mechanism (Schipper *et al*., 1996). Due to increased levels of oxidative stress, astrocytes and microglia display an inflammation response. It has been demonstrated that in the substantia nigra and striatum of PD patients, there is an increase in astrocyte neuroinflammatory products TNFα-, IL-1ß, and TGF-ß (Nagatsu *et al*., 2000). Under these conditions astrocytes display altered protein handling, with the glutamate-glutamine cycle becoming dysfunctional causing the levels of extracellular glutamate to rise. These high levels of extracellular glutamate have an excitotoxic effect upon neurons (Schapira and Jenner 2011). The combination of increased neuroinflammation products and

excitotoxicity may lead to neuron cell death (Markiewicz and Lukomska 2006).

-Vanishing white matter leukodystrophy

Vanishing white matter leukodystrophy (VWM) is an autosomal recessive disorder caused by mutations in the subunits that encode the eukaryotic initiation factor 2B (eIF2B), a protein complex essential for protein synthesis (Leegwater *et al*., 2001). It has been suggested that the pathophysiology of VWM involves inappropriate activation of the unfolded protein response (UPR) in astrocytes and oligodendrocytes (van Kollenburg *et al*., 2006). Neuroblast cultures from a patient with an *EIF2B5* mutation showed normal differentiation of oligodendrocytes while astrocytic induction and morphology were severely affected, raising the possibility that a deficiency in astrocyte function may contribute to the loss of white matter in VWM leukodystrophy (Dietrich *et al*., 2005).

-Down syndrome

Down syndrome (DS) is the most common disorder of intellectual disability. DS is caused by a nondisjunction event leading to trisomy of chromosome 21 with subsequent increase in dosage of linked genes. The cognitive deficits of DS have been connected to alterations in dendritic spines (Benavides-Piccione et al., 2004). Using a human astrocyte/rat hippocampal neuron co-culture system, Garcia *et al*. showed that patient-derived DS astrocytes affect neuron spine morphology through a decrease of the secreted protein thrombospondin 1 (TSP-1) (2010). Additionally, another study implicated an impairment of neurogenesis through the use of human neural progenitors

derived from Down syndrome patients, showing that gliogenesis was increased in these cells at the expense of neurogenesis (Lu *et al*., 2011).

- Fragile X

Fragile X (FXS) is a form of inherited intellectual disability that results from expansion of a CGG repeat in the *FMR1* (fragile X mental retardation 1) gene (Santoro *et al*., 2012). Repeat expansion leads to transcriptional silencing of the *FMR1* gene and loss of the encoded protein, FMRP (Bhakar et al., 2012). FMRP plays an important role in modulating the translation of mRNAs that have been implicated in dendritic growth (Brown et al., 2001; Lee et al., 2003) and in the development of synapses (Greenough et al., 2001). It has been shown both in vitro and in vivo that FMRP is expressed in early development in cells of the glial lineage (Pacey and Doering 2007). Astrocyte secreted factors from the *Fmr1* knockout mouse Fragile X model have been shown to inhibit dendritic growth of both wild type and *Fmr1* KO neurons, with elevated levels of neurotrophin-3 (NT-3) being implicated in the phenotype (Yang *et al*., 2012).

Initial studies implicating glia in RTT pathology

In addition to misregulated neural transcripts, several glia-specific transcripts have been shown to be misregulated in the RTT brain (Colantuoni *et al*., 2001). These include alpha B-crystallin, glial fibrillary acidic protein (GFAP), glial excitatory amino acid transporter 1 (EAAT1) and S100A13 (Colantuoni *et al*., 2001). All of these gene products have been implicated in neuropathological mechanisms (Iwaki *et al*., 1993; Goldman *et al*., 1988; Scott *et al*., 2002; Landriscina *et al*., 2006). These findings were

surprising; early analysis of MeCP2 expression throughout the brain failed to show detectable levels of the protein in cell types other than neurons (Shahbazian *et al*., 2002; Akbarian *et al*., 2001). In conjunction with high levels of MeCP2 protein found in neurons along with the presence of clear morphological deficits in neurons, RTT was considered to predominately affect neurons. Yet, multiple lines of evidence have begun to challenge this model, arguing that MeCP2 is important for the proper functioning in multiple cell types within the CNS.

In vitro evidence: RTT astrocytes affect neuron morphology

Initial studies to determine the glial role in RTT utilized *in vitro* co-cultures of *Mecp2* null astrocytes and wild type neurons. Two independent groups confirmed that unlike wild type astrocytes, mutant astrocytes could not support normal neuronal growth, resulting in neurons with shorter, less complex neurites (Maezawa *et al*., 2009, Ballas *et al*., 2009). This effect appears to be mediated by soluble factors released by astrocytes (either lack of necessary factors or gain of deleterious factors), as *Mecp2* mutant astrocyte conditioned media (ACM) failed to support neuronal growth (Ballas *et al*., 2009). This effect holds true when wild type and mutant ACM is mixed in equal portions, mirroring the mosaic expression of MeCP2 in the glia of heterozygous RTT females (Ballas *et al*., 2009).

In vivo mouse: astrocytes affect disease course

Further analysis of the involvement of astrocytes in RTT pathology was performed *in vivo*. In work performed by Gail Mandel's group using an inducible astrocyte-specific

Mecp2 expression line, it has been shown that restoration of MeCP2 specifically in astrocytes after the onset of disease progression can ameliorate RTT-like symptoms (Lioy *et al*., 2011). This provides the first definitive physiological link between MeCP2 expression in astrocytes and RTT features. Studying the interplay between the different cell types involved in RTT syndrome may be the only way to fully appreciate the disease course and thus, the only way to shed light on potential therapeutic approaches.

Patient iPSC study

Using our RTT patient-specific iPSC system, we developed a model to test the interplay between neurons and astrocytes. Adopting a method from Dr. Su-chun Zhang's laboratory (Krencik *et al*., 2011), we generated astrocytes from three different isogenic pairs for the V247X, R294X, and R306C RTT mutations. We showed isogenic RTT iPSC pairs can be differentiated into an enriched population of glial fibrillary acidic protein (GFAP) expressing astrocytes that maintained allelic *MECP2*/MECP2 expression, and that RTT mutant astrocytes and their secreted factors have non-cell autonomous adverse effects upon both neuron morphology and function. Additionally, we showed an amelioration of the non-cell autonomous effects of mutant neurons upon wild type interneurons through treatment with IGF-1 and its tripeptide cleavage product, Glycine-Proline-Glutamine (GPE). Our findings provide support for a glial contribution to RTT pathology in a patient-specific *in vitro* system that 1) displays robust genotype-dependent phenotypes and 2) allows for testing potential treatment compounds.

VI) Treatment development for RTT

Indications RTT may be treatable

There is critical need to develop treatments for RTT. The only available therapies are geared towards lessening symptoms and/or providing supportive measures including physical and speech therapies or administration of anti-seizure medication when applicable. Despite the lack of complete understanding in RTT's etiology, there is reason to believe that treatment may be possible. The first evidence comes from the disease time course RTT presents several months after birth. Key embryonic and perinatal developmental steps take place normally; and no gross malformation of the brain is evident (Neul *et al*., 2004). Second, most RTT-like symptoms are recapitulated when MeCP2 is inactivated in adult animals (Cheval *et al*., 2012; McGraw *et al*., 2011; Nguyen *et al*., 2012). Third, RTT-like symptoms in mouse models appear to be reversible following replacement or reactivation of *Mecp2*/MeCP2 (Guy *et al*., 2007; Lioy *et al*., 2011; Robinson *et al*., 2012; Alvarez-Saavedra *et al*., 2007; Giacometti *et al*., 2007; Jugloff *et al*., 2008; Luikenhuis *et al*., 2004). These data argue RTT disease phenotypes may be reversible.

Results of completed clinical trials

To date, four controlled clinical trials in RTT individuals have been reported, using various study designs (Percy *et al*., 1994; Ellaway *et al*., 1999; Ellaway *et al*., 2001, Glaze *et al*., 2009). These trials involved the administration of naltrexone (Percy *et al*., 1994), L-carnitine, (Ellaway *et al*., 1999; Ellaway *et al*., 2001), and folate-betaine (Glaze *et al*., 2009). None of the studies showed significant efficacy, while one highlighted the

detrimental effects of Naltrexone, an opioid antagonist (Percy *et al*., 1994). The Naltrexone study was a randomized, double blind, placebo-controlled crossover design with two treatment periods, 4 months each, and an intervening 1-month washout period. While Naltrexone was shown to slightly improve respiratory disturbance, this benefit was outweighed by a decline in motor function and more rapid progression of the disorder in subjects (Percy *et al*., 1994). L-carnitine, an amino acid that is involved in fatty acid metabolism, did not show significant improvement with drug administration but may provide a benefit in quality-of-life parameters, as was shown in a 1994 clinical trail with a follow-up 2001 study. The 1994 study was a randomized, placebo controlled, double-blind crossover designed trial with two treatment periods, 8 weeks each, with a 1-month washout period (Ellaway *et al*., 1999). Well-being and hand apraxia were slightly improved in treated subjects. The 2001 study was a cohort open label trial design wherein subjects in the treatment group showed slight improvements in sleep efficiency, energy levels, and expressive language skills (Ellaway *et al*., 2001). With these subjects, there was no improvement in hand function as was noted in the 1994 study with the same drug. The reason behind this discrepancy may warrant clarification in the future. Finally, folate-betaine, which has been shown to increase the available pool of methyl-donors, was used in a 12-month, double-blind, placebo-controlled trial. There was no objective evidence of improvement in treated subjects (Glaze *et al*., 2009).

Ongoing clinical trails

Additional clinical trials have been initiated to test the efficacy of the following compounds: EPI-743, NNZ-2566, rhIGF-1, and Dextromethorphan. The EPI-743 clinical

trial (ClinicalTrials.gov Identifier: NCT01822249) is a Phase 2A randomized, placebo controlled trial lead by a group at the University of Siena, Italy through collaboration with Edison Pharmaceutical Incorporated with an estimated primary completion date of December 2013. EPI-743 will be administered by subcutaneous injection. Past work with EPI-743 in the treatment of oxidative stress disorders has demonstrated it to be both safe and efficacious (Goldstein and Wolfe 2013). It has been hypothesized that free radicals generated from oxidation reactions are involved in the pathogenesis of Rett syndrome (Sierra *et al*., 2001). The NNZ-2566 clinical trail (ClinicalTrials.gov Identifier: NCT01703533) is a Phase 2A randomized, double blind, placebo controlled, parallel group, with dose-escalation lead by a group at Baylor Children's Hospital through collaboration with Neuren and the International Rett Syndrome Foundation (IRSF). The projected primary completion date is March 2014. NNZ-2566 will be administered orally rather than by subcutaneous injection. NNZ-2566 is an analog of the N-terminal Glypromate (Gly-Pro-Glu, GPE) cleavage product of human insulin-like growth factor-1 (IGF-1). Glypromate has been shown to have neuroprotective effects in both *in vitro* and *in vivo* models of brain injury (Bickerdike *et al*., 2009). Specifically, Glypromate has been shown to reverse behavioral phenotypes and increase survival in a RTT mouse model (Tropea *et al*., 2009). As a structural analogue of Glypromate, NNZ-2566 has improved stability and oral bioavailability. NNZ-2566 is also currently being tested in a clinical trial for traumatic brain injury patients (ClinicalTrials.gov Identifier: NCT00805818). The rhIGF-1 (Mecasermin/ INCRELEX) clinical trial (ClinicalTrials.gov Identifier: NCT01777542) is a Phase 2A randomized, double blind, placebo controlled, crossover study lead by a group at Boston Children's Hospital

through collaboration with the IRSF. The estimated primary completion date is July 2014. IGF-1 has been approved by the Food & Drug Administration (FDA) for use in children with growth hormone insensitivity syndrome, but in the context of RTT, it is currently considered an investigational drug. The Dextromethorphan (DM) clinical trial (ClinicalTrials.gov Identifier: NCT01520363) is a randomized double blinded placebo controlled trial being led by a group at the Kennedy Krieger Institute/ John's Hopkins School of Medicine. The estimated primary completion date is September 2014. DM was identified by its ability to block NMDA receptors (Gorman *et al*., 1997). In the early (<10 years of age) RTT brain, there is an increase in NMDA receptors that has been hypothesized to lead to misregulated excitatory neurotransmission (Blue *et al*., 1999).

Neurotrophic factors as RTT treatment candidates: IGF-1 and GPE

Neurotrophic growth factors are noteworthy treatment candidates for RTT. This was first shown in a pivotal study performed by Chang *et al*., that demonstrated overexpression of the neurotrophic growth factor BDNF was able to counteract MeCP2 deficiency (Chang *et al*., 2006). BDNF'S application in RTT treatment is limited due to its large size, impeding its pharmacological activity in the brain following peripheral administration due to its inability to cross the BBB (Pardridge *et al*., 1998). Thus, various agonists against the BDNF receptor TrkB have recently become of interest in RTT animal studies. When given systemically, the small molecule 7,8-dihydroxyflavone (7,8-DHF) selectively activates TrkB (Jang *et al*., 2010), leading to some improvement of RTT-like symptoms *in vivo* (Johnson *et al*., 2012). Although the mode of 7,8-DHF action is not well resolved, the specific activation of TrkB receptors remains a potential topic for

future RTT studies (Johnson *et al*., 2012).

An additional growth factor, insulin-like growth factor 1 (IGF1), has been shown to pass the BBB by regulated transport (Reinhardt et al., 1994; Pan and Kastin 2000). A small number of studies have tested components of the IGF-1 signaling pathway in RTT mouse models, with one study showing improvement of RTT-like phenotypes (Pitcher *et al*., 2013; Tropea *et al*., 2009). Also, to date, there are two clinical drug trails testing the efficacy of IGF-1 components in the treatment of RTT patients (ClinicalTrials.gov Identifier: NCT01703533 and NCT01777542). IGF-1 is produced for systemic circulation and locally within the brain. IGF-I is highly expressed in neurons (Garcia-Segura *et al*., 1991) and at lower levels in developing oligodendrocytes and astrocytes (Chernausek *et al*., 1993; Shinar and McMorris, 1995). Serum IGF-I is predominately produced by the liver, mediating the actions of growth hormones that lead to body growth, tissue remodeling and with recent evidence, neurodevelopment and cognition (Sjögren et al., 2002; Wang, 1997, Yakar et al., 2002, Nishijima et al., 2010). Peripheral IGF-I shows a wide neuroactive profile that hints to pleiotropic effects upon the brain (Nishijima et al., 2010). Specifically, peripheral administration of IGF-I has been shown to modulate brain vessel growth in adult mice (Lopez-Lopez et al., 2004), to stimulate adult neurogenesis (Aberg et al., 2000), and to influence hippocampal-dependent cognitive function in adult mice (Trejo *et al*., 2007). It should be noted that in these *in vivo* studies, test animals had low circulating levels of IGF-1 due to either liver specific IGF-1 knock-out (Lopez-Lopez *et al*., 2004; Trejo *et al*., 2007) or were hypophysectomized (Aberg *et al*., 2000). Thus, these studies provide strong evidence for

a specific role in systemic IGF-1 leading to downstream neurological effects.

It has been demonstrated *in vivo* that neurovascular coupling drives uptake of systemic IGF-1 to active brain regions (Nishijima *et al*., 2010). Using a variety of experimental approaches, Nishijima *et a,l* has shown that IGF-I penetrates the BBB in response to neuronal activity (2010). Results of this study indicate that cerebrospinal fluid IGF-I does not redistribute to active brain regions, but rather that circulating IGF-I is allowed entrance into active brain areas through the local vasculature of the BBB. While the exact mechanism is not well resolved, there appears to be a complex interplay between brain uptake of serum IGF-1 and CNS-derived IGF-1 that may affect different aspects of neurodevelopment and cognition. Future work to characterize the signaling mechanisms involved in the uptake of IGF-1 in conjunction to the actions of resident brain-derived IGF-1 may help explain the specific dysfunction in disorders in which IGF-1 has been implicated, such as Alzheimer's disease and Huntington's Disease, and with new evidence, RTT (Gasparini and Xu 2003; Humbert *et al*., 2002; Tropea *et al*., 2009).

The actions of IGF-1 are regulated by its association with IGF binding proteins 1-6 (IGFBPs). Binding to IGFBPs increases IGF-1's half-life and modulates its interaction with the IGF-1 receptor (IGF1R) (Duan *et al*., 1999). Additionally, overexpression of IGFBPs has been shown to retard postnatal brain growth, an effect postulated to be due to the decrease of available IGF-I (Lee *et al*., 1999). When IGF-1 is dissociated from an IGFBP, the peptide may in turn bind to the IGF-1 receptor (IGF-1R), initiating a signaling cascade. The IGF-1R is a cell surface tyrosine kinase that autophosporylates upon ligand binding. This autophosporylation leads to the association of the receptor to

insulin receptor substrate (IRS) adapter proteins. IRS proteins bind to tyrosine phosphate docking sites on the activated IGF1R and undergo phosphorylation themselves. Following this, immediate second messengers are recruited to transduce IGF-1 actions. A number of immediate second messengers have been implicated in IGF-1 action, including phosphatidylinositol 3 kinase (PI3K), growth factor receptor bound protein 2 (GRB-2) and Janus kinase (JAK) (Banerjee *et al*., 2012). PI3K activation leads to signal transduction through the AKT and mTOR pathway. Growth factor receptor bound protein 2 (GRB-2) leads to MAPK and extracellular signal-regulated kinase (ERK) signaling. Finally, JAK phosphorylation leads to the activation of the STAT pathway.

IGF-1's effects upon the CNS through the PI3K/AKT pathway include neuronal growth and neuroprotection (Brywe *et al*., 2005; Laurino *et al*., 2005). IGF-1's 'insulin-like' anabolic effects upon neuronal growth appears to be by mediating glucose utilization and protein synthesis to supply the huge biosynthetic needs of dendritogenesis and axonal growth cone assembly (Trejo *et al*., 2007; Laurino *et al*., 2005), while its role in neuroprotection is due to combating the pro-apoptotic proteins BAD, GSK-3, and caspase-9 and TNFα (Brywe *et al*., 2005; Zhao *et al*., 2006; Pang *et al*., 2007). *In vitro*, it appears that the MAPK (mitogen-activated protein kinase) signaling pathway is required for IGF-I–stimulated proliferation of adult progenitor cells, which was shown through the use of inhibitors and dominant negative constructs (Aberg *et al*., 2003). IGF-1 actions in neurons through the JAK-STAT pathway appear to counteract the neurodegenerative effects of the cytokine TNFα (Yadav *et al*., 2005). It is likely that IGF-1 simultaneously acts through various signaling pathways to be involved in such various processes such as the control of cell proliferation, gliogenesis, neurogenesis, neuron survival,

differentiation, synaptogenesis and myelination (Aberg *et al*., 2006). Moreover, IGF-I expression in the brain is spatiotemporally correlated to regions and periods of axon outgrowth, dendritic maturation, and synaptogenesis (Bondy *et al*., 1992; D'Ercole *et al*., 1996; Niblock *et al*., 2000).

Coupled with the increased interest of IGF-1 in nervous system therapeutics, there has been an insurgence of studies to improve its delivery method to guarantee more specific neurological improvements. One such approach was to look at how IGF-1 is utilized within the brain. In the brain, IGF-1 has been shown to be cleaved into two fragments, the N-terminal tripeptide of IGF-I, glycine-proline-glutamate (GPE) and the remaining des(1-3)IGF-1 (Yamamoto and Murphy, 1994; Yamamoto and Murphy, 1995). GPE was especially interesting due to its small size, allowing the peptide to efficiently cross the BBB (Baker *el al*., 2005). Although the precise mode of action of GPE is still unknown, initial reports showed that it was indeed neuroactive (Nilsson-Hakansson *et al*., 1993). *In vivo*, GPE was first shown to reduce neuronal loss after hypoxic-ischemic brain injury (Baker *et al*., 2005) and is currently in clinical trials for the treatment of traumatic brain injury (ClinicalTrials.gov Identifier: NCT00805818). *In vitro*, GPE was shown to protect neurons from glutamate-induced neurotoxicity (Saura *et al*., 1999). Specifically, GPE has been shown to activate PI3K signaling in glia, which could lead to downstream neuroprotective effects (Corvin *et al*., 2012). Later studies implicated GPE and its structural analogues in the modulation of inflammation, promotion of astrocytosis, inhibition of apoptosis and vascular remodeling (Guan and Gluckman, 2009). Systemic administration of GPE has been shown to improve several RTT-like phenotypes MeCP2 null mice (Tropea *et al*., 2009). Specifically, GPE was shown to extend life span,

improve locomotor function, ameliorate breathing patterns, and to reduce irregularity in heart rate. In addition, treatment with GPE increases the brain weight of the mutant mice. On the subcellular level, GPE was shown to partially restore spine density, PSD-95 expression and synaptic amplitude, increases, and stabilizes cortical plasticity to wild-type levels.

Conclusion

In conclusion, RTT is a debilitating neurodevelopmental disorder with no cure or effective treatment. While RTT is caused by mutations to a single gene, *MECP2*, the vast number of causative mutations and the influence of epigenetics upon this X-linked disorder present certain challenges for disease modeling. RTT mouse models have greatly advanced the understanding of the molecular mechanism underlying the disease, but have limitations that necessitate the development of human based systems. Thus, we have developed a unique *in vitro* experimental system based on several isogenic pairs of RTT patient-derived iPSC lines that harbor different *MECP2* mutations. Through this system, we have demonstrated the ability to model RTT *in vitro*. We have differentiated these isogenic pairs of RTT patient-specific iPSC lines into both specific subtypes of neurons and a highly enriched population of astrocytes, and observed cell autonomous deficits in RTT neurons and non-cell autonomous deficits in RTT astrocytes. Finally, we have demonstrated the tractability of our system as a drug-screening platform through a proof-of-principle assay testing the ability of the growth factors IGF-1 and GPE to modulate RTT-like cellular pathologies. In this work, we present results that are highly relevant for the understanding of the disease mechanism and therapeutic development.

Group	Fibroblasts reprogrammed	Reprogramming Method	XCI status	Article
Chang	GM17880 (**T158M**), GM07982 (V247X), GM11270 (**R306C**), RS0502 (**R294X**)	Retroviral for R294X (OCT4, SOX2, KLF4, c-MYC), Lentiviral for reminder (OCT4, SOX2, NANOG, LIN28)	Post XCI	Ananiev *et al*., 2011
Colman	GM17880 (**T158M**), GM11272 (1155del32)	Retroviral (OCT4, SOX2, KLF4, c-MYC)	Post XCI	Pomp *et al*., 2011
Ellis	Exon 3-4 deletion, GM17880 (**T158M**), GM11270 (**R306C**)	Retroviral (OCT4, SOX2, KLF4, c-MYC)	Post XCI	Cheung *et al*., 2011
Muotri	GM17880 (**T158M**), GM11272 (1155del32), GM16548 (Q244X), GM11270 (**R306C**)	Retroviral (OCT4, SOX2, KLF4, c-MYC)	Pre and Post XCI	Marchetto *et al*., 2010
Park	GM17880 (**T158M**), GM16548 (Q244X), GM07928 (E235fs), GM11270 (**R306C**), GM17567 (X487X)	Retroviral (OCT4, SOX2, KLF4, c-MYC)	Pre and Post XCI	Kim *et al*., 2011

Table I. RTT iPSC lines currently available to the RTT research community.

Bold text in table denotes a common RTT causing *MECP2* mutation.

References

Aberg, M. A., Aberg, N. D., Hedbacker, H., Oscarsson, J. & Eriksson, P. S. Peripheral infusion of IGF-I selectively induces neurogenesis in the adult rat hippocampus. *J Neurosci* **20**, 2896-2903 (2000).

Aberg, M. A. *et al*. IGF-I has a direct proliferative effect in adult hippocampal progenitor cells. *Mol Cell Neurosci* **24**, 23-40 (2003).

Aberg, N. D., Brywe, K. G. & Isgaard, J. Aspects of growth hormone and insulin-like growth factor-I related to neuroprotection, regeneration, and functional plasticity in the adult brain. *ScientificWorldJournal* **6**, 53-80 (2006).

Abuhatzira, L., Makedonski, K., Kaufman, Y., Razin, A. & Shemer, R. MeCP2 deficiency in the brain decreases BDNF levels by REST/CoREST-mediated repression and increases TRKB production. *Epigenetics* **2**, 214-222 (2007).

Adachi, M., Autry, A. E., III, H. E. C. & Monteggia, L. M. MeCP2-Mediated Transcription Repression in the Basolateral Amygdala May Underlie Heightened Anxiety in a Mouse Model of Rett Syndrome. doi:10.1523/JNEUROSCI.4225-08.2009 (2009).

Akbarian, S. *et al*. Expression pattern of the Rett syndrome gene MeCP2 in primate prefrontal cortex. *Neurobiol Dis* **8**, 784-791, doi:10.1006/nbdi.2001.0420 (2001).

Allaman, I., Bélanger, M. & Magistretti, P. J. Astrocyte–neuron metabolic relationships: for better and for worse. *Trends in Neurosciences* **34**, 76-87 (2011).

Allen, N. J. *et al*. Astrocyte glypicans 4 and 6 promote formation of excitatory synapses via GluA1 AMPA receptors. *Nature* **486**, 410-414 (2012).

Alvarez-Saavedra, M., Sáez, M. A., Kang, D., Zoghbi, H. Y. & Young, J. I. Cell-specific expression of wild-type MeCP2 in mouse models of Rett syndrome yields insight about pathogenesis. Hum Mol Genet. 19, 2315-25 (2007).

Amir, R. E. *et al*. Rett syndrome is caused by mutations in X-linked MECP2, encoding methyl-CpG-binding protein 2. *Nat Genet* **23**, 185-188 (1999).

Amir, R. E. *et al*. Influence of mutation type and X chromosome inactivation on Rett syndrome phenotypes. *Ann Neurol* **47**, 670-679 (2000).

Ananiev, G., Williams, E. C., Li, H. & Chang, Q. Isogenic pairs of wild type and mutant induced pluripotent stem cell (iPSC) lines from Rett syndrome patients as in vitro disease model. *PLoS One* **6**, e25255 (2011).

Anvret, M., Wahlstrom, J., Skogsberg, P. & Hagberg, B. Segregation analysis of the X-chromosome in a family with Rett syndrome in two generations. *Am J Med Genet* **37**, 31-35 (1990).

Arber, S. & Caroni, P. Thrombospondin-4, an extracellular matrix protein expressed in the developing and adult nervous system promotes neurite outgrowth. *J Cell Biol* **131**, 1083-1094 (1995).

Archidiacono, N. *et al*. Rett syndrome: exclusion mapping following the hypothesis of germinal mosaicism for new X-linked mutations. *Hum Genet* **86**, 604-606 (1991).

Armstrong, D., Dunn, J. K., Antalffy, B. & Trivedi, R. Selective dendritic alterations in the cortex of Rett syndrome. *J Neuropathol Exp Neurol* **54**, 195-201 (1995).

Armstrong, D. D., Dunn, K. & Antalffy, B. Decreased dendritic branching in frontal, motor and limbic cortex in Rett syndrome compared with trisomy 21. *J Neuropathol Exp Neurol* **57**, 1013-1017 (1998).

Baker, A. M. *et al*. Central penetration and stability of N-terminal tripeptide of insulin-like growth factor-I, glycine-proline-glutamate in adult rat. *Neuropeptides* **39**, 81-87, (2005).

Baker, S. A. *et al*. An AT-Hook Domain in MeCP2 Determines the Clinical Course of Rett Syndrome and Related Disorders. *Cell* **152**, 984-996 (2013).

Ballas, N., Lioy, D. T., Grunseich, C. & Mandel, G. in *Nat Neurosci* Vol. 12 311-317 (2009).

Banerjee, A., Castro, J. & Sur, M. Rett syndrome: genes, synapses, circuits, and therapeutics. *Front Psychiatry* **3**, 34 (2012).

Barbeito, L. H. *et al*. A role for astrocytes in motor neuron loss in amyotrophic lateral sclerosis. *Brain Res Brain Res Rev* **47**, 263-274 (2004).

Bauman, M. L., Kemper, T. L. & Arin, D. M. Microscopic observations of the brain in Rett syndrome. *Neuropediatrics* **26**, 105-108 (1995).

Bauman, M. L., Kemper, T. L. & Arin, D. M. Pervasive neuroanatomic abnormalities of the brain in three cases of Rett's syndrome. *Neurology* **45**, 1581-1586 (1995).

Belichenko, N. P., Belichenko, P. V. & Mobley, W. C. in *Neurobiol Dis* Vol. 34 71-77 (2009).

Belichenko, P. V., Oldfors, A., Hagberg, B. & Dahlstrom, A. Rett syndrome: 3-D confocal microscopy of cortical pyramidal dendrites and afferents. *Neuroreport* **5**, 1509-1513 (1994).

Benavides-Piccione, R. *et al*. On dendrites in Down syndrome and DS murine models: a spiny way to learn. *Prog Neurobiol* **74**, 111-126 (2004).

Bhakar, A. L., Dolen, G. & Bear, M. F. The pathophysiology of fragile X (and what it teaches us about synapses). *Annu Rev Neurosci* **35**, 417-443 (2012).

Bickerdike, M. J. *et al*. NNZ-2566: a Gly-Pro-Glu analogue with neuroprotective efficacy in a rat model of. *J Neurol Sci* **278**, 85-90 (2009).

Bird, A. P. & Wolffe, A. P. Methylation-induced repression--belts, braces, and chromatin. *Cell* **99**, 451-454 (1999).

Blue, M. E., Naidu, S. & Johnston, M. V. Development of amino acid receptors in frontal cortex from girls with Rett. *Ann Neurol* **45**, 541-545 (1999).

Bondy, C. A. & Cheng, C. M. Signaling by insulin-like growth factor 1 in brain. *European Journal of Pharmacology* **490**, 25-31 (2004).

Bradford, J. *et al*. Expression of mutant huntingtin in mouse brain astrocytes causes age-dependent neurological symptoms. *Proc Natl Acad Sci U S A* **106**, 22480-22485 (2009).

Brown, V. *et al*. Microarray identification of FMRP-associated brain mRNAs and altered mRNA translational profiles in fragile X syndrome. *Cell* **107**, 477-487 (2001).

Brywe, K. G. *et al*. IGF-I neuroprotection in the immature brain after hypoxia-ischemia, involvement of Akt and GSK3beta? *Eur J Neurosci* **21**, 1489-1502 (2005).

Bushong, E. A., Martone, M. E., Jones, Y. Z. & Ellisman, M. H. Protoplasmic astrocytes in CA1 stratum radiatum occupy separate anatomical domains. *J Neurosci* **22**, 183-192 (2002).

Cajal S, R. y. Un nuevo proceder para la impregnación de la neuroglía. *Bol Soc Esp Biol*, 104-108 (1913).

Calfa, G., Percy, A. K. & Pozzo-Miller, L. Experimental models of Rett syndrome based on Mecp2 dysfunction. *Exp Biol Med* **236** 3-19 (2011).

Chahrour, M. *et al*. MeCP2, a key contributor to neurological disease, activates and represses transcription. *Science* **320**, 1224-1229 (2008).

Chahrour, M. & Zoghbi, H. Y. The Story of Rett Syndrome: From Clinic to Neurobiology. *Neuron* **56**, 422-437 (2007).

Chandler, S., Guschin, D., Landsberger, N., & Wolffe, A. P. The Methyl-CpG Binding Transcriptional Repressor MeCP2 Stably Associates with Nucleosomal DNA. *Biochemistry*. 22, 7008-18 (1999).

Chang, Q., Khare, G., Dani, V., Nelson, S. & Jaenisch, R. The Disease Progression of Mecp2 Mutant Mice Is Affected by the Level of BDNF Expression. *Neuron* **49**, 341-348 (2006).

Chao, H. T. *et al*. Dysfunction in GABA signalling mediates autism-like stereotypies and Rett syndrome phenotypes. *Nature* **468**, 263-269 (2010).

Chapleau, C. A. *et al*. Dendritic spine pathologies in hippocampal pyramidal neurons from Rett syndrome brain and after expression of Rett-associated MECP2 mutations. *Neurobiol Dis* **35**, 219-233 (2009).

Chen, R. Z., Akbarian, S., Tudor, M. & Jaenisch, R. Deficiency of methyl-CpG binding protein-2 in CNS neurons results in a Rett-like phenotype in mice. *Nature Genetics* **27**, 327-331 (2001).

Chen, W. G. *et al*. Derepression of BDNF transcription involves calcium-dependent phosphorylation of MeCP2. *Science* **302**, 885-889 (2003).

Chernausek, S. D., Backeljauw, P. F., Frane, J., Kuntze, J. & Underwood, L. E. Long-term treatment with recombinant insulin-like growth factor (IGF)-I in. *J Clin Endocrinol Metab* **92**, 902-910 (2007).

Cheung, A. Y., Horvath, L. M., Carrel, L. & Ellis, J. X-chromosome inactivation in rett syndrome human induced pluripotent stem cells. *Front Psychiatry* **3**, 24 (2012).

Cheung, A. Y. *et al*. Isolation of MECP2-null Rett Syndrome patient hiPS cells and isogenic controls. *Hum Mol Genet* **20**, 2103-2115 (2011).

Cheval, H. et al. Postnatal inactivation reveals enhanced requirement for MeCP2 at distinct age windows. *Hum Mol Genet* **21**, 3806-3814 (2012).

Christopherson, K. S. *et al*. Thrombospondins are astrocyte-secreted proteins that promote CNS synaptogenesis. *Cell* **120**, 421-433 (2005).

Cleveland, D. W. & Rothstein, J. D. From Charcot to Lou Gehrig: deciphering selective motor neuron death in ALS. *Nat Rev Neurosci* **2**, 806-819 (2001).

Colantuoni C., Jeon O.H., Hyder K., Chenchik A., Khimani A.H., *et al*. Gene expression profiling in postmortem Rett Syndrome brain: differential gene expression and patient classification. *Neurobiol Dis*. **8,** 847–865. (2001)

Collins, A. L. *et al*. Mild overexpression of MeCP2 causes a progressive neurological disorder in mice. *Hum Mol Genet*. **13,** 2679-89 (2004).

Corvin, A. P. et al. Insulin-like growth factor 1 (IGF1) and its active peptide (1-3)IGF1 enhance the expression of synaptic markers in neuronal circuits through different cellular mechanisms. *Neurosci Lett* **520,** 51-56 (2012).

Coy, J. F., Sedlacek, Z., Bachner, D., Delius, H. & Poustka, A. A complex pattern of evolutionary conservation and alternative polyadenylation within the long 3"-untranslated region of the methyl-CpG-binding protein 2 gene (MeCP2) suggests a regulatory role in gene expression. *Hum Mol Genet* **8** 1253-1262 (1999).

Cunha, C., Brambilla, R. & Thomas, K. L. A Simple Role for BDNF in Learning and Memory? *Front Mol Neurosci* **3**, (2010).

D'Ercole, A. J., Ye, P., Calikoglu, A. S. & Gutierrez-Ospina, G. The role of the insulin-like growth factors in the central nervous system. *Mol Neurobiol* **13**, 227-255 (1996).

D'Esposito, M. *et al*. Isolation, physical mapping, and northern analysis of the X-linked human gene encoding methyl CpG-binding protein, MECP2. *Mamm Genome* **7**, 533-535 (1996).

Danbolt, N. C. Glutamate uptake. *Prog Neurobiol* **65**, 1-105 (2001).

Davies, S. & Ramsden, D. B. Huntington's disease. *Mol Pathol* **54**, 409-413 (2001).

De Keyser, J., Mostert, J. P. & Koch, M. W. Dysfunctional astrocytes as key players in the pathogenesis of central nervous system disorders. *J Neurol Sci* **267**, 3-16 (2008).

Dietrich, J. *et al*. EIF2B5 mutations compromise GFAP+ astrocyte generation in vanishing white matter leukodystrophy. *Nat Med* **11**, 277-283 (2005).

Djukic, A. & McDermott, M. V. in *Pediatr Neurol* **46**, 240-242 (2012).

Doble, A. The role of excitotoxicity in neurodegenerative disease: implications for therapy. *Pharmacol Ther* **81**, 163-221 (1999).

Duan, C. Specifying the cellular responses to IGF signals: roles of IGF-binding proteins. *J Endocrinol* **175**, 41-54 (2002).

Ebert, D. H. *et al*. Activity-dependent phosphorylation of MECP2 threonine 308 regulates interaction with NcoR. *Nature* **499**, 341-5 (2013).

Ellaway, C. *et al*. Rett syndrome: randomized controlled trial of L-carnitine. *J Child Neurol* **14**, 162-167 (1999).

Ellaway, C. J., Peat, J., Williams, K., Leonard, H. & Christodoulou, J. Medium-term open label trial of L-carnitine in Rett syndrome. *Brain Dev* **23 Suppl 1**, S85-89 (2001).

Ellison, K. A. *et al*. Examination of X chromosome markers in Rett syndrome: exclusion mapping with a novel variation on multilocus linkage analysis. *Am J Hum Genet* **50**, 278-287 (1992).

Ferguson, T. A. & Scherer, S. S. Neuronal cadherin (NCAD) increases sensory neurite formation and outgrowth on astrocytes. *Neurosci Lett* **522**, 108-112, (2012).

Ferrer, I. & Galofré, E. Dendritic Spine Anomalies in Fetal Alcohol Syndrome. *Neuropediatrics* **18**, 161-163 (2008).

Freeman, M. R. Specification and Morphogenesis of Astrocytes. *Science* **330**, 774-778, (2010).

Fyffe, S. L. *et al*. Deletion of Mecp2 in Sim1-expressing neurons reveals a critical role for MeCP2 in. *Neuron* **59**, 947-958 (2008).

Garcia, O., Torres, M., Helguera, P., Coskun, P. & Busciglio, J. A role for thrombospondin-1 deficits in astrocyte-mediated spine and synaptic pathology in Down's syndrome. *PLoS One* **5**, e14200, doi:10.1371/journal.pone.0014200 (2010).

Garcia-Segura, L. M., Perez, J., Pons, S., Rejas, M. T. & Torres-Aleman, I. Localization of insulin-like growth factor I (IGF-I)-like immunoreactivity in the developing and adult rat brain. *Brain Res* **560**, 167-174 (1991).

Gasparini, L. & Xu, H. Potential roles of insulin and IGF-1 in Alzheimer's disease. *Trends Neurosci* **26**, 404-406 (2003).

Gemelli, T. *et al*. Postnatal loss of methyl-CpG binding protein 2 in the forebrain is sufficient to. *Biol Psychiatry* **59**, 468-476 (2006).

Giacometti, E., Luikenhuis, S., Beard, C. & Jaenisch, R. Partial rescue of MeCP2 deficiency by postnatal activation of MeCP2. *Proc Natl Acad Sci U S A* **104**, 1931-1936 (2007).

Glaze, D. G. *et al*. A study of the treatment of Rett syndrome with folate and betaine. *J Child Neurol* **24**, 551-556 (2009).

Goffin, D. *et al*. Rett syndrome mutation MeCP2 T158A disrupts DNA binding, protein stability and ERP responses Nat Neurosci. **15**, 274-283 (2012).

Goldman, J. E. & Corbin, E. Isolation of a major protein component of Rosenthal fibers. *Am J Pathol* **130**, 569-578 (1988).

Goldstein, A. *et al*., The Elusive Magic Pill: Finding Effective Therapies for Mitochondrial Disorders. *Neurotherapeutics* **10**, 320-328 (2013).

Golgi, C. Suella struttura della sostanza grigia del cervello (comunicazione preventiva). *Gazz. Med. Ital. Lombardia* **33**, 244–246 (1873).

Golgi, C. Das diffuse nervose Netz der Centralorgane des Nervensystems. *Untersuchungen uber den feineren Bau des centralen und peripherischen Nevensystems*, doi:10.1016/j.brainresrev.2010.05.002 (1894).

Gorman, A.L, Elliott, K. J. & Inturrisi, C. E. The d- and l- isomers of methadone bind to the non-competitive site on the N-methyl-d-aspartate (NMDA) receptor in rat forebrain and spinal cord. *Neuroscience Letters* **223**, 5-8 (1997).

Greenberg, M. E., Xu, B., Lu, B. & Hempstead, B. L. New insights in the biology of BDNF synthesis and release: implications in CNS function. *J Neurosci* **29**, 12764-12767, (2009).

Greenough, W. T. *et al*. Synaptic regulation of protein synthesis and the fragile X protein. *Proc Natl Acad Sci U S A* **98**, 7101-7106 (2001).

Group, H. s. D. C. R. A novel gene containing a trinucleotide repeat that is expanded and unstable on Huntington's disease chromosomes. The Huntington's Disease Collaborative Research Group. *Cell* **72**, 971-983 (1993).

Guan, J. & Gluckman, P. D. IGF-1 derived small neuropeptides and analogues: a novel strategy for the development of pharmaceuticals for neurological conditions. *Br J Pharmacol* **157**, 881-891 (2009).

Guy, J., Hendrich, B., Holmes, M., Martin, J. E. & Bird, A. A mouse Mecp2-null mutation causes neurological symptoms that mimic Rett syndrome. *Nature Genetics* **27**, 322-326 (2001).

Guy, J., Gan, J., Selfridge, J., Cobb, S. & Bird, A. Reversal of Neurological Defects in a Mouse Model of Rett Syndrome. *Science*.1138389 (2007).

Hagberg, B. Clinical manifestations and stages of Rett syndrome. *Ment Retard Dev Disabil Res Rev* **8**, 61-65 (2002).

Hagberg, B., Aicardi, J., Dias, K. & Ramos, O. A progressive syndrome of autism, dementia, ataxia, and loss of purposeful hand use in girls: Rett's syndrome: report of 35 cases. *Ann Neurol* **14**, 471-479 (1983).

Halassa, M. M., Fellin, T., Takano, H., Dong, J. H. & Haydon, P. G. Synaptic islands defined by the territory of a single astrocyte. *J Neurosci* **27**, 6473-6477 (2007).

Harris, Z. L. *et al*. Aceruloplasminemia: molecular characterization of this disorder of iron metabolism. *Proc Natl Acad Sci U S A* **92**, 2539-2543 (1995).

Holroyd, S. & Shepherd, M. L. Alzheimer's disease: a review for the ophthalmologist. *Surv Ophthalmol* **45**, 516-524 (2001).

Hotta, A. *et al*. Isolation of human iPS cells using EOS lentiviral vectors to select for. *Nat Methods* **6**, 370-376 (2009).

Humbert, S. *et al*. The IGF-1/Akt pathway is neuroprotective in Huntington's disease and involves Huntingtin phosphorylation by Akt. *Dev Cell* **2**, 831-837 (2002).

Iadecola, C. & Nedergaard, M. Glial regulation of the cerebral microvasculature. *Nat Neurosci* **10**, 1369-1376 (2007).

Ilieva, H., Polymenidou, M. & Cleveland, D. W. Non-cell autonomous toxicity in neurodegenerative disorders: ALS and beyond. *J Cell Biol* **187**, 761-772 (2009).

Irwin, S. A., Galvez, R. & Greenough, W. T. Dendritic Spine Structural Anomalies in Fragile-X Mental Retardation Syndrome. *Cereb Cortex* **10,** 1038-44 (2000).

Itoh, M. *et al*. Methyl CpG-binding Protein Isoform MeCP2_e2 Is Dispensable for Rett Syndrome Phenotypes but Essential for Embryo Viability and Placenta Development. *J Biol Chem* **287**, 13859-67 (2012).

Iwaki, T., Iwaki, A., Tateishi, J., Sakaki, Y. & Goldman, J. E. Alpha B-crystallin and 27-kd heat shock protein are regulated by stress conditions in the central nervous system and accumulate in Rosenthal fibers. *Am J Pathol* **143**, 487-495 (1993).

Jacobs, S. & Doering, L. C. Astrocytes prevent abnormal neuronal development in the fragile x mouse. *J Neurosci* **30**, 4508-4514 (2010).

Jang, S.-W. *et al*. A selective TrkB agonist with potent neurotrophic activities by 7,8-dihydroxyflavone. *Proceedings of the National Academy of Sciences* **107**, 2687-92 (2010).

Jellinger, K., Armstrong, D., Zoghbi, H. Y. & Percy, A. K. Neuropathology of Rett syndrome. *Acta Neuropathol* **76**, 142-158 (1988).

Jentarra, G. M. et al. Abnormalities of cell packing density and dendritic complexity in the MeCP2 A140V mouse model of Rett syndrome/X-linked mental retardation. *BMC Neurosci* **11** 19 (2010).

Johnson, R. A. *et al*. 7,8-dihydroxyflavone exhibits therapeutic efficacy in a mouse model of Rett syndrome. *J Appl Physiol* (2012).

Jones, P. L. *et al*. Methylated DNA and MeCP2 recruit histone deacetylase to repress transcription. *Nat Genet* **19**, 187-191 (1998).

Jordan, C., Li, H. H., Kwan, H. C. & Francke, U. Cerebellar gene expression profiles of mouse models for Rett syndrome reveal novel MeCP2 targets. *BMC Medical Genetics* **8**, 36 (2007).

Jugloff, D. G. *et al*. Targeted delivery of an Mecp2 transgene to forebrain neurons improves the. *Hum Mol Genet* **17**, 1386-1396 (2008).

Kacem, K., Lacombe, P., Seylaz, J. & Bonvento, G. Structural organization of the perivascular astrocyte endfeet and their relationship with the endothelial glucose transporter: a confocal microscopy study. *Glia* **23**, 1-10 (1998).

Katz, D. M. *et al*. Preclinical research in Rett syndrome: setting the foundation for translational. *Dis Model Mech* **5**, 733-745 (2012).

Kerr, A. M., Armstrong, D. D., Prescott, R. J., Doyle, D. & Kearney, D. L. Rett syndrome: analysis of deaths in the British survey. *Eur Child Adolesc Psychiatry* **6 Suppl 1**, 71-74 (1997).

Kimelberg, H. K. Receptors on astrocytes--what possible functions? *Neurochem Int* **26**, 27-40 (1995).

Kishi, N. & Macklis, J. D. MECP2 is progressively expressed in post-migratory neurons and is involved in neuronal maturation rather than cell fate decisions. *Mol Cell Neurosci* **27**, 306-321 (2004).

Kishi, N. & Macklis, J. D. Dissecting MECP2 function in the central nervous system. *Exp Neurol* **222**, 51-58 (2010).

Klose, R. J. *et al*. DNA binding selectivity of MeCP2 due to a requirement for A/T sequences adjacent to methyl-CpG. *Mol Cell* **19**, 667-678 (2005).

Kortum, F. *et al*. The core FOXG1 syndrome phenotype consists of postnatal microcephaly, severe mental retardation, absent language, dyskinesia, and corpus callosum hypogenesis *J Med Genet* **48**, 396-406 (2011).

Kriaucionis, S. & Bird, A. The major form of MeCP2 has a novel N-terminus generated by alternative splicing. *Nucleic Acids Res* **32**, 1818-1823 (2004).

Kim, K.-Y., Hysolli, E. & Park, I.-H. Neuronal maturation defect in induced pluripotent stem cells from patients with Rett syndrome. *Proc Natl Acad Sci U S A*. **108**, 14169-74 (2011).

Krencik, R. & Zhang, S.-C. Directed differentiation of functional astroglial subtypes from human pluripotent stem cells. *Nature Protocols* **6**, 1710-1717 (2011).

Landriscina, M. *et al*. S100A13, a new marker of angiogenesis in human astrocytic gliomas. *J Neurooncol* **80**, 251-259 (2006).

Laurino, L. *et al*. PI3K activation by IGF-1 is essential for the regulation of membrane expansion at the nerve growth cone. *J Cell Sci* **118**, 3653-3662 (2005).

Lawson-Yuen, A. et al. Ube3a mRNA and protein expression are not decreased in Mecp2R168X mutant mice *Brain Res* 1180, 1-6 (2007).

Le Guen, T. *et al*. A FOXG1 mutation in a boy with congenital variant of Rett syndrome. *Neurogenetics* **12**, 1-8 (2011).

Lee, A. *et al*. Control of dendritic development by the Drosophila fragile X-related gene involves the small GTPase Rac1. *Development* **130**, 5543-5552 (2003).

Lee, K. H., Calikoglu, A. S., Ye, P. & D'Ercole, A. J. Insulin-like growth factor-I (IGF-I) ameliorates and IGF binding protein-1 (IGFBP-1) exacerbates the effects of undernutrition on brain growth during early postnatal life: studies in IGF-I and IGFBP-1 transgenic mice. *Pediatr Res* **45**, 331-336 (1999).

Leegwater, P. A. *et al*. Subunits of the translation initiation factor eIF2B are mutant in leukoencephalopathy with vanishing white matter. *Nat Genet* **29**, 383-388 (2001).

Lenhossek, M. V. Zur Kenntnis der Neuroglia des menschlichen Ruckenmarkes. *Verh. Anat. Ges.*, 193–221 (1891).

Lennon, V. A., Kryzer, T. J., Pittock, S. J., Verkman, A. S. & Hinson, S. R. IgG marker of optic-spinal multiple sclerosis binds to the aquaporin-4 water channel. *J Exp Med* **202**, 473-477 (2005).

Li, R., Messing, A., Goldman, J. E. & Brenner, M. GFAP mutations in Alexander disease. *Int J Dev Neurosci* **20**, 259-268 (2002).

Liberto, C. M., Albrecht, P. J., Herx, L. M., Yong, V. W. & Levison, S. W. Pro-regenerative properties of cytokine-activated astrocytes. *J Neurochem* **89**, 1092-1100 (2004).

Lioy, D. T. *et al*. A role for glia in the progression of Rett's syndrome. *Nature* **475**, 497-500 (2011).

Lopez-Lopez, C., LeRoith, D. & Torres-Aleman, I. Insulin-like growth factor I is required for vessel remodeling in the adult brain. *Proc Natl Acad Sci U S A* **101**, 9833-9838 (2004).

Lu, J. *et al*. S100B and APP promote a gliocentric shift and impaired neurogenesis in Down syndrome neural progenitors. *PLoS One* **6**, e22126 (2011).

Luikenhuis, S., Giacometti, E., Beard, C. F. & Jaenisch, R. Expression of MeCP2 in postmitotic neurons rescues Rett syndrome in mice. *Proc Natl Acad Sci U S A* **101,** 6033-8 (2004).

Maezawa, I., Swanberg, S., Harvey, D., LaSalle, J. M. & Jin, L. W. in *J Neurosci* Vol. 29 5051-5061 (2009).

Lyst, M. J. *et al*. Rett syndrome mutations abolish the interaction of MeCP2 with the NCoR/SMRT co-repressor. *Nat Neurosci* **16**, 898-902 (2013).

Maezawa, I. & Jin, L.-W. Rett Syndrome Microglia Damage Dendrites and Synapses by the Elevated Release of Glutamate. *J Neurosci* **30**, 5346-56 (2010).

Mari, F. *et al*. Germline mosaicism in Rett syndrome identified by prenatal diagnosis. *Clin Genet* **67**, 258-260 (2005).

Marchetto, M. C. N. *et al*. A Model for Neural Development and Treatment of Rett Syndrome Using Human Induced Pluripotent Stem Cells. *Cell* **143**, 527-539 (2010).

Marignier, R. *et al*. Oligodendrocytes are damaged by neuromyelitis optica immunoglobulin G via astrocyte injury. *Brain* **133**, 2578-2591 (2010).

Marin-Padilla, M. Structural abnormalities of the cerebral cortex in human chromosomal aberrations: a Golgi study. *Brain Res* **44** 625-629 (1972).

Markiewicz, I. & Lukomska, B. The role of astrocytes in the physiology and pathology of the central nervous system. *Acta Neurobiol Exp (Wars)* **66**, 343-358 (2006).

Martinez-Hernandez, A., Bell, K. P. & Norenberg, M. D. Glutamine synthetase: glial localization in brain. *Science* **195**, 1356-1358 (1977).

McCaslin, A. F., Chen, B. R., Radosevich, A. J., Cauli, B. & Hillman, E. M. In vivo 3D morphology of astrocyte-vasculature interactions in the somatosensory cortex: implications for neurovascular coupling. *J Cereb Blood Flow Metab* **31**, 795-806 (2011).

McGraw, C. M., Samaco, R. C. & Zoghbi, H. Y. Adult Neural Function Requires MeCP2. *Science* **333**, 6039 (2011).

McKeon, R. J., Schreiber, R. C., Rudge, J. S. & Silver, J. Reduction of neurite outgrowth in a model of glial scarring following CNS injury is correlated with the expression of inhibitory molecules on reactive astrocytes. *J Neurosci* **11**, 3398-3411 (1991).

Messing, A., Brenner, M., Feany, M. B., Nedergaard, M. & Goldman, J. E. Alexander disease. *J Neurosci* **32**, 5017-5023 (2012).

Messing, A. *et al*. Fatal encephalopathy with astrocyte inclusions in GFAP transgenic mice. *Am J Pathol* **152**, 391-398 (1998).

Miyajima, H. Aceruloplasminemia, an iron metabolic disorder. *Neuropathology* **23**, 345-350 (2003).

Mnatzakanian, G. N. *et al*. A previously unidentified MECP2 open reading frame defines a new protein isoform relevant to Rett syndrome. *Nature Genetics* **36**, 339-341 (2004).

Murer, M. G., Yan, Q. & Raisman-Vozari, R. Brain-derived neurotrophic factor in the control human brain, and in Alzheimer's disease and Parkinson's disease. *Prog Neurobiol* **63**, 71-124 (2001).

Nagatsu, T., Mogi, M., Ichinose, H. & Togari, A. Changes in cytokines and neurotrophins in Parkinson's disease. *J Neural Transm Suppl*, 277-290 (2000).

Nan, X., Meehan, R. R. & Bird, A. Dissection of the methyl-CpG binding domain from the chromosomal protein MeCP2. *Nucleic Acids Res* **21**, 4886-4892 (1993).

Nan, X., Campoy, F. J. & Bird, A. MeCP2 is a transcriptional repressor with abundant binding sites in genomic chromatin. *Cell* **88,** 471-481 (1997).

Nan, X., Tate, P., Li, E. & Bird, A. DNA methylation specifies chromosomal localization of MeCP2. *Mol Cell Biol* **16** 414-421 (1996).

Neugebauer, K. M., Tomaselli, K. J., Lilien, J. & Reichardt, L. F. N-cadherin, NCAM, and integrins promote retinal neurite outgrowth on astrocytes in vitro. *J Cell Biol* **107**, 1177-1187 (1988).

Neul, J. L. & Zoghbi, H. Y. Rett syndrome: a prototypical neurodevelopmental disorder. *Neuroscientist* **10**, 118-128 (2004).

Neul, J. L. *et al*. Specific mutations in Methyl-CpG-Binding Protein 2 confer different severity in Rett syndrome. **16**, 1313-21 (2008).

Nguyen, M. V. *et al*. MeCP2 is critical for maintaining mature neuronal networks and global brain anatomy during late stages of postnatal brain development and in the mature adult brain *J Neurosci* **32,** 10021-10034 (2012).

Niblock, M. M., Brunso-Bechtold, J. K. & Riddle, D. R. Insulin-like growth factor I stimulates dendritic growth in primary somatosensory cortex. *J Neurosci* **20**, 4165-4176 (2000).

Nilsson-Hakansson, L. *et al*. Effects of IGF-1, truncated IGF-1 and the tripeptide Gly-Pro-Glu on acetylcholine release from parietal cortex of rat brain. *Neuroreport* **4**, 1111-1114 (1993).

Nishijima, T. *et al*. Neuronal activity drives localized blood-brain-barrier transport of serum insulin-like growth factor-I into the CNS. *Neuron* **67**, 834-846 (2010).

Nuber, U. A. *et al*. Up-regulation of glucocorticoid-regulated genes in a mouse model of Rett syndrome. *Hum Mol Genet* **14**, 2247-2256 (2005).

Obata, K. *et al*. Mutation analysis of the methyl-CpG binding protein 2 gene (MECP2) in patients with Rett syndrome. *J Med Genet* **37**, 608-610 (2000).

Pacey, L. K. & Doering, L. C. Developmental expression of FMRP in the astrocyte lineage: implications for fragile X syndrome. *Glia* **55**, 1601-1609 (2007).

Pan, W. & Kastin, A. J. Interactions of IGF-1 with the blood-brain barrier in vivo and in situ. *Neuroendocrinology* **72**, 171-178 (2000).

Pang, Y., Zheng, B., Fan, L. W., Rhodes, P. G. & Cai, Z. IGF-1 protects oligodendrocyte progenitors against TNFalpha-induced damage by activation of PI3K/Akt and interruption of the mitochondrial apoptotic pathway. *Glia* **55**, 1099-1107 (2007).

Pardridge, W. M., Wu, D. & Sakane, T. Combined use of carboxyl-directed protein pegylation and vector-mediated blood-brain barrier drug delivery system optimizes brain uptake of brain-derived neurotrophic factor following intravenous administration. *Pharm Res* **15**, 576-582 (1998).

Park, W. D. *et al*. Identification of 58 novel mutations in Niemann-Pick disease type C: correlation with biochemical phenotype and importance of PTC1-like domains in NPC1. *Hum Mutat* **22**, 313-325 (2003).

Patel, S. C. *et al*. Localization of Niemann-Pick C1 protein in astrocytes: implications for neuronal degeneration in Niemann- Pick type C disease. *Proc Natl Acad Sci U S A* **96**, 1657-1662 (1999).

Pelka, G. J. *et al*. Mecp2 deficiency is associated with learning and cognitive deficits and altered gene activity in the hippocampal region of mice *Brain* **129**, 887-898 (2006).

Pellerin, L. & Magistretti, P. J. Glutamate uptake into astrocytes stimulates aerobic glycolysis: a mechanism coupling neuronal activity to glucose utilization. *Proceedings of the National Academy of Sciences* **91**, 10625-10629 (1994).

Percy, A. K. *et al*. Rett syndrome: controlled study of an oral opiate antagonist, naltrexone. *Ann Neurol* **35**, 464-470 (1994).

Pfrieger, F. W. & Barres, B. A. Synaptic efficacy enhanced by glial cells in vitro. *Science* **277**, 1684-1687 (1997).

Pitcher, M. R. *et al*. Insulinotropic treatments exacerbate metabolic syndrome in mice lacking MeCP2 function. *Hum Mol Genet* **22**, 2626-2633 (2013).

Pogacar, S., Nora, N. F. & Kemper, T. L. Neuropathological findings in the rubinstein-taybi syndrome. *R I Med J* **56**, 114-121 (1973).

Pomp, O. *et al*. Unexpected X chromosome skewing during culture and reprogramming of human somatic cells can be alleviated by exogenous telomerase. *Cell Stem Cell* **9**, 156-165 (2011).

Pruunsild, P., Kazantseva, A., Aid, T., Palm, K. & Timmusk, T. Dissecting the human BDNF locus: bidirectional transcription, complex splicing, and multiple promoters. *Genomics* **90**, 397-406 (2007).

Purpura, D. P. Dendritic Spine "Dysgenesis" and Mental Retardation. *Science* **186**, 1126-1128 (1974).

Quaderi, N. A. *et al*. Genetic and physical mapping of a gene encoding a methyl CpG binding protein, Mecp2, to the mouse X chromosome. *Genomics* **22**, 648-651 (1994).

Rao, S. D., Yin, H. Z. & Weiss, J. H. Disruption of glial glutamate transport by reactive oxygen species produced in motor neurons. *J Neurosci* **23**, 2627-2633 (2003).

Regan, M. R. *et al*. Variations in promoter activity reveal a differential expression and physiology of glutamate transporters by glia in the developing and mature CNS. *J Neurosci* **27**, 6607-6619 (2007).

Reichardt, L. F. Neurotrophin-regulated signalling pathways. *Philos Trans R Soc Lond B Biol Sci* **361**, 1545-1564 (2006).

Reichwald, K. *et al*. Comparative sequence analysis of the MECP2-locus in human and mouse reveals new transcribed regions. *Mamm Genome* **11**, 182-190 (2000).

Reinhardt, R. R. & Bondy, C. A. Insulin-like growth factors cross the blood-brain barrier. *Endocrinology* **135**, 1753-1761 (1994).

Reiss, A. L. *et al*. Neuroanatomy of Rett syndrome: a volumetric imaging study. *Ann Neurol* **34**, 227-234 (1993).

Robinson, L. *et al*. Morphological and functional reversal of phenotypes in a mouse model of Rett. *Brain* **135** (2012).

Rose, E. M. *et al*. Glutamate transporter coupling to Na,K-ATPase. *J Neurosci* **29**, 8143-8155, (2009).

Roux, J. C., Dura, E., Moncla, A., Mancini, J. & Villard, L. Treatment with desipramine improves breathing and survival in a mouse model for Rett syndrome. *Eur J Neurosci* **25**, 1915-1922 (2007).

Schwartzman, J.S. *et al*. Rett syndrome in a boy with a 47,XXY karyotype confirmed by a rare mutation in the MECP2 gene *Am J Hum Genet* **64**, 1781-1785 (1999).

Schwartzman, J. S., Bernardino, A., Nishimura, A., Gomes, R. R. & Zatz, M. Rett syndrome in a boy with a 47,XXY karyotype confirmed by a rare mutation in the MECP2 gene. *Neuropediatrics* **32**, 162-164 (2001).

Samaco, R. C. *et al*. Loss of MeCP2 in aminergic neurons causes cell-autonomous defects in neurotransmitter synthesis and specific behavioral abnormalities. *Proc Natl Acad Sci U S A* **106**, 21966-21971 (2009).

Samaco, R. C., Nagarajan, R. P., Braunschweig, D. & LaSalle, J. M. Multiple pathways regulate MeCP2 expression in normal brain development and exhibit defects in autism-spectrum disorders. *Hum Mol Genet* **13**, 629-639 (2004).

Samaco, R. C. & Neul, J. L. Complexities of Rett syndrome and MeCP2. *J Neurosci* **31**, 7951-7959 (2011).

Santoro, M. R., Bray, S. M. & Warren, S. T. Molecular mechanisms of fragile X syndrome: a twenty-year perspective. *Annu Rev Pathol* **7**, 219-245 (2012).

Saura, J. *et al*. Neuroprotective effects of Gly-Pro-Glu, the N-terminal tripeptide of IGF-1, in the hippocampus in vitro. *Neuroreport* **10**, 161-164 (1999).

Scala, E. *et al*. CDKL5/STK9 is mutated in Rett syndrome variant with infantile spasms *J Med Genet* **42**, 103-107 (2005).

Schapira, A. H. & Jenner, P. Etiology and pathogenesis of Parkinson's disease. *Mov Disord* **26**, 1049-1055 (2011).

Schipper, H. M. Astrocytes, brain aging, and neurodegeneration. *Neurobiol Aging* **17**, 467-480 (1996).

Schools, G. P. & Kimelberg, H. K. mGluR3 and mGluR5 are the predominant metabotropic glutamate receptor mRNAs expressed in hippocampal astrocytes acutely isolated from young rats. *J Neurosci Res* **58**, 533-543 (1999).

Schwartzman, J. S., Bernardino, A., Nishimura, A., Gomes, R. R. & Zatz, M. Rett syndrome in a boy with a 47,XXY karyotype confirmed by a rare mutation in the MECP2 gene. *Neuropediatrics* **32**, 162-164 (2001).

Scott, H. L., Pow, D. V., Tannenberg, A. E. & Dodd, P. R. Aberrant expression of the glutamate transporter excitatory amino acid transporter 1 (EAAT1) in Alzheimer's disease *J Neurosci* **22**, RC206 (2002).

Shinar, Y. & McMorris, F. A. Developing oligodendroglia express mRNA for insulin-like growth factor-I, a regulator of oligodendrocyte development. *J Neurosci Res* **42**, 516-527 (1995).

Sierra, C. *et al*. Oxidative stress in Rett syndrome. *Brain Dev* **23 Suppl 1**, S236-239 (2001).

Singh, J., Saxena, A., Christodoulou, J. & Ravine, D. MECP2 genomic structure and function: insights from ENCODE. Nucleic Acids Res **19**, 6035–6047 (2008).

Sirianni, N., Naidu, S., Pereira, J., Pillotto, R. F. & Hoffman, E. P. in *Am J Hum Genet* **63**, 1552-1558 (1998).

Sjogren, K., Jansson, J. O., Isaksson, O. G. & Ohlsson, C. A transgenic model to determine the physiological role of liver-derived insulin-like growth factor I. *Minerva Endocrinol* **27**, 299-311 (2002).

Smrt, R. D. *et al*. Mecp2 deficiency leads to delayed maturation and altered gene expression in hippocampal neurons. *Neurobiol Dis* **27**, 77-89 (2007).

Stobart, J. L. & Anderson, C. M. Multifunctional role of astrocytes as gatekeepers of neuronal energy supply. *Front Cell Neurosci* **7**, 38 (2013).

Strong, M. J. The basic aspects of therapeutics in amyotrophic lateral sclerosis. *Pharmacol Ther* **98**, 379-414 (2003).

Takahashi, K. *et al*. Induction of pluripotent stem cells from adult human fibroblasts by defined factors. *Cell* **131**, 861-872 (2007).

Takano, T. *et al*. Astrocyte-mediated control of cerebral blood flow. *Nat Neurosci* **9**, 260-267 (2006).

Taneja, P. *et al*. Pathophysiology of locus ceruleus neurons in a mouse model of Rett syndrome. *J Neurosci* **29**, 12187-12195 (2009).

Tchieu, J. *et al*. Female human iPSCs retain an inactive X chromosome. *Cell Stem Cell* **7**, 329-342 (2010).

Tian, R. *et al*. Alexander Disease Mutant Glial Fibrillary Acidic Protein Compromises Glutamate Transport in Astrocytes. *J Neuropathol Exp Neurol* **69**, 335-345 (2010).

Trejo, J. L. *et al*. Central actions of liver-derived insulin-like growth factor I underlying its pro-cognitive effects. *Mol Psychiatry* **12**, 1118-1128 (2007).

Tropea, D. *et al*. Partial reversal of Rett Syndrome-like symptoms in MeCP2 mutant mice. *Proc Natl Acad Sci U S A* **106**, 2029-34 (2009).

Tsacopoulos, M. & Magistretti, P. J. Metabolic coupling between glia and neurons. *J Neurosci* **16**, 877-885 (1996).

Tudor, M., Akbarian, S., Chen, R. Z. & Jaenisch, R. Transcriptional profiling of a mouse model for Rett syndrome reveals subtle transcriptional changes in the brain. *Proc Natl Acad Sci U S A* **99**, 15536-15541 (2002).

Tuppo, E. E. & Arias, H. R. The role of inflammation in Alzheimer's disease. *Int J Biochem Cell Biol* **37**, 289-305 (2005).

Ullian, E. M., Sapperstein, S. K., Christopherson, K. S. & Barres, B. A. Control of synapse number by glia. *Science* **291**, 657-661 (2001).

Ullian, E. M., Harris, B. T., Wu, A., Chan, J. R. & Barres, B. A. Schwann cells and astrocytes induce synapse formation by spinal motor neurons in culture. *Mol Cell Neurosci* **25**, 241-251 (2004).

Van der Aa, N. *et al*. Analysis of FOXG1 Is Highly Recommended in Male and Female Patients with Rett Syndrome. *Mol Syndromol* **1**, 290-293 (2011).

Van Esch, H. *et al*. Duplication of the MECP2 region is a frequent cause of severe mental retardation and progressive neurological symptoms in males. *Am J Hum Genet* **77**, 442-453 (2005).

van Kollenburg, B. *et al*. Glia-specific activation of all pathways of the unfolded protein response in vanishing white matter disease. *J Neuropathol Exp Neurol* **65**, 707-715 (2006).

Virchow, R. Gesammelte Abbildung zur wissenschaftlichen Medizin. *Verlag von Meidinger Sohn & Comp* (1856).

Wang, J. *et al*. Targeted overexpression of IGF-I evokes distinct patterns of organ remodeling in smooth muscle cell tissue beds of transgenic mice. *J Clin Invest* **100**, 1425-1439 (1997).

Weaving, L. S. *et al*. Mutations of CDKL5 cause a severe neurodevelopmental disorder with infantile spasms and mental retardation *Am J Hum Genet* **75**, 1079-1093 (2004).

Weaving, L. S., Ellaway, C. J., Gecz, J. & Christodoulou, J. Rett syndrome: clinical review and genetic update. *J Med Genet* **42**, 1-7 (2005).

Williams, R. S., Hauser, S. L., Purpura, D. P., DeLong, G. R. & Swisher, C. N. Autism and Mental Retardation: Neuropathologic Studies Performed in Four Retarded Persons With Autistic Behavior. *Archives of Neurology* **37**, 749-753 (1980).

Williamson, S. L. & Christodoulou, J. Rett syndrome: new clinical and molecular insights. *European Journal of Human Genetics* **14**, 896-903 (2006).

Xiang, F. *et al*. Chromosome mapping of Rett syndrome: a likely candidate region on the telomere of Xq. *J Med Genet* **35**, 297-300 (1998).

Yadav, A., Kalita, A., Dhillon, S. & Banerjee, K. JAK/STAT3 pathway is involved in survival of neurons in response to insulin-like growth factor and negatively regulated by suppressor of cytokine signaling-3. *J Biol Chem* **280**, 31830-31840 (2005).

Yakar, S. *et al*. Circulating levels of IGF-1 directly regulate bone growth and density. *J Clin Invest* **110**, 771-781 (2002).

Yamamoto, H. & Murphy, L. J. Generation of des-(1-3) insulin-like growth factor-I in serum by an acid protease. *Endocrinology* **135**, 2432-2439 (1994).

Yamamoto, H. & Murphy, L. J. Enzymatic conversion of IGF-I to des(1-3)IGF-I in rat serum and tissues: a further potential site of growth hormone regulation of IGF-I action. *J Endocrinol* **146**, 141-148 (1995).

Yang, Q. *et al*. Excessive astrocyte-derived neurotrophin-3 contributes to the abnormal neuronal dendritic development in a mouse model of fragile X syndrome. *PLoS Genet* **8**, e1003172 (2012).

Young, J. I. *et al*. Regulation of RNA splicing by the methylation-dependent transcriptional repressor methyl-CpG binding protein 2 *Proc Natl Acad Sci U S A* **102**, 17551-17558 (2005).

Yu, J. *et al*. Induced pluripotent stem cell lines derived from human somatic cells. *Science* **318**, 1917-1920 (2007).

Yu, W. *et al*. Altered cholesterol metabolism in Niemann-Pick type C1 mouse brains affects mitochondrial function. *J Biol Chem* **280**, 11731-11739 (2005).

Zanella, S. *et al*. Oral treatment with desipramine improves breathing and life span in Rett syndrome mouse model. *Respir Physiol Neurobiol* **160**, 116-121 (2008).

Zhao, H., Sapolsky, R. M. & Steinberg, G. K. Phosphoinositide-3-kinase/akt survival signal pathways are implicated in neuronal survival after stroke. *Mol Neurobiol* **34**, 249-270 (2006).

Zhou, Z. *et al*. Brain-specific phosphorylation of MeCP2 regulates activity-dependent Bdnf transcription, dendritic growth, and spine maturation. *Neuron* **52**, 255-269 (2006).

Chapter I

Isogenic Pairs of Wild Type and Mutant Induced Pluripotent Stem Cell (iPSC) Lines from Rett Syndrome Patients as *In Vitro* Disease Model

Abstract

Rett syndrome (RTT) is an autism spectrum developmental disorder caused by mutations in the X-linked methyl-CpG binding protein 2 (*MECP2*) gene. Excellent RTT mouse models have been created to study the disease mechanisms, leading to many important findings with potential therapeutic implications. These include the identification of many MeCP2 target genes, better understanding of the neurobiological consequences of the loss- or mis-function of MeCP2, and drug testing in RTT mice and clinical trials in human RTT patients. However, because of potential differences in the underlying biology between humans and common research animals, there is a need to establish cell culture-based human models for studying disease mechanisms to validate and expand the knowledge acquired in animal models. Taking advantage of the nonrandom pattern of X chromosome inactivation in female induced pluripotent stem cells (iPSC), we have generated isogenic pairs of wild type and mutant iPSC lines from several female RTT patients with common and rare RTT mutations. R294X (arginine 294 to stop codon) is a common mutation carried by 5–6% of RTT patients. iPSCs carrying the R294X mutation has not been studied. We differentiated three R294X iPSC lines and their isogenic wild type control iPSC into neurons with high efficiency and consistency, and observed characteristic RTT pathology in R294X neurons. These isogenic iPSC lines provide unique resources to the RTT research community for studying disease pathology, screening for novel drugs, and testing toxicology.

Introduction

Rett syndrome (RTT) is a debilitating autism spectrum developmental disorder that predominantly affects females (Hagberg 1985, Hagberg and Hagberg 1997). RTT patients often experience normal development for the first 6–18 months of their lives, which is followed by a rapid developmental regression between the ages of 1 to 3 years. Major symptoms of RTT include reduced head growth, social withdrawal, loss of previously acquired skills including purposeful hand use and expressive language, gait ataxia, stereotypic movement of the hands, and autonomic dysfunctions such as respiratory distress (Chahrour and Zoghbi 2007). At an estimated prevalence of 1 in 10,000–15,000 girls, RTT is the second most common cause of X-linked mental retardation (XLMR).

Mutations in the X-linked methyl-CpG binding protein 2 (*MECP2*) gene were identified to account for almost all of the classic RTT cases (Amir *et al.,* 1999, van den Veyver and Zoghbi 2000, Wan *et al*., 1999, Xiang *et al*., 2000). MeCP2 is involved in modulating chromatin structure and gene transcription through its binding to methylated DNA (Bird and Wolffe 1999). To study RTT disease mechanisms, mouse models have been generated by engineering *Mecp2* gene deletions (Chen *et al*., 2001, Guy *et al*., 2001, Shahbazian *et al*., 2002). Male mutant mice that lack either the entire *Mecp2* gene (Guy *et al*., 2001) or the essential methyl-DNA binding domain (Chen *et al*., 2001) develop normally until 5 weeks of age when RTT-like symptoms are first observed, including reduced brain weight, hindlimb clasping and impaired locomotor function. These mice later develop respiratory abnormalities (Katz *et al*., 2009) and die prematurely around 8–

10 weeks of age. Female mutant mice heterozygous for these deletions also display RTT-like symptoms, yet the onset is typically much later than in their male counterparts. At the cellular level, the most noticeable pathologies in these mice are the decrease in the size of neuronal nuclei (Chen *et al*., 2001) and the reduced complexity of neuronal dendritic arborization (Kishi and Macklis 2004, Jugloff *et al*., 2005, Belichenko *et al*., 2008, Belichenko *et al*., 2009), which are also observed in human autopsy samples (Armstrong *et al*., 1995).

Although they have been extremely useful in studying the molecular mechanism of RTT, mouse models may have limitations in mimicking human RTT mutations and in drug screening. To date, almost all the available RTT mouse models are loss-of-function alleles that either lacks the whole gene or harbors large deletions in the *Mecp2* gene (Chen *et al*., 2001, Guy *et al*., 2001, Shahbazian *et al*., 2002). In contrast, many human RTT patients carry missense mutations in the *MECP2* gene. Moreover, 92% of new drugs that pass preclinical tests, including tests on animals, fail to reach the market either because of safety or efficacy failures (US FDA: Report on Challenge and Opportunity on the Critical Path to New Medical Products, March 2004). This highlights the potential differences in the underlying biology between humans and common research animals. Therefore there is a need to establish cell culture-based human models for studying disease mechanisms to validate and expand the knowledge gained from animal models.

Groundbreaking work from the Yamanaka group showed that it is feasible to generate induced pluripotent stem cells (iPSC) from mouse embryonic fibroblasts (Takahashi and Yamanaka 2006) and human fibroblasts (Takahashi *et al*., 2007) by

retrovirus mediated expression of four key stem cell transcription factors: OCT4, SOX2, c-Myc, and KLF4. The Thomson group independently demonstrated that iPSCs could be generated from human adult fibroblasts (Yu *et al*., 2007) by lentivirus mediated expression of overlapping but different combination of stem cell factors: OCT4, SOX2, NANOG, and LIN28. These early studies have established the iPSC technology as a novel tool to model human diseases and screen for drugs. Since then, patient-specific iPSCs have been successfully generated for several diseases (Dimos *et al*., 2008, Park *et al*., 2008, Ebert *et al*., 2009, Soldner *et al*., 2009), including Rett syndrome (Hotta *et al*., 2009, Marchetto *et al*., 2010, Cheung *et al*., 2011, Amenduni *et al*., 2011, Kim *et al*., 2011).

Taking advantage of the nonrandom pattern of X chromosome inactivation in female iPSCs (Tchieu *et al*., 2010), we have generated several novel isogenic pairs of wild type and mutant iPSC lines from patient fibroblasts carrying common RTT mutations, as well as from an unrelated healthy individual. We show here that all female RTT iPSC lines have highly skewed XCI pattern, and clonally express either the wild type or the mutant, but not both, alleles of the *MECP2* gene. Both the wild type and mutant RTT iPSC lines can be consistently and efficiently differentiated into neurons. For phenotypic characterization, we focused our study on the R294X neurons and their isogenic wild type controls, because iPSCs with this common RTT mutation have not been described previously. Our extensive analysis revealed that the R294X neurons were smaller than their isogenic controls, which is a characteristic RTT pathology observed in both RTT patients and Mecp2 mutant mice.

Results

Generation of RTT patient-derived iPSC lines

RTT patient induced pluripotent stem cell (iPSC) lines were previously derived via lentiviral transduction or retroviral transduction of female RTT patient fibroblasts as described in (Ananiev *et al*., 2011). The lentiviral transduced lines were as follows: GM17880 was derived from a patient carrying the T158M mutation, GM07982 was derived from a patient carrying the V247X mutation, GM11270 was derived from a patient carrying the R306C mutation, and the control line, AG07306, was derived from a healthy female. The retroviral transduced line, RS0502, was derived from a patient carrying the R294X mutation. The percent occurrence and location of each RTT patient mutation in relation to the known functional domains of the MECP2 protein is shown in **Figure 1**.

RTT iPSCs are bona fide induced pluripotent stem cells

For each RTT patient mutation, multiple lines were derived from individual induced cells and the resultant iPSC colonies were expanded and validated for pluripotent character. RTT iPSC colonies were found to have characteristic hESC-like morphology with clearly defined borders and were composed of cells with high nucleoli to cytoplasm ratio as shown in **Figure 2** (leftmost column). Similar to previously characterized hESCs and iPSCs, RTT iPSCs expressed high levels of the pluripotency markers OCT4, SOX2 and Nanog, were positive for the presence of the surface antigens Ssea4 and TRA-1-81 and expressed high levels of alkaline phosphatase (AP) (**Fig 2**).

RTT iPSCs were found to display characteristic hESC demethylation of the OCT4 promoter, and the retroviral transduced line, R294X, was found to silence retroviral transcription when compared to newly infected fibroblasts (Ananiev *et al*., 2011). Additionally, RTT iPSCs were able to generate teratomas in SCID mice representing all three germ layers (Ananiev *et al*., 2011). Chromosomal stability of select iPSCs was verified by G-band analysis at WiCell Research Institute and found to be karyotypically normal by a certified cytogeneticist. As such, RTT lines were validated as bona fide iPSCs.

XCI is clonal and nonrandom in RTT iPSCs

The female patient fibroblast samples and corresponding iPSC lines were verified for MECP2 allelic heterozygousity at the genomic level (Ananiev *et al*., 2011). Due to the X-linked nature of MECP2, characterization of the XCI pattern in each iPSC line was necessary to determine whether lines on a cell population level were a mosaic for WT and MT MECP2 expression due to random XCI or if lines were homozygous for expression of either the WT or the MT MECP2 allele due to nonrandom XCI.

To determine the XCI status and the resultant MECP2 allelic expression of each of the RTT iPSCs, three independent assays were performed. First, a previously documented methylation-specific PCR based assay that utilizes of the presence of a CAG repeat polymorphism at the X-linked Androgen Receptor locus (AR), was used as a methylation status surrogate marker of XCI (Allen *et al*., 1992). In this assay (**Fig. 3**), heterozygosity at the AR locus is determined by amplification at the locus without prior exposure to the methylation sensitive enzyme *HhaI* (uncut traces). If there is heterozygosity at the locus,

both parental AR alleles are amplified, with a shorter trace with fewer CAG repeats (red peaks) and a longer trace with more numerous CAG repeats (blue peaks). When exposed to *HhaI* (cut traces), the highly methylated AR allele on the inactive X chromosome is protected while the AR allele on the active X chromosome is cleaved numerous times, becoming incompatible to amplification. In all fibroblast lines, both alleles were present in a comparatively 50:50 ratio (red and blue peaks), indicating a non-skewed random pattern of XCI (**Fig. 4** top traces in each section). In contrast, the hiPSC's had one allele present as the majority (13:87 for R294X-WT, 100:0 for R294X-MT, 81:19 for R306C-WT, 2:98 for T158M-WT, 89:11 for V247X-WT, and 0:100 for V247X-MT), indicating a skewed, non-random pattern of XCI (**Fig. 4**). This pattern appeared to be clonal and remained fixed for an iPSC line throughout passaging.

Second, XCI status was screened by an assay that utilizes the presence of single nucleotide polymorphisms (SNPs) in the X-linked XIST locus transcripts (previously described by Tchieu *et al*., 2010). In genomic DNA, T158M, R294X and R306C fibroblasts were found to be heterozygous for one of the described SNPs. When transcripts from the fibroblasts were sequenced, both alleles of XIST were detectable (Ananiev *et al*., 2011), indicating a random pattern of XCI. In contrast, when iPSC lines were sequenced for the XIST SNP's, transcription from only one allele was detected (**Fig. 5, panel A**). This result further indicates a nonrandom pattern of XCI wherein only one X is active in each iPSC line.

Third, the MECP2 mutational loci were sequenced using primers that spanned an intron to reduce the potential of genomic contamination. RTT iPSC lines were found to express only one allele, either mutant or wildtype, but not both alleles (**Fig. 5, panel B**).

Additionally, verification of the maintenance of MECP2 allelic expression throughout neuronal differentiation was performed. As can be seen when the V247X-MT iPSC was assayed at the EB, NE and NS stage of the differentiation scheme, the V247X-MT MECP2 allele remained expressed (**Fig. 5, panel C**).

RTT iPSC isogenic pairs

Individual RTT lines were genotyped using the three assays listed above; a compilation of results is listed in **Table 1**. As a result of extensive genotyping of lines, isogenic pairs of wildtype and mutant V247X, R294X and R306C iPSCs were obtained as annotated in **Table 1**. For these mutant iPSC lines and those cells differentiated from them, an internal control exists in the same genetic background, from the same individual.

Isogenic RTT iPSCs can be differentiated into neurons

To model RTT in vitro, the R294X isogenic RTT iPSC pair was differentiated into neurons, a major cell type affected in RTT's pathogenesis. For directed neuronal differentiation, a well-established protocol was used that mirrors human *in vivo* neuronal differentiation to pattern cells (Johnson *et al*., 2007) and schematic shown in **Figure 6**. Briefly, R294X-WT-iPSC and R294X-MT-iPSCs and control hESCs were lifted enzymatically from their MEF layer and allowed to differentiate in suspension in the absence of exogenous morphogens for regionalization cues (**Fig. 7, columns 1-2**). After a week in suspension culture, EB's were plated down on an adherent culture that eventually matured into neuroepithelia cells reminiscent of the neural tube formation (**Fig. 7, columns 3-4**). Neural rosettes of the neuroepithelia cells from all lines were found to

express high levels of the neural progenitor cell transcription factor PAX6 (**Fig. 7, column 5**). After a week of neural rosette maturation, cells were lifted off the substrate and transferred to a suspension culture that eventually formed neurospheres. These neurospheres were allowed to mature for one week, were enzymatically treated and titurated and then plated on a laminin coated surface. Hours after plating, post-mitotic neurons were visible migrating from the broken neurospheres. Neurons differentiated from R294X-WT-iPSC and R294X-MT-iPSCs and hESCs were found to be positive for expression of the neuron specific microtubular element protein ß-tubulin III (**Fig. 7, column 6**).

Phenotypic characterization of patient iPSC-derived R294X neurons

A consistent RTT phenotype is a reduction in brain size due to greater cell compaction in certain brain regions and a global reduction in neuron cell size. Due to the positive correlation between somal and nuclear size, the nuclear size of RTT iPSC-derived neurons was assayed (Fig 7). Recapitulating a hallmark pathology of RTT that is present in both post-mortem patient samples and in mouse models, R294X-MT post-mitotic neurons were statistically significantly smaller (R294X-MT-1: -17%, R294X-MT-2: -9%, and R294X-MT-3: -9%) than the neurons expressing the WT MECP2 allele, indicating a cell autonomous effect.

Discussion

Two recent studies have reported the generation and phenotypic analyses of iPSCs from RTT patients. The Muotri group (Marchetto *et al*., 2010) generated iPSC lines from RTT patients and an unrelated healthy individual (control), observed random XCI in most of their RTT iPSC lines, and compared phenotypes in neurons differentiated from RTT iPSC lines and control iPSC and hESC lines. The Ellis group (Cheung *et al*., 2011) generated iPSC lines from female RTT patients carrying mutations different from those included in the Muotri study, observed nonrandom XCI in all of their iPSC lines, and compared cell size in mutant neurons differentiated from an iPSC line with a rare deletion of almost the entire MECP2 gene and their isogenic controls. These studies appear to contrast each other in the XCI status of female RTT iPSC lines. This is a critical issue because the MECP2 gene, mutations in which cause RTT, is located on the X chromosome. Thus the XCI status in RTT iPSC lines directly determines which allele of MECP2 is expressed in the neurons differentiated from these iPSC lines. And the expression status of MECP2 directly influences the interpretation of results from phenotypic analyses of neurons differentiated from such RTT iPSC lines. Our results are consistent with the finding of the Ellis group, as well as the original discovery of nonrandom XCI in female human iPSC lines (Tchieu *et al*., 2010).

To rule out potential difference in reprogramming procedures, we used two methods (Yamanaka factors delivered by retroviruses and Thompson factors delivered by lentiviruses) to generate iPSCs from 3 female RTT patients with common mutations (R294X, R306C, and T158M) and 1 female RTT patients with a rare mutation (V247X),

and observed nonrandom XCI in a total of 23 iPSC lines regardless of the reprogramming methods used or the inherent RTT mutations. However, at this early stage of iPSC technology development, there are likely many unknown technical variations across different labs that may have caused the different XCI status in female iPSCs generated in these studies.

There may be certain advantages in using isogenic pairs of wild type and mutant disease-specific iPSC lines and their derivatives to studying disease mechanism. For instance, comparison within the isogenic pair may reduce the phenotypic variation across different iPSC lines from individuals with diverse genetic background. However, the failure to reactivate the inactivated X chromosome clearly demonstrates the incomplete reprogramming of the somatic epigenome, which may interfere with subsequent phenotypic analyses. As a first step to assess phenotypic variation caused by epigenetic difference among iPSC lines, we analyzed neurons differentiated from 3 different isogenic mutant R294X iPSC lines. Our results showed that although there was variation among neurons from the three mutant lines, they were all significantly smaller than neurons differentiated from the isogenic wild type R294X iPSC line. Future analysis of additional isogenic wild type iPSC lines from the same patient will define the phenotypic variation among wild type lines, and conclusively answer the question of whether epigenetic difference among iPSC lines may mask genotype-dependent phenotypes.

To date, more than 600 mutations have been identified in the MECP2 gene, all of which cause RTT. Since no clear genotype-phenotype correlation has been established between a certain mutation and the resulting spectrum of disease symptoms, it is

necessary to generate and analyze RTT iPSC lines with different mutations (varying in the nature of mutation and the location of the mutation), when using RTT iPSCs and their derivatives to studying disease mechanisms. Compared with RTT iPSC that carry rare RTT mutation (such as the deletion mutation in Cheung *et al*., 2011), our R294X isogenic pair carries a common RTT mutation that is identified in ~5% of RTT patients. At the molecular level, the $MeCP2^{R294X}$ protein may retain some of the important functions of the wild type protein (i.e. binding to methylated DNA because it still has the MBD domain), while lack other functions. Therefore, difference in the spectrum of phenotypes and the underlying mechanisms may exist between the R294X neurons and the MECP2 null neurons described in (Cheung *et al*., 2011).

In summary, we have established two novel isogenic pairs of RTT iPSC lines with either a common (R294X) or a rare (V247X) RTT mutation, and characterized the R294X pair. Together with the RTT iPSC lines generated by the Muotri group (Marchetto *et al*., 2010) and the Ellis group (Cheung *et al*., 2011), these unique isogenic pairs of iPSC lines generated in our study are valuable tools for the RTT research community.

Materials and Methods

All work related to generating iPSC from fibroblast lines from the Coriell Institute for Medical Research (Camden, NJ) has been approved by the Stem Cell Research Oversight (SCRO) Committee at the University of Wisconsin-Madison (protocol # SC-2009-0006), and has been exempted from Institution Review Board (IRB) review (IRB protocol # M-2009-1424).

The work related to generating iPSC from patient RS0502 has been approved by the IRB at University of Wisconsin-Madison (protocol # H-2009-0110). Written informed consent was obtained from patient RS0502/her guardian. All procedures were in accordance with the Helsinki Declaration and established guidelines at University of Wisconsin-Madison.

Methods

Cell culture

Media compositions:

Pluripotent stem cell media (PSCM): DMEM/F12 with 20% KOSR, 1x NEAA, 1x pen/strep, and 1 mM L-glutamine (all from Invitrogen) and 0.1 mM ß-mercaptoethanol (Sigma).

Neuronal media (NM): DMEM/F12 with 1% N2, 1x NEAA, 1x pen/strep and 2 μg/ml heparin (Sigma H3149).

Neurobasal media (NBM): Neurobasal media with 1% N2, 2% B27, 0.5% Glutamax and 1x pen/strep (all from Invitrogen).

iPSC/hESC maintenance

RTT patient-derived iPSCs used in this study were reprogrammed as described in (Ananiev 2011). During the patient fibroblast reprogramming process, cells were fed daily with PSCM supplemented with 100 ng/ml recombinant zebra fish bFGF (kind gift of the Thompson lab), or recombinant human FGF2 (Waisman Biomanufactoring Core). Distinct iPSC colonies appeared as early as 21 days. The average time of colony picking was 30 days post infection. Initial colonies were mechanically picked and split for the first 4–6 passages. Following the initial mechanical splitting, cells were propagated with pluripotent stem cell media (PSCM) containing 4 ng/ml recombinant human FGF and passaged using 1 unit/ml dispase (Invitrogen) upon a layer of irradiated mouse embryonic fibroblasts supplied by WiCell Research Institute. The human embryonic stem cell (hESC) line H9 was used as a control and cultured as reported in (Amir *et al*., 2000).

Karyotyping

G-band chromosome analysis of the iPSC lines was conducted by the cytogenetics lab at the WiCell Research Institute (Madison, WI).

Teratoma formation

Teratoma formation and histological analysis of teratoma were conducted by the WiCell Research Institute (Madison, WI). A certified pathologist was consulted for identification of the three germ layers.

Immunocytochemistry

Cultures were fixed on ice with 4% paraformaldehyde for 20 minutes, washed 3 times with PBS for 15 minutes each wash at room temperature (RT), permeablized with 1% Triton X100 (Sigma) for 30 minutes at RT, blocked with 3% normal donkey serum, 0.25% Triton X100 in PBS for 60 minutes at RT, incubated with primary antibodies overnight at 4°C, washed 3 times with PBS for 15 minutes at RT, incubated with the corresponding secondary antibodies for 60 minutes at RT, and washed 3 times with PBS for 15 minutes at RT. Primary antibody dilutions were as follows: anti-Oct4 1:200 (Santa Cruz sc-5279), anti-Sox2 1:500 (R&D systems AF2018), anti-NANOG 1:500 (R&D systems AF1997), anti-Ssea4 1:20 (DSHB), anti-Tra-1-81 1:500 (Millipore MAB4381), anti-beta III tubulin 1:500 (Sigma T8660), anti-Pax6 1:5000 (DSHB). Secondary antibody dilutions were as follows: Cy 2 Donkey anti-Rabbit antibody, Cy 2 Donkey anti-Mouse antibody, Cy 3 Donkey anti-Rabbit antibody, Cy 3 Donkey anti-Mouse antibody, Cy 3 Donkey anti-Goat antibody (all from Jackson ImmunoResearch). DAPI was used at 3nM for counterstaining.

Post-mitotic neuron differentiation

iPSCs and hESCs were differentiated to neurons as previously described (Johnson *et al*., 2007). Briefly, embryoid bodies (EB) were formed via Dispase disassociation of mature iPSC and hESC colonies from the mouse feeder layer. Differentiating cells were grown in suspension for four days and were fed daily with hES media without FGF. To begin neural induction, EBs were cultured in suspension for an additional three days, feeding every other day with Neuronal induction media (NIM). Seven days after dissociation, the

EBs were plated down into six well tissue culture plates using NIM supplemented with 10% FBS (HyClone). 12 to 16 hours after plating, the FBS supplemented media was replaced with NIM without serum. The attached EBs were fed with NIM every other day for 10 days and allowed to differentiate into neuroepithelial cells. At day 15-17, the neuroepithelial cells were mechanically dissociated, and grown into neurospheres in a suspension of NIM augmented with 2% B27 to aid in survival. At day 23, neurospheres were incubated with accutase (Innovative Cell Technology) for 3 minutes at 37°C and broken into small clusters by mechanical force. Neurosphere particles were plated on 48 well tissue culture plates precoated with 20 μg/ml mouse laminin in NBM for 2 hours. Neurons migrating from the dissociated neurosphere clusters were visible ~2 hours post plating.

Neuronal nuclei phenotypic assay

Fixed neuronal cultures (3 days after plating) were immunostained for ß- tubulin III, counterstained with DAPI, and imaged at 40× magnification. Neurons were identified by ß- tubulin III immunoreactivity and characteristic neuronal morphology under transmitted light. The nuclear area was measured by defining the outer perimeter of DAPI stained nuclei in Adobe Photoshop CS4 Extended.

Allele-specific transcription of MECP2 and XIST

RNA was prepared using the SV Total RNA Isolation kit (Promega). cDNA was made using the qScript cDNA SuperMix (Quanta Biosciences), and used as PCR template to examine allele-specific transcription of MECP2 and XIST. To eliminate the possibility of

genomic DNA being amplified, the MECP2 PCR primers were designed to span an intron. Primers: Forward GCAAAGCAGAGACATCAGAA, reverse 1 (for T158M, V247X) CAGATCGGATAGAAGACTCC, reverse 2 (for R294X, R306C) GCCCAGGGCTCTTACAGGTC. XIST SNP assay was performed as previously described (Tchieu, 2010). Primers: Forward AATGGGCAAAGTGGTTATGC (XIST SNP 1 for R294X), and reverse AGGCCCCTTTCTCAAACTGT. Forward AGTGCCTAGCACAGGGACAG (XIST SNP 2 for T158M and R306C), and reverse ACTTCCCTCAGGAGCAGACA. Purified PCR products were directly sequenced.

The human androgen receptor assay (HUMARA)

The human androgen receptor assay was preformed as previously described (Allen *et al*., 1992). Briefly, 500 ng of genomic DNA was digested to completion with the methylation sensitive restriction enzyme *Hha I*. Both the cut and uncut samples were used as template in PCR reactions, using primers flanking the polymorphic repeats upstream of the human androgen receptor locus. PCR amplification was performed as previously described (Cheung *et al*., 2011) using a forward primer labeled with 6-FAM on the 5′end. The fluorescently labeled PCR amplicons were resolved on a genetic analyzer. The GeneScan data was analyzed and the peak area were measured using ABI Peak Scanner software.

Statistical analysis

For all statistical analyses in this report, an F-test was first performed to determine whether the samples had equal or unequal variance. Then the Student's t-test (2-tailed)

was performed assuming either equal or unequal variance as determined by the F-test. The threshold of statistical significance was set at $p = 0.01$.

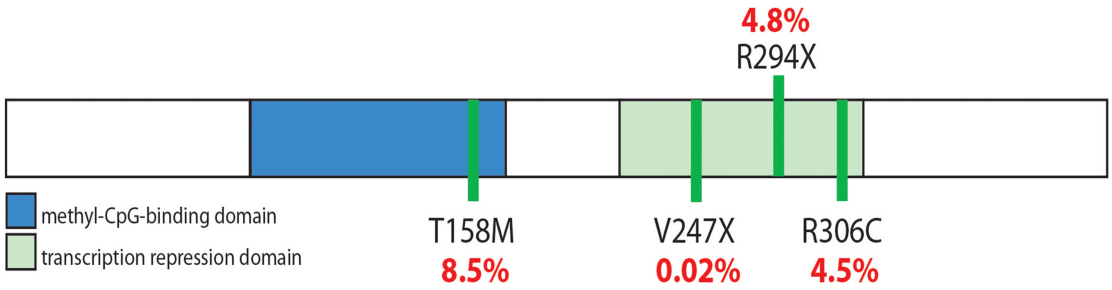

Figure 1. RTT mutations used in this study

Schematic of the location of RTT mutations used in this study in relation to the known functional domains of the MECP2 protein. Values in red indicate the percent occurrence of each mutation in relation to total documented cases (occurrence updated 2/10/13 via RettBASE: IRSF MECP2 Variation Database).

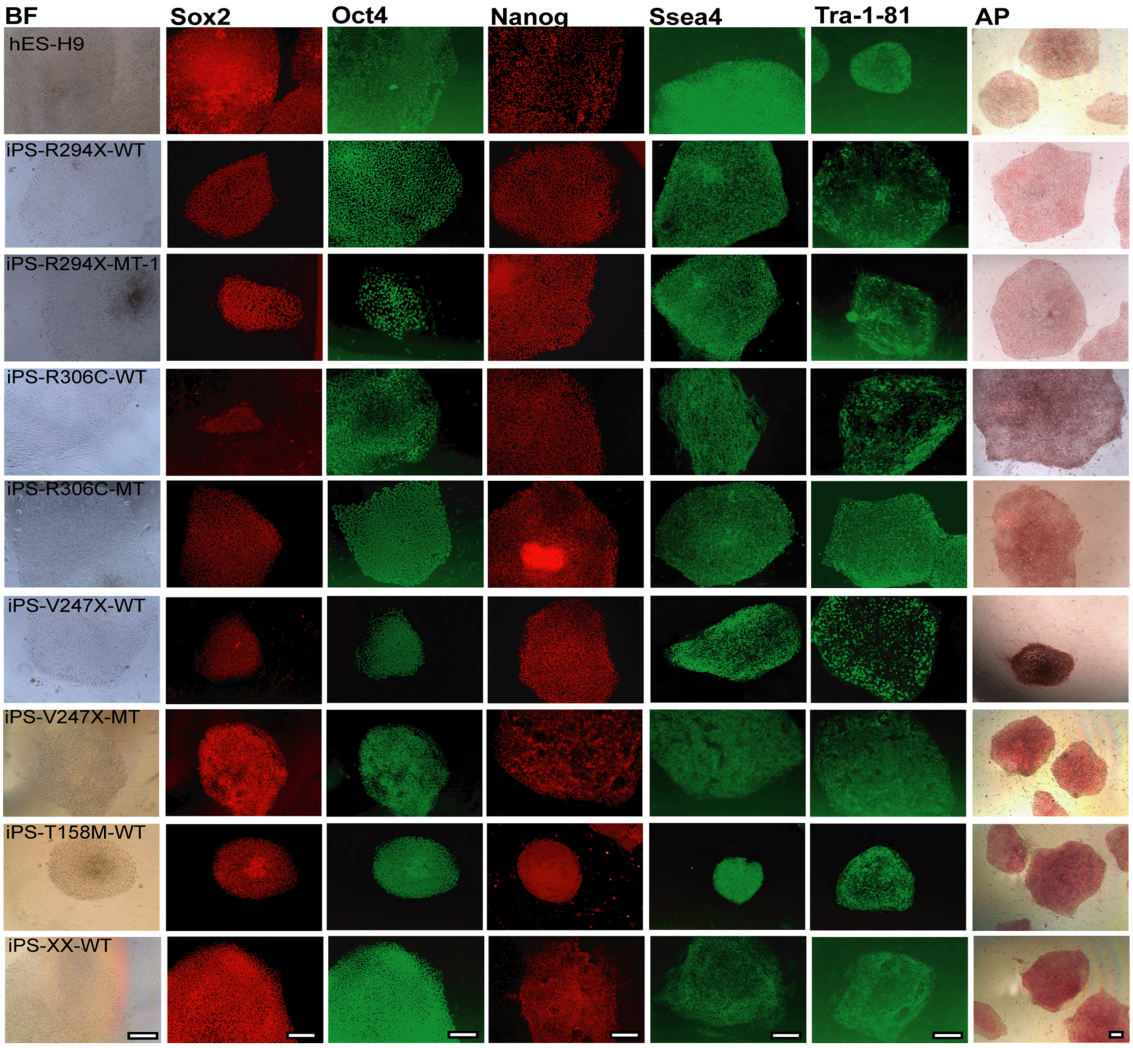

Figure 2. RTT iPSCs are bona fide induced pluripotent stem cells

Representative images of hESC (H9) and hiPSC colonies displaying characteristic stem cell morphology (left-most column) and stained with antibodies against the pluripotency markers Sox2, Oct4, Nanog, Ssea4, and Tra-1-81, and processed for alkaline phosphatase reaction (listed in left to right columns). Each row represents colonies from one hESC or hiPSC line. iPS-XX-WT was derived from the AG07306 healthy female control. BF stands for bright field. Scale bars = 200 μm.

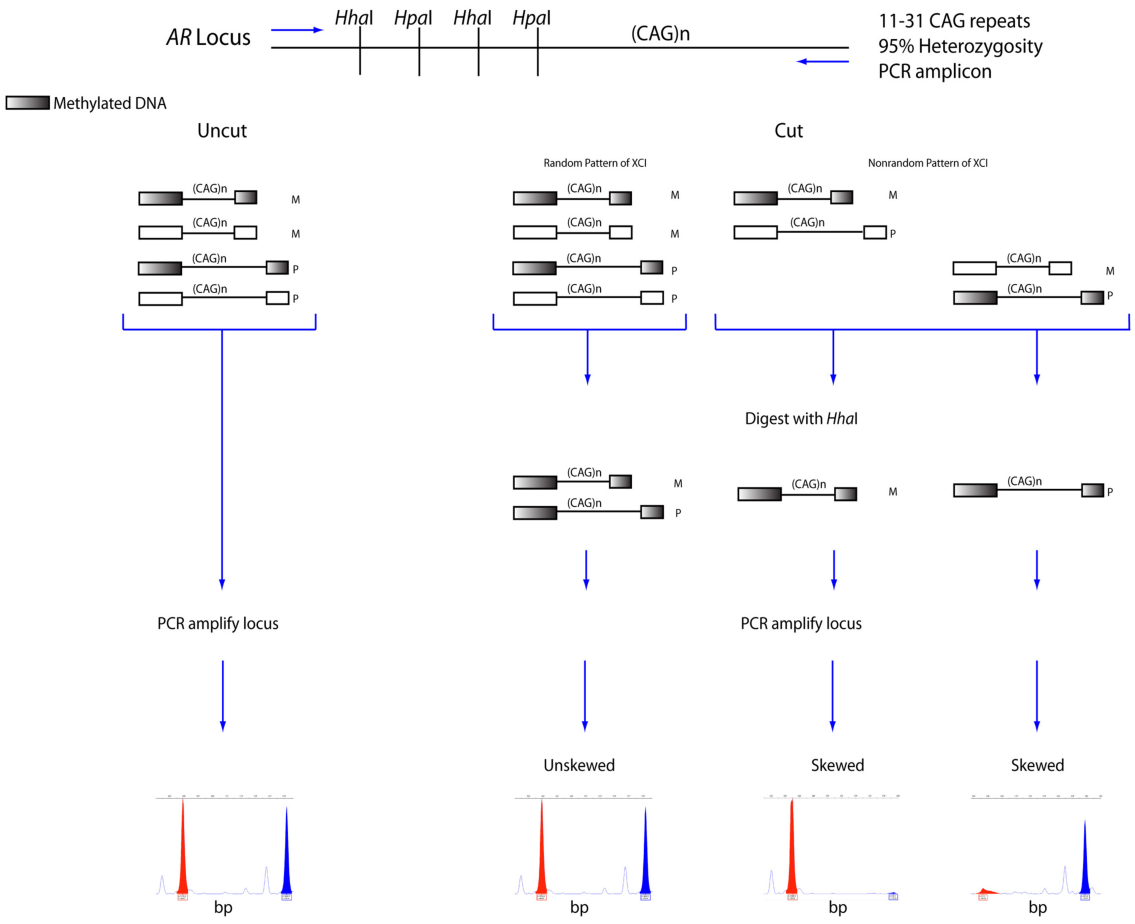

Figure 3. The *Androgen Receptor* assay

Schematic of the *Androgen Receptor* locus displaying the location of methylation sensitive restriction enzyme cleavage sites (*HhaI* and *HpaI*) in relation to PCR amplification sites (top). Adapted from Allen *et al*., (1992). Heterozygosity is verified by direct PCR amplification at locus resulting in a chromatograph with a two peaks, one with a short "M" amplicon and one with a long "P" amplicon (Uncut column). In Random XCI, the "M" and "P" X chromosomes are present in both methylated and unmethylated states. When digested with *HhaI*, the methylated X chromosomes are protected and amplification of both alleles occurs. This results in an Unskewed pattern. In Nonrandom XCI, either only with "M" X chromosome is methylated or only the "P" X

chromosome is methylated, which confers protection against *HhaI* digestion and only one allele is amplified. This results in a skewed pattern. Methylated DNA is shown darkened. M= the "maternal" X-chromosome and P= the "paternal" X-chromosome for schematic explanation purposes only. Chromatographs display signal height on the Y-axis and size in base pairs on the X-axis.

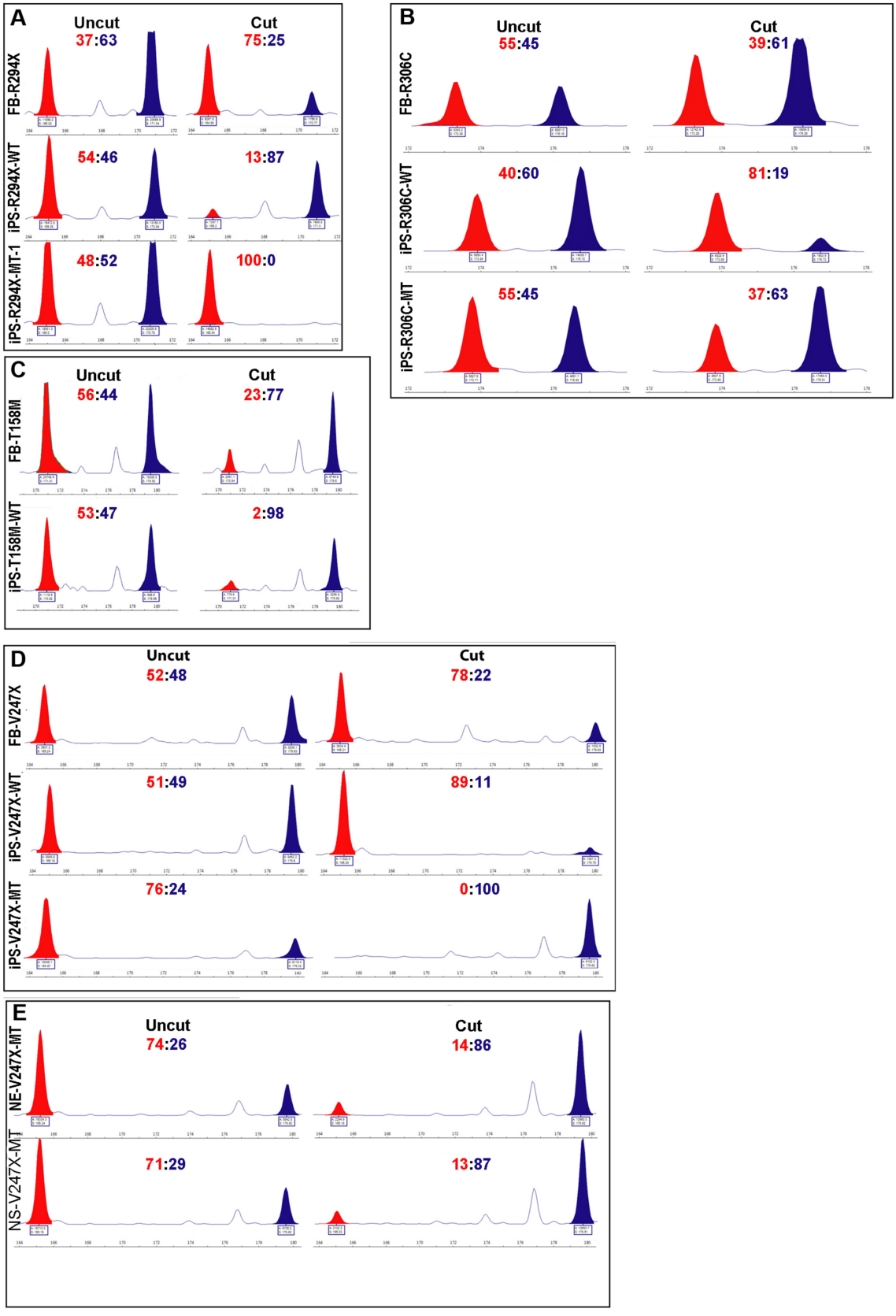
A
Uncut
Cut
FB-R294X
37:63
75:25
iPS-R294X-WT
54:46
13:87
iPS-R294X-MT-1
48:52
100:0
B
Uncut
Cut
FB-R306C
55:45
39:61
iPS-R306C-WT
40:60
81:19
iPS-R306C-MT
55:45
37:63
C
Uncut
Cut
FB-T158M
56:44
23:77
iPS-T158M-WT
53:47
2:98
D
Uncut
Cut
FB-V247X
52:48
78:22
iPS-V247X-WT
51:49
89:11
iPS-V247X-MT
76:24
0:100
E
Uncut
Cut
NE-V247X-MT
74:26
14:86
NS-V247X-MT
71:29
13:87

Figure 4. RTT iPSCs exhibit a nonrandom, skewed pattern of XCI that remains constant through differentiation

The AR assay was used to determine the XCI pattern of RTT fibroblasts, iPSC lines and their differentiation products. (A) Results from the R294X fibroblast and iPSC lines. (B) Results from the R306C fibroblast and iPSC lines. (C) Results from the T158M fibroblast and iPSC T158M-WT line. (D) Results from the V247X fibroblast and iPSC lines. (E) Results from the neuroepithelia (NE-V247X-MT) and neurospheres (NS-V247X-MT) differentiated from iPS-V247X-MT and displaying continued allele-specific methylation of the AR locus. Uncut traces verified the presence of both parental AR alleles: 165 bp and 171 bp for the R294X lines; 173 bp and 176 bp for the R306C lines; 171 bp and 180 bp for the T158M lines; and 165 bp and 180 bp for the V247X lines. Cut traces for fibroblasts verified the presence of both AR alleles due to unskewed, random XCI while cut traces for iPSCs verified the presence of only one AR allele from the hypermethylated, inactive X chromosome and as such displayed skewed, nonrandom XCI. The source of genomic DNA is labeled to the left of each trace. The ratio between the two AR alleles is at the top of each trace. The molecular weight standard is provided under each trace.

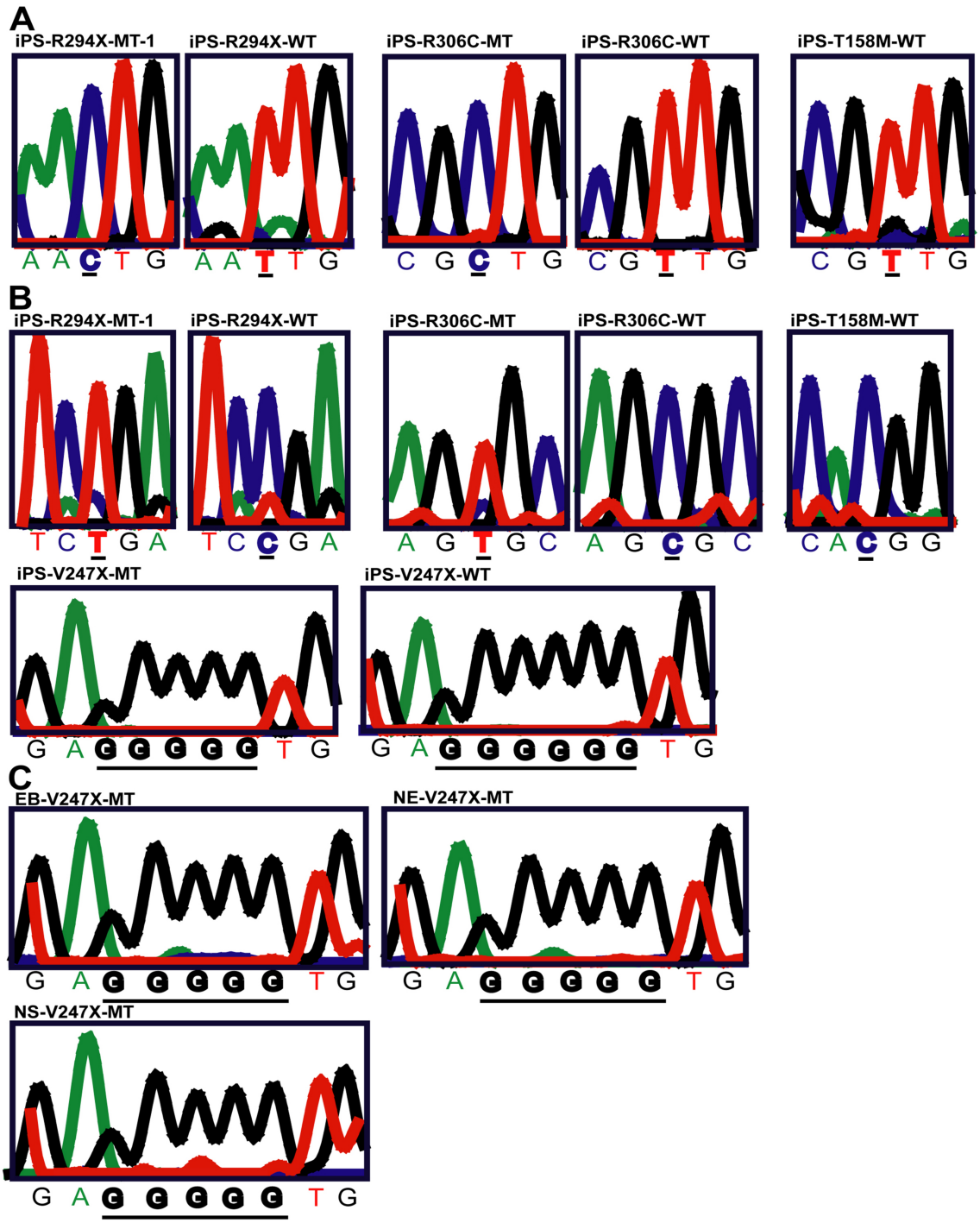

Figure 5. Clonal and allele-specific expression of *XIST* SNPs and *MECP2* in female human iPSC lines and their differentiation products

(A) Sequencing traces of XIST SNP analysis to distinguish allele-specific transcription in iPS-R294X-MT-1, iPS-R294X-WT, iPS-R306C-MT, iPS-R306C-WT, and iPS-T158M-

WT. SNP 1 (C or T) was examined in iPS-R306C-MT, iPS-R306C-WT, and iPS-T158M-WT. SNP 2 (C or T) was examined in iPS-R294X-MT-1, iPS-R294X-WT. (B) Sequencing traces of regions of the MECP2 gene that contain RTT mutations to distinguish allele-specific transcription of MECP2 in iPS-R294X-MT-1, iPS-R294X-WT, iPS-R306C-MT, iPS-R306C-WT, and iPS-T158M-WT, iPS-V247X-MT, and iPS-V247X-WT. MT denotes expression of the mutant MECP2 allele. WT denotes expression of the wild type MECP2 allele. (C) Representative sequencing traces of the region of the MECP2 gene that contains RTT mutation V247X (705delG) to distinguish allele-specific transcription of MECP2 at the stages of embryoid body (EB), neuroepithelia (NE) and neurosphere (NS) during directed neural differentiation from iPS-V247X-MT.

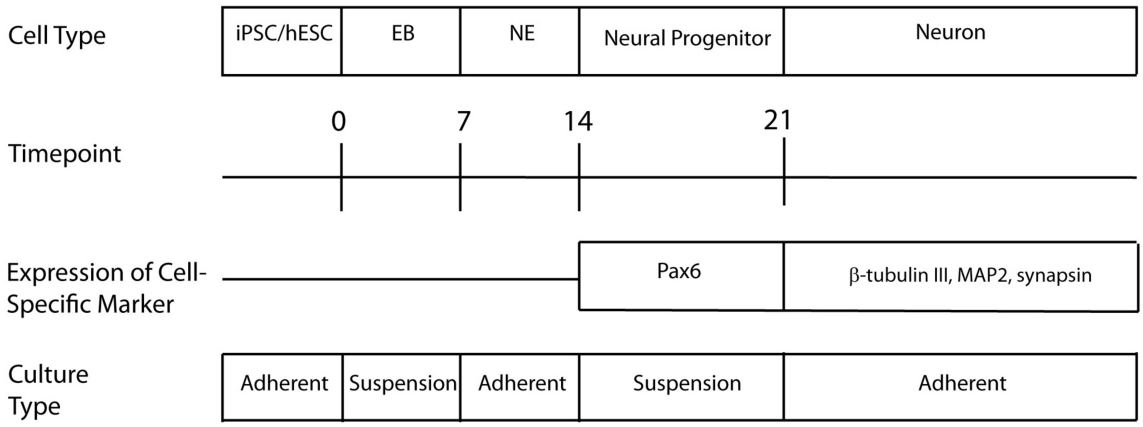

Figure 6. Directed neuronal differentiation of iPSC/hESCs

Major stages are listed as follows: embryoid body (EB), neural epithelia (NE), neurosphere (NS) and neuron. Timepoints are listed in days beginning with iPSC/hESCs being lifted from the MEF layer = 0. Adapted from Johnson *et al*., 2007.

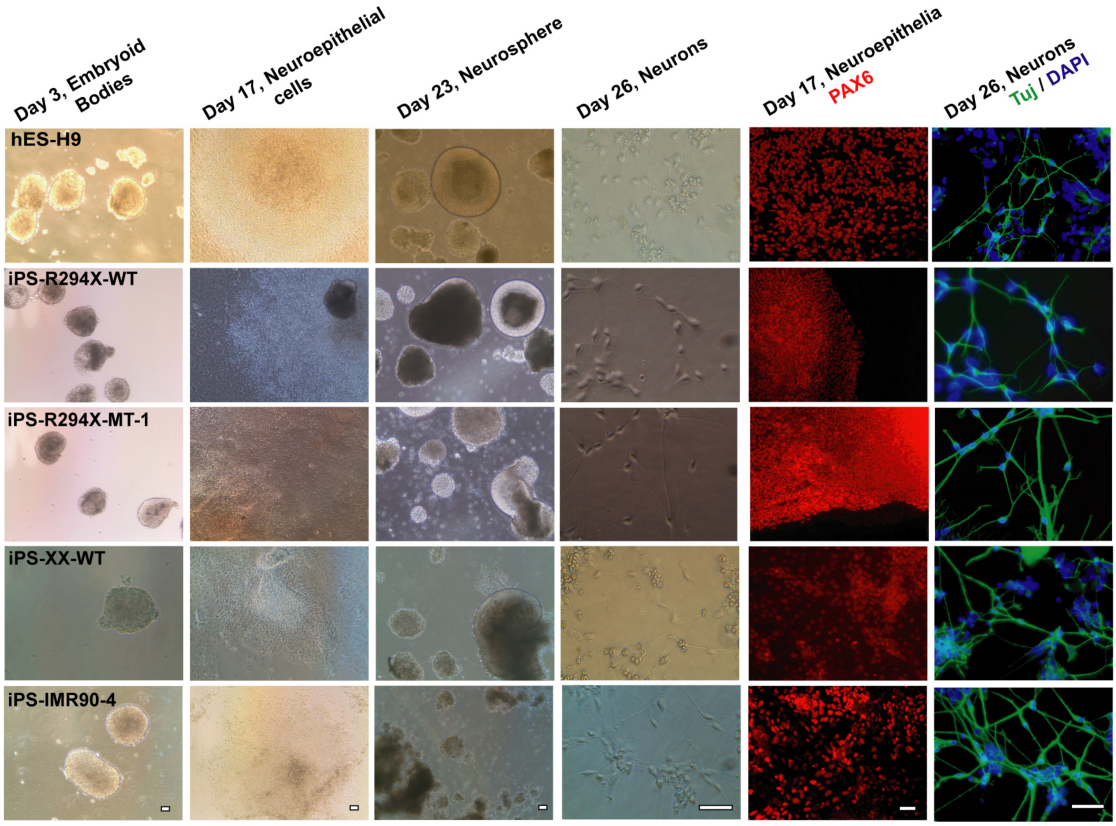

Figure 7. Isogenic pairs of wild type and mutant RTT iPSC lines can be differentiated into post mitotic neurons

Columns 1-4: transmitted light microscropy images of major sequential stages of the directed neuronal differentiation. Columns 5-6: fluorescence images of expression of neuroepithelial marker PAX6 and postmitotic neuron marker ß tubulin III (Tuj). Each row represents differentiation of one hESC or hiPSC line. Each column represents one key stage of the differentiation. Scale bars = 200 μm.

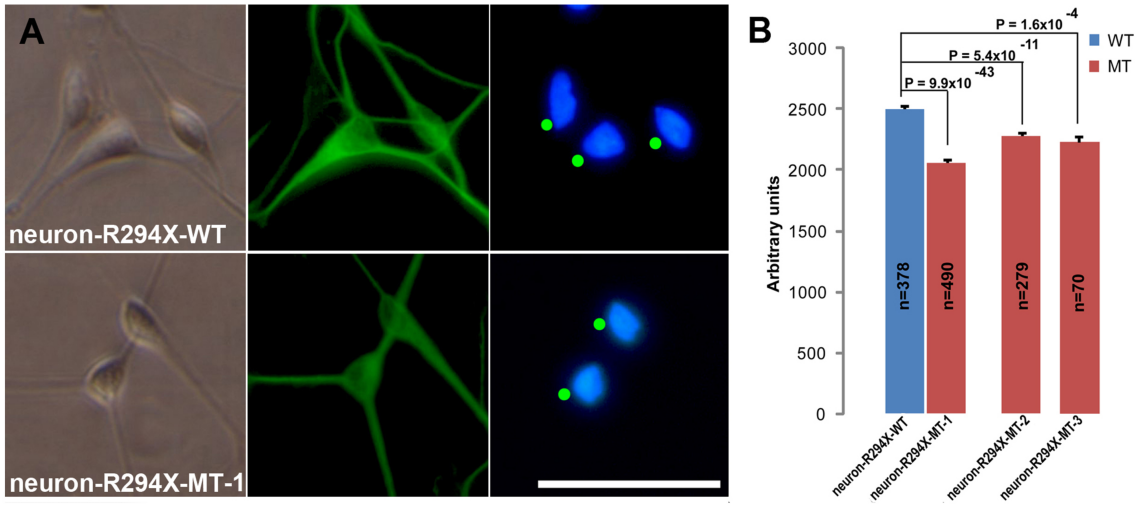

Figure 8. Phenotypic characterization of R294X isogenic pair neurons

(A) High magnification transmitted light images of neurons (neuron-R294X-WT and neuron-R294X-MT-1) derived from the isogenic pair of iPS-R294X-WT and iPS-R294X-MT-1 to demonstrate characteristic neuronal morphology (left), which was used in conjunction with ß tubulin III immunoreactivity (middle) to identify neurons for measuring DAPI stained nuclear area (right). Green dots in the DAPI images indicate neuronal nuclei identified for size analysis to avoid double sampling. Scale bar = 200 μm. (B) Bar graph of neuronal nuclei area measurements using artificial units. Average nuclear area measurements from R294X neurons (red, neuron-R294X-MT-1, -2, and –3 which were differentiated from three isogenic iPSC-R294X-MT lines, respectively, and analyzed 3 days after plating) and their isogenic controls (blue, neuron-R294X-WT which was differentiated from the isogenic iPSC-R294X-WT line). Error bars = standard error of the mean (SEM). Total number of nuclei measured for each line is shown in each bar. All p values are from two-tailed Student's t-tests.

iPSC line	Allele specific *MECP2* transcription	Allele specific *AR* methylation	*XIST* SNP analysis	
			SNP 1	SNP 2
T158M-1	WT	Not tested	T	N/A
T158M-3	WT	skewed	T	N/A
T158M-4	WT	Not tested	T	N/A
T158M-5	WT	Not tested	Not tested	N/A
T158M-6	WT	skewed	T	N/A
T158M-7	WT	Not tested	T	N/A
T158M-8	WT	Not tested	Not tested	N/A
V247X-1	WT	skewed	N/A	N/A
V247X-2	**WT**	**skewed**	**N/A**	**N/A**
V247X-4	**MT**	**skewed**	**N/A**	**N/A**
V247X-5	WT	skewed	N/A	N/A
R306C-1	MT	Not tested	C	N/A
R306C-23	**MT**	**skewed**	**C**	**N/A**
R306C-33	**WT**	**skewed**	**T**	**N/A**
R306C-24	WT	Not tested	Not tested	N/A
R306C-325	MT	skewed	C	N/A
R294X-1	**MT**	**skewed**	**N/A**	**C**
R294X-4	**MT**	**skewed**	**N/A**	**C**
R294X-5	**MT**	**skewed**	**N/A**	**C**
R294X-6	MT	Not tested	N/A	C
R294X-10	MT	Not tested	N/A	C
R294X-11	**WT**	**skewed**	**N/A**	**T**
R294X-12	MT	Not tested	N/A	C

Table 1. Summary of XCI status screening and allele-specific expression of *MECP2* in multiple RTT iPSC lines

WT: wild type allele of *MECP2*. MT: mutant allele of *MECP2*. N/A: not applicable. The **WT** chosen for each pair is in **bold black** while the **MT** chosen for each pair is in **bold red**.

References

Allen, R.C., Zoghbi, H.Y., Moseley, A.B., Rosenblatt, H.M., Belmont, J.W. Methylation of *HpaII* and *HhaI* sites near the polymorphic CAG repeat in the human androgen-receptor gene correlates with X chromosome inactivation. *Am J Hum Genet* **51**, 1229–1239 (1992).

Amenduni, M., De Filippis, R., Cheung, A.Y., Disciglio, V., Epistolato, M.C., *et al*. iPS cells to model CDKL5-related disorders. *Eur J Hum Genet* **190**, 812–5 (2011).

Amir, R.E., van den Veyver, I.B., Wan, M., Tran, C.Q., Francke, U., *et al*. Rett syndrome is caused by mutations in X-linked MECP2, encoding methyl-CpG-binding protein 2. *Nat Genet* **23**, 185–188 (1999).

Ananiev, G., Williams, E.C., Li, H., & Chang, Q. Isogenic Pairs of Wild Type and Mutant Induced Pluripotent Stem Cell (iPSC) Lines from Rett Syndrome Patients as *In Vitro* Disease Model. *PLoS ONE* **6**, e25255 (2011).

Armstrong, D., Dunn, J.K., Antalffy, B., Trivedi, R. Selective dendritic alterations in the cortex of Rett syndrome. *J Neuropathol Exp Neurol* **54**, 195–201 (1995).

Bird, A.P,. Wolffe, A.P. Methylation-induced repression–belts, braces, and chromatin. *Cell* **99**, 451–454 (1999).

Belichenko, N.P., Belichenko, P.V., Li, H.H., Mobley, W.C., Francke, U. Comparative study of brain morphology in Mecp2 mutant mouse models of Rett syndrome. *J Comp Neurol* **508**, 184–195 (2008).

Belichenko, P.V., Wright, E.E., Belichenko, N.P., Masliah, E., Li H.H., *et al*. Widespread changes in dendritic and axonal morphology in Mecp2-mutant mouse models of Rett syndrome: evidence for disruption of neuronal networks. *J Comp Neurol* **514**, 240–258 (2009).

Chahrour, M., Zoghbi, H.Y. The story of Rett syndrome: from clinic to neurobiology. *Neuron* **56**, 422–437 (2007).

Chen, R.Z., Akbarian, S., Tudo,r M., Jaenisch, R. Deficiency of methyl-CpG binding protein-2 in CNS neurons results in a Rett-like phenotype in mice. *Nat Genet* **27**, 327–331 (2001).

Cheung, A.Y., Horvath, L.M., Grafodatskaya, D., Pasceri, P., Weksberg, R., *et al*. Isolation of MECP2-null Rett Syndrome patient hiPS cells and isogenic controls through X-chromosome inactivation. *Hum Mol Genet* **20**, 2103–2115 (2011).

Dimos, J.T., Rodolfa, K.T., Niakan, K.K., Weisenthal, L.M., Mitsumoto, H., *et al*. Induced pluripotent stem cells generated from patients with ALS can be differentiated into motor neurons. *Science* **321**, 1218–1221 (2008).

Ebert, A.D., Yu, J., Rose, F.F. Jr, Mattis, V.B., Lorson, C.L., *et al*. Induced pluripotent stem cells from a spinal muscular atrophy patient. *Nature* **457,** 277–280 (2009).

Esteban, M.A., Wang, T., Qin, B., Yang, J., Qin, D., *et al*. Vitamin C enhances the generation of mouse and human induced pluripotent stem cells. *Cell Stem Cell* **6**, 71–79 (2010).

Guy, J., Hendrich, B., Holmes, M., Martin, J.E., Bird, A. A mouse *Mecp2*-null mutation causes neurological symptoms that mimic Rett syndrome. *Nat Genet* **27**, 322–326 (2001).

Hagberg, B. Rett's syndrome: prevalence and impact on progressive severe mental retardation in girls. *Acta Paediatr Scand* **74**, 405–408 (1985).

Hagberg, B., Hagberg, G. Rett syndrome: epidemiology and geographical variability. *Eur Child Adolesc Psychiatry* **6**, Suppl 15–7 (1997).

Hotta, A., Cheung, A.Y., Farra ,N., Vijayaragavan, K., Seguin, C.A., *et al*. (2009) Isolation of human iPS cells using EOS lentiviral vectors to select for pluripotency. *Nat Methods* **6**, 370–376.

Johnson, M.A., Weick, J.P., Pearce, R.A., Zhang, S.C. Functional neural development from human embryonic stem cells: accelerated synaptic activity via astrocyte coculture. *J Neurosci* **27**, 3069–3077 (2007).

Jugloff, D.G., Jung, B.P., Purushotham, D., Logan, R., Eubanks, J.H. Increased dendritic complexity and axonal length in cultured mouse cortical neurons overexpressing methyl-CpG-binding protein MeCP2. *Neurobiol Dis* **19**, 18–27 (2005).

Katz, D.M., Dutschmann, M., Ramirez, J.M., Hilaire, G. Breathing disorders in Rett syndrome: progressive neurochemical dysfunction in the respiratory network after birth. Respir *Physiol Neurobiol* **168**, 101–108 (2009).

Kim, K.Y., Hysolli, E., Park, I.H. Neuronal maturation defect in induced pluripotent stem cells from patients with Rett syndrome. *Proc Natl Acad Sci U S A* **108**, 14169–74 (2011).

Kishi, N., Macklis, J.D. MECP2 is progressively expressed in post-migratory neurons and is involved in neuronal maturation rather than cell fate decisions. *Mol Cell Neurosci* **27**, 306–321 (2004).

Marchetto, M.C., Carromeu, C., Acab, A., Yu, D., Yeo, G.W., *et al*. A model for neural development and treatment of Rett syndrome using human induced pluripotent stem cells. *Cell* **143**, 527–539 (2010).

Park, I.H., Arora, N., Huo, H., Maherali, N., Ahfeldt, T., *et al*. Disease-specific induced pluripotent stem cells. *Cell* **134**, 877–886 (2008).

Shahbazian, M.D., Sun, Y., Zoghbi, H.Y. Balanced X chromosome inactivation patterns in the Rett syndrome brain. *Am J Med Genet* **111**, 164–168 (2002).

Shahbazian, M., Young, J., Yuva-Paylor, L,. Spencer, C., Antalffy, B., *et al*. Mice with truncated MeCP2 recapitulate many Rett syndrome features and display hyperacetylation of histone H3. *Neuron* **35**, 243–254 (2002).

Soldner, F., Hockemeyer, D., Beard, C., Gao, Q., Bell, G.W., *et al*. Parkinson's disease patient-derived induced pluripotent stem cells free of viral reprogramming factors. *Cell* **136**, 964–977 (2009).

Takahashi, K., Yamanaka, S. Induction of pluripotent stem cells from mouse embryonic and adult fibroblast cultures by defined factors. *Cell* **126**, 663–676 (2006).

Takahashi, K., Tanabe, K., Ohnuki, M., Narita, M., Ichisaka, T., *et al*. Induction of pluripotent stem cells from adult human fibroblasts by defined factors. *Cell* **131**, 861–872 (2007).

Tchieu, J., Kuoy, E., Chin, M.H., Trinh, H., Patterson, M., *et al*. Female human iPSCs retain an inactive X chromosome. *Cell Stem Cell* **7**, 329–342 (2010).

Tiscornia, G,. Singer, O., Verma, I.M. Production and purification of lentiviral vectors. *Nat Protoc* **1**, 241–245 (2006).

van den Veyver, I.B., Zoghbi, H.Y. Methyl-CpG-binding protein 2 mutations in Rett syndrome. *Curr Opin Genet Dev* **10**, 275–279 (2000).

Wan, M., Lee, S.S., Zhang, X., Houwink-Manville, I., Song, H.R., *et al*. Rett syndrome and beyond: recurrent spontaneous and familial MECP2 mutations at CpG hotspots. *Am J Hum Genet* **65**, 1520–1529 (1999).

Xiang, F., Buervenich, S., Nicolao, P., Bailey, M.E., Zhang, Z., *et a*l. Mutation screening in Rett syndrome patients. *J Med Genet* **37,** 250–255 (2000).

Yu, J., Vodyanik, M.A., Smuga-Otto, K., Antosiewicz-Bourget, J., Frane, J.L., *et al*. Induced pluripotent stem cell lines derived from human somatic cells. *Science* **318**, 1917–1920 (2007).

Chapter II

Mutant Astrocytes Differentiated from Rett Syndrome Patient-specific iPSCs Have Adverse Effects on Wild Type Neurons

Abstract

The disease mechanism of Rett syndrome (RTT) is not well understood. Studies in RTT mouse models have suggested a non-cell autonomous role for astrocytes in RTT pathogenesis. However, it is not clear whether this is also true for human RTT astrocytes. To establish an *in vitro* human RTT model, we have previously generated isogenic induced pluripotent stem cell (iPSC) lines from several RTT patients carrying different disease-causing mutations. Here we show that these RTT iPSC lines can be efficiently differentiated into astroglial progenitors and glial fibrillary acidic protein expressing ($GFAP^+$) astrocytes that maintain such isogenic status, that the mutant RTT astrocytes carrying three different RTT mutations and their conditioned media have adverse effects on the morphology and function of wild type neurons, and the glial effect on neuronal morphology is independent of the intrinsic neuronal deficit in mutant neurons. Moreover, both Insulin-like Growth Factor 1 (IGF-1) and (1-3)IGF-1 (GPE) partially rescued the neuronal deficits caused by mutant RTT astrocytes. Our findings confirm the critical glial contribution to RTT pathology, reveal potential cellular targets of IGF-1 therapy, and further validate patient-specific iPSCs and their derivatives as valuable tools to study RTT disease mechanism.

Introduction

Mutations in the X-linked methyl-CpG binding protein 2 (*MECP2*) gene cause Rett syndrome (RTT) (Amir *et al*., 1999), a devastating neurological disease that predominantly affects females (Hagberg 1985). In order to fully understand the disease mechanism and develop effective treatments, it is necessary to determine what cells/tissues express MeCP2 and study the contributions of each MeCP2-expressing cell/tissue to the overall disease.

Earlier studies showed that MeCP2 is highly expressed in mature neurons throughout the mammalian brains (Akbarian *et al*., 2001; Shahbazian *et al*., 2001), suggesting the loss of function or malfunction of MeCP2 in neurons plays a key role in RTT pathogenesis. This hypothesis is strongly supported by several later studies demonstrating that specific genetic deletion of *Mecp2* in different neuronal subtypes leads to distinct subsets of RTT-like phenotypes in mouse models (Chao *et al*., 2010; Samaco *et al*., 2009; Fyffe *et al*., 2008).

More recently, it was discovered that astrocytes, another major cell type in the brain, also express MeCP2, and that the loss of MeCP2 in astrocytes has a non-cell autonomous influence on neuronal morphology (Ballas *et al*., 2009; Maezawa *et al*., 2009). Furthermore, the restoration of normal MeCP2 expression only in astrocytes is sufficient to rescue RTT disease symptoms in mouse models (Lioy *et al*., 2011). However, it is unclear whether human astrocytes also express MECP2 and whether human RTT astrocytes adversely affect neuronal morphology and function. (1-3)IGF-1 (or GPE) has been show to partially rescue RTT-like phenotypes in *Mecp2* mutant mice

(Tropea *et al*., 2009), which led to ongoing clinical trials of IGF-1 and GPE in RTT patients. Yet the cellular targets of these IGF-1 related therapies remain unclear.

We have previously generated and characterized isogenic pairs of wild type and mutant induced pluripotent stem cell (iPSC) lines from RTT patients carrying the V247X (valine 247 to stop codon, nonsense, rare in RTT patients), R294X (arginine 294 to stop codon, nonsense, present in 5-6% of RTT patients) and R306C (arginine 306 to cysteine, missense, present in 4-7% of RTT patients) mutations (Ananiev *et al*., 2011). While it has long been feasible to differentiate human embryonic stem cells (hESCs) into various types of neurons, methods to efficiently differentiate hESCs and iPSCs into functional astrocytes have only recently become available (Krencik *et al*., 2011; Emdad *et al*., 2011; Yuan *et al*., 2011). Using one of these methods (Krencik *et al*., 2011), we have differentiated isogenic pairs of RTT iPSC lines carrying the V247X, R294X and R306C mutations into astrocytes and examined their influence on the morphology of wild type neurons. We show here that astrocytes differentiated from the RTT iPSCs maintain the nonrandom X chromosome inactivation (XCI) status of their parental RTT iPSC lines, clonally express either the wild type or mutant, but not both, allele of *MECP2*, that the mutant RTT astrocytes adversely affect the morphology and function of wild type mouse neurons, that similar negative influence also applies to human neurons co-cultured with these astrocytes, and that such a non-cell autonomous influence is partially mediated by factors secreted from the astrocytes. Furthermore, using different combinations of GABAergic interneurons and astrocytes differentiated from the same isogenic pair of RTT iPSC lines, our *in vitro* co-culture system was able to clearly separate the neuronal

and glial contribution to the observed neuronal deficits. Finally, both IGF-1 and GPE were effective in rescuing neuronal deficits caused by mutant RTT astrocytes.

Our findings provide the first direct evidence that human astrocytes express detectable level of MECP2, and confirm the significant glial contribution to RTT pathology in human cells. In addition, our results demonstrate that the isogenic RTT iPSC lines and their derivatives as a valid *in vitro* system for studying RTT disease mechanisms and testing drug candidates.

Results

The isogenic RTT iPSC lines can be efficiently differentiated into GFAP$^+$ astrocytes

Using isogenic pairs of RTT iPSC lines to study disease mechanisms may reduce phenotypic variations across different individuals with diverse genetic backgrounds. However, it has been reported that female iPSC lines could undergo an erosion of XCI (Mekhoubad *et al*., 2012) in culture over time. Thus, we reconfirmed the XCI status of all of our isogenic RTT iPSC lines by examining the methylation profile of the androgen receptor (*AR*) locus, the allele-specific transcription of a single nucleotide polymorphism (SNP) from the *XIST* locus, and the allele-specific transcription of the *MECP2* gene. Our results clearly demonstrated that all the RTT iPSC lines used for astroglial differentiation in this study maintained their original XCI pattern (**Fig. 1**), likely because they were still at relatively early passages (passage 13-38, details on each line provided in methods). We first generated astroglial progenitors from the of the RTT iPSC lines by growing neurospheres in the presence of epidermal growth factor (EGF) and fibroblast growth factor 2 (FGF2) in alternating suspension and adherent culture. To carefully monitor the astrogenic potential of each of the RTT astroglial progenitor lines, terminal differentiation of the astroglial progenitors was performed in the presence of ciliary neurotrophic factor (CNTF) and the absence of EGF and FGF2 every month from 90 days to over 300 days after the start of differentiation (**Fig. 2A**). While all RTT astroglial progenitor cells efficiently differentiated into S100β positive cells, the number of glial fibrillary acidic protein (GFAP) positive cells continued to increase when terminal differentiation was performed from early phase (90-150 days), intermediate phase (150-270 days) and late phase (270-300+ days) astroglial progenitors (**Fig. 2B**). Stereological

counting determined that 70-85% of cells terminally differentiated from late phase RTT astroglial progenitors were positive for GFAP (**Fig. 2C**). 2-5 independent differentiations from each RTT astroglial progenitor line were included in this analysis. Although astroglial progenitors differentiated from each RTT iPSC lines appeared to mature at slightly different times, there was no significant difference in proliferation rate and differentiation efficiency between the wild type and mutant RTT astroglial progenitor cells. Consistent with the increase of S100β and GFAP levels through astrocyte differentiation, we observed increased expression of *NFIX*-a astroglial transcription factor and decreased expression of *OCT4*-a pluripotency transcription factor (**Fig. 3A-B**).

Astroglial progenitors differentiated from isogenic RTT iPSC lines maintain their original isogenic status

We next examined the XCI status and allelic *MECP2* expression in all the astroglial progenitors differentiated from these iPSC lines to make sure they maintained the original isogenic status. The methylation status of the *AR* locus has been established as a surrogate marker of XCI status (Allen *et al*., 1992). In this assay, without digestion with methylation sensitive enzymes (uncut traces), both parental alleles of *AR* can be readily detected and unequivocally distinguished by the presence of two different-sized peaks (165bp and 180bp for the V247X lines, 165bp and 171bp for the R294X lines, 173 and 176bp for the R306C lines, as indicated by the red and blue color) in all the RTT astroglial progenitors throughout the early, intermediate and late phases (**Fig. 4A**). The non-skewed ratio between the red and blue peaks (ranging from 33:67 to 63:37) indicated similar amplification efficiency of the two parental alleles. After digestion with

methylation sensitive enzymes (cut traces), only the hypermethylated *AR* allele (on the inactivated X chromosome) could be amplified (**Fig. 4A**). In all RTT astroglial progenitors across the early, intermediate and late phases, the ratio between the red and the blue peaks was highly skewed (**Fig. 4A**), suggesting XCI was not random in these RTT astroglial progenitors. Moreover, the RTT astroglial progenitors had the same *AR* allele hypermethylated as the RTT iPSC lines they were differentiated from (**compare Fig. 1 and Fig. 4A**). Allele-specific transcription of the *MECP2* gene in all the late phase RTT astroglial progenitors was also examined as previously reported *(*Ananiev *et al*., 2011), which showed either the wild type or the mutant, but not both, alleles of the *MECP2* gene (**Fig. 4B**). Finally, we performed Western blot to directly examine MECP2 protein expression in astrocytes terminally differentiated from late phase RTT astroglial progenitors. The MECP2 band was detected at ~75kDa in astrocytes differentiated from H9, V247X-WT, R294X-WT and R306C-WT astroglial progenitors, but not in astrocytes differentiated from V247X-MT and R294X-MT astroglial progenitors (**Fig. 5**). Because the antibody cannot distinguish the R306C missense mutation, a MECP2 band was also detected in the R306C-MT astrocytes. Taken together, our data suggest that all RTT astroglial progenitors/astrocytes maintained the isogenic status throughout the differentiation procedure and clonally express either the wild type or mutant MECP2.

Mutant RTT astrocytes have adverse effects on the morphology and function of co-cultured wild type mouse hippocampal neurons

To determine whether human RTT mutant astrocytes have non-cell autonomous influence on wild type neurons, we isolated primary hippocampal neurons from postnatal day 0

(P0) mice and co-cultured them with either wild type or mutant astrocytes differentiated from late phase isogenic astroglial progenitors. We chose the P0 hippocampal neurons for our first co-culture experiment because they are easier to obtain, more mature and more homogenous in their morphology than hESC- of iPSC-derived neurons. After 24 and 72 hours of co-culture with astrocytes with various genotypes, a detailed analysis of neuronal morphology was performed on MAP2 positive neurons using the Neurolucida tracing tool and the Neurolucida Explorer software (**Fig. 6**). After 24 hours of co-culture, the wild type P0 mouse hippocampal neurons had significantly smaller soma size, shorter total neurite length, and fewer number of terminal ends when cultured on mutant V247X, R294X and R306C astrocytes as compared with those cultured on their respective isogenic wild type astrocytes (**Fig. 7A**). The only exception to this the number of terminal ends in the isogenic R294X pair. 100-200 MAP2 positive neurons from co-culture experiments with astrocytes of each genotype were included for analysis at this time point. When those three morphological features were analyzed after 72 hours of co-culture, it appeared that neurons grew bigger in soma size, longer in total neurite length and more terminal ends on both the wild type and mutant astrocytes as compared with their respective marks at the 24-hour time point. More importantly, the neuron co-cultured with the mutant V247X, R294X and R306C astrocytes had significantly smaller soma size, shorter total neurite length, and fewer number of terminal ends when compared with those co-cultured with their respective isogenic wild type counterparts at the 72-hour time point (**Fig. 7B**). One exception was that the soma size was not different between neurons co-cultured on the wild type and mutant astrocytes from the isogenic R306C pair. 97-188 MAP2 positive neurons from co-culture experiments with astrocytes

of each genotype were included for analysis at this time point. Similar morphological deficits were observed in wild type hESC (H9)-derived forebrain neurons co-cultured with mutant RTT astrocytes (**Fig. 8**). To find out whether the morphological deficits may lead to functional changes in these neurons, we co-cultured the wild type hippocampal neurons with either wild type or mutant astrocytes from the R306C pair for 8 days and recording miniature excitatory postsynaptic currents (mEPSCs). While the average mEPSC amplitude was similar between neurons co-cultured with either wild type or mutant astrocytes, the average mEPSC frequency of neurons co-cultured with mutant astrocytes was significantly lower than that of neurons co-cultured with wild type astrocytes (**Fig. 7C-E**). Together, these results revealed both morphological and functional deficits in wild type neurons co-cultured with RTT mutant astrocytes.

Media conditioned by mutant RTT astrocytes have adverse effects on the morphology of wild type mouse hippocampal neurons

Having observed the adverse influence of mutant RTT astrocytes on both mouse and human wild type neurons, we decided to test whether such a non-cell autonomous effect was mediated by factors secreted from the astrocytes as demonstrated in *Mecp2* null mouse astrocytes (Ballas *et al.,* 2009). In this series of experiments, we cultured wild type primary P0 mouse hippocampal neurons in astrocytes-conditioned medium (ACM) collected from each isogenic pair of the wild type and mutant astrocytes, and examined neuronal morphology after 24 and 72 hours of culture (**Fig 9**). At the 24-hour time point, neurons grown in ACM from mutant V247X, R294X and R306C astrocytes had significantly smaller soma size, shorter dendrites and fewer terminal ends than those

grown in ACM from their respective isogenic wild type astrocytes (**Fig. 10A**). 49-122 neurons cultured in ACM from astrocytes of each genotype were included in analysis for this time point. At the 72-hour time point, neurons grown in ACM from mutant R294X and R306C astrocytes had significantly smaller soma size than those grown in ACM from their respective isogenic wild type astrocytes, yet no difference was found when neurons were grown in ACM from the V247X pair; neurons grown in ACM from mutant V247X, R294X and R306C astrocytes had significantly shorter neurites than those grown in ACM from their respective isogenic wild type astrocytes; neurons grown in ACM from mutant R294X astrocytes has significantly fewer terminal ends than those grown in ACM from wild type R294X astrocytes, yet no difference was found when neurons were grown in ACM from the V247X pair and the R306C pair (**Fig. 10B**). 43-123 neurons cultured in ACM from astrocytes of each genotype were included in analysis for this time point.

Mutant RTT astrocytes negatively influence the morphology of co-cultured wild type human interneurons, while wild type RTT astrocytes positively influence the morphology of co-cultured mutant human interneurons

Since the brains of female RTT patients have a mixture of both mutant and wild type neurons and astrocytes due to random XCI, there are four possible interactions concerning these two cell types with two different genotypes. To model each interaction, we differentiated the isogenic pair of R294X iPSC lines into GABAergic interneurons (Liu *et al.,* 2013) and astrocytes, generated co-cultures of all four possible combinations (WT interneuron/WT astrocyte, WT interneuron/MT astrocyte, MT interneuron/WT astrocyte, and MT interneuron/MT astrocyte), and analyzed neuronal morphology after

72 hours of co-culture (**Fig. 11A-B**). To ensure sensitivity and consistency, only GABA-positive interneurons were included in our analysis. For both the total neurite length and the number of terminal ends, mutant astrocytes had a significant negative effect on wild type interneurons (**Fig. 12A**, WT interneuron/WT astrocyte vs. WT interneuron/MT astrocyte, p=0.000004 for neurite length, p=0.02 for terminal ends), while wild type astrocytes had a significant positive effect on mutant interneurons (**Fig. 12A**, MT interneuron/WT astrocyte vs. MT interneuron/MT astrocyte, p=0.0002 for neurite length, p=0.0009 for terminal ends). In addition to the non-cell autonomous effect of astrocytes on neuronal morphology, *MECP2* mutations in interneurons also had negative effect on neuronal morphology (**Fig. 12A**, WT interneuron/WT astrocyte vs. MT interneuron/WT astrocyte, p=0.0001 for neurite length, p=0.01 for terminal ends; WT interneuron/MT astrocyte vs. MT interneuron/MT astrocyte, p=0.02 for neurite length, p=0.006 for terminal ends). Moreover, the astroglial effect and the neuronal effect on neuronal morphology appeared additive (no significant interaction between interneuron and astrocyte detected by two-way ANOVA). Finally, no significant difference was observed in neuronal soma size across the four combinations (**Fig. 12A**).

The effects of IGF-1 and GPE treatment on neuronal morphology in RTT interneuron/astrocyte co-cultures

Currently, both IGF-1 and a modified form of GPE are on clinical trial for treating RTT patients. Yet it is not clear what either reagent may do to RTT human neurons/astrocytes at the cellular level. Thus we examined the effect of short-term treatment with either 100 ng/ml of IGF-1 or 300 ng/ml of GPE on neuronal morphology

in our co-culture system (**Fig. 11A, C, D**). Despite the fact that no difference in neuronal soma size was observed among all four co-culture combinations in the absence of any treatment (**Fig. 12A**), both IGF-1 and GPE significantly increased the neuronal soma size over the untreated condition in almost all combinations (**Fig. 12B**). For the total neurite length, GPE had a significant benefit for both the WT interneuron/MT astrocyte combination and the MT interneuron/MT astrocyte combination (**Fig. 12C**). The beneficial effect of IGF-1, however, was more modest, reaching statistical significance in the MT interneuron/MT astrocyte combination and barely missing the cutoff in the WT interneuron/MT astrocyte combination ($p=0.052$). As for the number of terminal ends, except in the GPE treatment of the MT interneuron/MT astrocyte combination, no significant improvement over untreated condition was observed for either IGF-1 or GPE treatment in any co-culture combination (**Fig. 12D**). Surprisingly, IGF-1 negatively affected the total neurite length and the number of terminal ends in both the WT interneuron/WT astrocyte combination and the MT interneuron/WT astrocyte combination; while GPE negatively affected the total neurite length and the number of terminal ends in the WT interneuron/WT astrocyte combination (**Fig. 12C, D**). Thus, the direction of IGF-1/GPE treatment effect appears to depend on the genotype of RTT astrocyte: IGF-1 and GPE had positive influence on neuronal morphology in co-cultures including mutant astrocytes, but negative morphology influence in co-cultures including wild type astrocytes. As the first step to identify the cellular targets of IGF-1/GPE in our co-cultures, we examined the expression/localization of the known receptor of IGF-1 (IGF-1R). While diffuse IGF-1R immunoreactivity was found in both MAP2-positive neurons and GFAP-positive astrocytes in the co-culture, punctate IGF-1R

immunoreactivity was only found in GFAP-positive astrocytes (**Fig. 13A, B**). Such punctate pattern of the IGF-1R signal was more obvious when astrocytes were cultured alone (**Fig**. **13C**).

Discussion

Previous mouse studies have implicated a potential glial contribution to RTT disease progression (Ballas *et al*., 2009; Maezawa *et al*., 2009; Lioy *et al*., 2011). However, it is critical to validate observations made in *Mecp2* null mice in human cells with actual RTT mutations, because significant differences in biology exist between mice and humans and the complete removal of a gene in mouse is not always the same as expressing a mutant gene in human. Moreover, an earlier study has hinted that some of the non-cell autonomous effect on neurons may be caused by contaminating microglia in the culture (Maezawa *et al*., 2011). In the current study, we have efficiently differentiated RTT iPSCs into $GFAP^+$ astrocytes, and demonstrated that wild type human astrocytes express detectable level of MECP2, and that mutant human astrocytes carrying 3 different RTT mutations have an adverse influence on the morphology and function of wild type neurons. The phenotypes of small neuron, shorter total neurite length and fewer terminal ends observed in our study are consistent with the hallmark pathologies observed in RTT human autopsy samples (Armstrong *et al*., 1995) and RTT mouse models (Chen *et al*., 2001; Kishi *et al*., 2004; Belichenko *et al*., 2008; Belichenko *et al*., 2009). It is worth noting that our *in vitro* differentiation protocol cannot generate microglia, which comes from the hematopoietic lineage. Thus, although our study cannot be used to exclude potential microglial contribution to RTT pathology, the phenotypes observed in our study cannot be caused by microglia. With this agreement between our human data and the previous mouse data, there should be little doubt left that astrocytes indeed express MECP2 and that loss of MECP2 in astrocytes contribute to neuronal abnormalities in addition to cell-autonomous dysfunctions caused by MECP2 deficiency

in neurons. This conclusion has important implications for developing treatments for RTT, because strategies aimed at neuronal defects in the absence of astrocytes may not work efficiently if glial defects are left untreated.

Since the initial discovery, the iPSC technology has been expected to become a powerful tool in modeling human diseases. Our study adds to the growing number of examples that demonstrate cell types of interest differentiated from patient-specific iPSCs may recapitulate certain disease phenotypes, and therefore provide a valid *in vitro* model to study disease mechanisms. In spite of the obvious variation for all three morphological features from neurons exposed to the three wild type astrocytes, our genotype-dependent phenotypes are still readily detectable when comparing the effects of wild type and mutant astrocytes within an isogenic pair. Thus, our study suggests that, as long as the XCI status in female iPSC lines and their derivatives is continuously and carefully monitored, using isogenic controls will significantly increase the sensitivity and reliability in identifying characteristic disease pathologies. Moreover, because our results are mostly consistent among astrocytes carrying 3 different RTT mutations, they strongly suggest that the phenotypes observed in our study were caused by mutations in the *MECP2* gene, but not due to variations inherent to the reprogramming process or the *in vitro* culture/differentiation of the iPSCs and their derivatives. As for the few phenotypic inconsistencies observed across different isogenic pairs, they could be either real differences caused by different RTT mutations or inherent experimental variations. Future studies involving human astrocytes differentiated from additional RTT iPSC lines,

either carrying these same or other RTT mutations, will help distinguish these possibilities.

Because the negative influence of mutant RTT astrocytes detected in the co-culture experiments is largely recapitulated in the ACM culture, cell-cell contact independent mechanisms, namely factors secreted by astrocytes, are at least partially responsible for the phenotypes. The negative effect on neuronal growth could be caused by either the presence of growth-inhibiting factors or the absence of growth-promoting factors in the medium conditioned by mutant RTT astrocytes. Future identification of these factors may facilitate the development of treatments for RTT patients.

By systematically comparing the same morphological features across all four possible combinations of interneurons and astrocytes differentiated from the same isogenic pair of RTT iPSCs, we were able to not only distinguish the contribution from each cell type to the same phenotype, but also determine that the contributions were additive. Such a clear understanding would have been difficult to achieve from studying the intact patient brains where all four types of interneuron-astrocyte interactions are intermingled. In contrast to the clear-cut results from the untreated conditions, the IGF-1/GPE treatment effects are much more complex. On one hand, consistent with their general function as growth factors, both IGF-1 and GPE had positive effects on neuronal soma size (which appeared not affected by the R294X mutation in this specific neuronal type in the absence of IGF-1/GPE) in almost all co-culture combinations. On the other hand, when the total neurite length was compared, the direction of effects of both

treatments showed strong a dependency on the genotype of astrocyte. One potential explanation is that, as suggested by the punctate localization pattern, functional IGF-1Rs are only present on the cell surface of astrocytes in our co-culture system. Maybe the level of IGF-1R is different between the wild type and mutant RTT astrocytes, leading to opposite signaling outcomes when the same amount of exogenous ligand is provided. Alternatively, the opposite treatment effects could be caused by inherent variations in the assay, the choice of drug dosage and treatment time, the maturation status of the interneuron and astrocyte, or a combination of these factors. Although more detailed studies are certainly necessary to distinguish these possibilities, our results nonetheless provide a cautionary note that the outcome of IGF-1 therapies may be complex at the cellular level.

Methods

Cell culture

Media compositions:

Pluripotent stem cell media (PSCM): DMEM/F12 with 20% KOSR, 1x NEAA, 1x pen/strep, and 1 mM L-glutamine (all from Invitrogen) and 0.1 mM ß mercaptoethanol (Sigma).

Neural media (NM): DMEM/F12 with 1% N2, 1x NEAA, 1x pen/strep and 2 µg/ml heparin (Sigma H3149). Supplemented with SHH (1,000 ng/ml; 1845-SH; R&D System)/or Purmorphamine (1.5μM, StemGent, cat. no. 04-0009) where noted.

Astroglial media (AM): NM with the addition of 10ng/ml EGF (PeproTech) and 10 ng/ml recombinant human FGF2.

Astroglial differentiation media (ADM): NM with the addition of 10 ng/mL CNTF (BioSensis).

Neurobasal media (NBM): Neurobasal media with 1% N2, 2% B27, 0.5% Glutamax and 1x pen/strep (all from Invitrogen). Supplemented with 10, 100 ng/mL IGF-1 (PeproTech) or 100, 300 ng/mL GPE (Bachem) where noted.

iPSC maintenance

RTT patient-specific iPSCs used in this study have been previously described in (Ananiev *et al*., 2011). In addition, a pair of isogenic iPSCs were derived from a RTT patient carrying the R306C mutation (a different patient from the GM11270 Corielle fibroblast line) at the Waisman Center iPSC Core using the originally reported retrovirus-based method (Takahashi *et al*., 2007). iPSC lines at the following passage numbers were used to derive the astroglial progenitor lines presented in this study: passage 27 (P27) and

P21 for V247X-WT, P23 and P25 for V247X-MT, P13-14 for R294X-WT, P25 and P39 for R294X-MT, P34 for R306C-WT, P38 for R306C-MT. Several astroglial progenitor lines were derived from each isogenic iPSC pair to verify the similarity in astroglial specification between wild type and mutant RTT lines. The human embryonic stem cell (hESC) line H9 at P41-P47 was used for forebrain neuron differentiation. iPSC lines at the following passage numbers were used for interneuron (IN) differentiation: P25-31 for R294X-WT and P48-54 for R294X-MT. iPSC and hESCs were propagated with pluripotent stem cell media (PSCM) containing 4 ng/ml recombinant human FGF (Waisman Center Biomanufactoring) and passaged using 1 unit/ml dispase (Invitrogen) on a layer of irradiated mouse embryonic fibroblasts (WiCell Research Institute).

Astroglial differentiation

Astroglial progenitors were differentiated from iPSCs as previously described (Krencik *et al*., 2011). Briefly, RTT iPSCs and hESCs (H9) were first differentiated to neuroepithelia in the absence of regionalizing morphogens with cells patterned toward the default forebrain fate. At day 14 of differentiation, adherent neural progenitors were expanded in a suspension culture with NM. On day 21, media was switched to AM. These neural progenitor spheres were propagated first by tituration with a flamed polished Pasteur pipette (days 21-90) followed by dissociation with 1x accutase (Innovative Cell Technologies), resulting in a rapidly dividing monolayer culture that eventually lifted and formed astroglial progenitor spheres. Terminal differentiation into astrocytes from astroglial progenitors was achieved by dissociating progenitors into single cell with 1x accutase, and plating at a density of $3x10^4$ cells per coverslip in ADM

with 10% FBS (Gibco). The following day, fresh ADM without FBS was added. Differentiated progenitors were then fed every other day and used for experimentation 7 days after the start of terminal differentiation.

Neuronal differentiation

RTT iPSCs were differentiated to GABAergic interneurons (IN) as described (Liu *et al.,* 2013). Briefly, to induce MGE-like progenitors, primitive neuroepithelial cells were treated with SHH or Purmorphamine on day 10–26. Neuroepithelia were gently blown off on day 26 and grown in suspension with NBM. At day 36-40, patterned neurospheres were treated with accutase, titurated into single cell and co-cultured at a density of 6 x10^4 cells per coverslip upon RTT iPSC-derived astrocytes for 72 hours. Upon plating, MGE-like progenitors produced GABAergic IN. IGF-1 and GPE 72 hour treated co-cultures were treated at plating, with fresh media replaced every 24 hours. Dr. Yan Liu from the laboratory of Dr. Su-Chun Zhang performed the initial patterning of neuroepithelia and provided technical expertise. hESCs (H9) were differentiated to neurons as previously described (Johnson *et al*., 2007). Day 21 neurospheres were subjected to a mild accutase treatment and were co-cultured with RTT iPSC-derived astrocytes for 72 hours, generating post-mitotic forebrain neurons upon plating.

Primary mouse hippocampal culture

Hippocampi from postnatal day 0 (P0) C57BL/6 pups were dissected and dissociated into single cells using the Papain Dissociation System (Worthington Biochemical Corporation LK003153).

Co-culture of mouse hippocampal neurons and RTT iPSC-derived astrocytes

On day 6 of astroglial terminal differentiation, NBM was added. The following day, mouse hippocampal neurons were plated at a density of $2x10^4$ cells per coverslip and co-cultured for 24 and 72 hours.

ACM culture

ACM was made by conditioning NBM with terminally differentiated astroglia for 24 hours and passing through a 70μm cell strainer (performed at plating, 24 and 48 hours post-plating). Mouse hippocampal neurons plated at a density of $2x10^4$ cells per coverslip were cultured in the presence of ACM for either 24 or 72 hours. In the 72 hour culture, fresh ACM was made and replaced every 24 hours.

Immunocytochemistry

Cultures were fixed on ice with 4% paraformaldehyde for 30 minutes, washed 3 times with PBS for 15 minutes each wash at room temperature (RT), permeablized with 1% Triton X100 (Sigma) for 30 minutes at RT, blocked with 3% normal donkey serum, 0.25% Triton X100 in PBS for 60 minutes at RT, incubated with primary antibodies overnight at 4°C, washed 3 times with PBS for 15 minutes at RT, incubated with the corresponding secondary antibodies for 60 minutes at RT, and washed 3 times with PBS for 15 minutes at RT. Primary antibody dilutions were as follows: anti-S100ß (Abcam ab868, 1:500), anti-GFAP (NeuroMab clone N20A/8, 1:500 and Millipore MAB3402, 1:500), anti-MAP2 (Abcam ab32454, 1:500), anti-GABA (Sigma A2052, 1:500), anti-IGF-1R (Abcam ab90657, 1:300). Secondary antibody dilutions were as follows: Alexa Fluor 568 Donkey anti-Rabbit antibody (Invitrogen A10042, 1:500), Alexa Fluor 488

Donkey anti-mouse antibody (Invitrogen A21202, 1:500). DAPI was used at 3nM for counterstaining.

Stereology

Terminally differentiated astroglia were immunostained with anti-GFAP antibody and counterstained with DAPI. Cells were viewed with a Zeiss photomicroscope at 20X. Stereology was performed with the Stereo Investigator software (MicroBrightField). At least two biological replicates were performed for each astroglial line. The optimal number of counting sites was determined empirically based upon a Scheaffer CE value less than 0.30. Results were quantified as percent of $GFAP^+$ cells of the total $DAPI^+$ cell count.

Western blot analysis

One million astroglial progenitors were differentiated for one week and collected. Western blot preparations were optimized by Ronghui Li from the laboratory of Dr. Qiang Chang. Nuclear extract from each culture was prepared using NE-PER Nuclear and Cytoplasmic Extraction Reagents (Thermo Scientific). Nuclear extracts were resolved on 10% SDSPAGE and transferred onto Protran BA85 nitrocellulose membranes (Whatman). The membrane was blotted with anti-MeCP2 antibody (either 1:4,000, Diagenode or 1:2,000, Abcam C-terminal epitope) and infrared dye-conjugated secondary antibody (1:10,000, Thermo Scientific), and scanned by the Odyssey infrared imaging system.

Morphological analysis of neurons co-cultured with RTT iPSC-derived astrocytes or cultured in ACM

H9 neuron and P0 hippocampal cultures were stained with anti-MAP2 antibody while IN co-cultures were stained with anti-GABA and anti-MAP2 antibodies and imaged with an Olympus BX51microscope. For IN co-cultures, $GABA^+$ cells were identified for analysis. MAP2 labeled neuronal soma and neurites were traced using Neurolucida (MicroBrightField) and analyzed with Neurolucida Explorer (MicroBrightField). The staining, imaging and tracing steps were performed by different researchers in the triple blind manner. Staining was performed by Ahmed Mohammed and Benjamin Lin of the laboratory of Dr. Qiang Chang, while imaging of coded samples was performed by Emily Cunningham Williams, also from the laboratory of Dr. Qiang Chang. The following undergraduates from the laboratory of Dr. Qiang Chang performed neuron tracing: Ahmed Mohammed, Benjamin Lin, Cassandra Chiao, Rachel Cherney, Jonathan Mok and Austin Becker.

Allele-specific transcription of *MECP2* and *XIST*

Genotyping was performed for iPSC and astroglial lines as previously described (Ananiev *et al*., 2011). RNA was prepared using the SV Total RNA Isolation kit (Promega). cDNA was made using the qScript cDNA SuperMix (Quanta Biosciences). Primers: Forward GCAAAGCAGAGACATCAGAA,
reverse 1 (for V247X) CAGATCGGATAGAAGACTCC,
reverse 2 (for R294X, R306C) GCCCAGGGCTCTTACAGGTC. The *XIST* SNP assay was performed as previously described (Ananiev *et al*., 2011). Purified PCR products were directly sequenced.

Human androgen receptor assay

The human androgen receptor assay was preformed as previously described (Ananiev *et al*., 2011). Briefly, 500 ng of genomic DNA was digested with Hha I (cut samples) with uncut samples processed in tandem. PCR amplification was performed as previously described (Ananiev *et al*., 2011), using a forward primer labeled with 6-FAM on the 5' end. PCR amplicons were resolved on a genetic analyzer. The GeneScan data was analyzed and the peak area measured using ABI Peak Scanner software.

qRT-PCR

One million astroglial progenitors were differentiated for one week and collected. Other cell types were collected at a density to obtain ~1μg total RNA. cDNA was prepared as described in genotyping. GAPDH was used as a normalization control. At least two separate astroglial differentiations were used for transcriptional analysis. Primers were as follows: OCT4 (Accession number NM_002701), Forward: 5'-CAGTGCCCGAAACCCACAC-3', Reverse: 5'-GGAGACCCAGCAGCCTCAAA-3'; NFIX (Accession number NM_002501), Forward: 5'- ATGTACTCCCCGTACTGCCTC -3', Reverse: 5'-ACATCCGCTTTTCATGCTTCTT -3'; GAPDH (Accession number NM_002046), Forward: 5'- GTGGACCTGACCTGCCGTCT-3', Reverse: 5'-GGAGGAGTGGGTGTCGCTGT-3'. Primers were obtained from Krencik *et al*., 2011 (*NFIX*) and Yu *et al*., 2007 (*GAPDH* and *OCT4*).

Electrophysiology

Dissociated hippocampal neurons were isolated from postnatal day 0-1 C57BL/6 pups and seeded on RTT iPSC-derived astrocytes. Recordings were performed by Dr.

Xiaofen Zhong, a former postdoc in the Chang lab. Whole-cell patch-clamp recording was performed on day 8 of co-culture at ambient temperature. Coverslips with the cultured hippocampal neurons were put into the chamber which was continuously perfused with external recording solution containing (in mM) 140 NaCl, 3 KCl, 15 Hepes, 1 MgCl2, 2 CaCl2, 20 Glucose (pH7.4, 300 ± 5 mmol/kg). 1 μM TTX and 10 μM Bicuculline were added to the bath solution during the duration of the recording process. The patch pipette (3 to 5 MΩ) solution contained (in mM) 140 K-gluconate, 7.5 KCl, 10 Hepes-K, 0.5 EGTA-K, 4 Mg-ATP and 0.3 Li-GTP (pH7.4, 290± 5 mmol/kg). Hippocampal neurons were visualized with an Olympus Optical (Tokyo, Japan) BX51WI microscope. The neurons were held at -70 mV. Whole-cell capacitance compensation was applied. The mEPSCs recording started 3 min after whole-cell voltage clamp configuration was established and lasted for 6 min on a gap free mode. Recordings with series resistance (Rs) greater than 20 MΩ were excluded. Raw data were amplified with a Multiclamp 700B amplifier, acquired with pClamp10.2 software (Molecular Devices, Sunnyvale, CA). Signals were filtered at 2 Hz and sampled at 10 kHz by Digidata 1440A (Molecular Devices). Digital Gaussian filter (1 kHz) was applied and mEPSCs were analyzed using the Template Search tool of the Clampfit10.2 software (Molecular Devices). The mEPSC events were accepted manually. All group data were shown as mean ± standard error of the mean (SEM). All results were analyzed via t-test with repeated measures. Significance for all tests was set at $p < 0.05$.

Statistical analyses

For neuronal morphological measures in the RTT interneuron/astrocyte co-culture with no treatment (**Fig. 12A**), a two-way ANOVA analysis was performed first, which

was followed by Post Hoc pairwise comparison between groups of interest. The outputs from SAS 9.3 for between-subject effects were presented as **Table 1** in the supplementary data file. For neuronal morphological measures in the RTT interneuron/astrocyte co-culture with IGF-1/GPE treatment (**Fig. 12**), a three-way ANOVA analysis was performed first, which was followed by Post Hoc pairwise comparison between groups of interest. The outputs from SAS 9.3 for between-subject effects were presented as **Table 2**. For all other experiments in this study, Student's two tailed t-tests were used for pairwise comparisons unless stated otherwise.

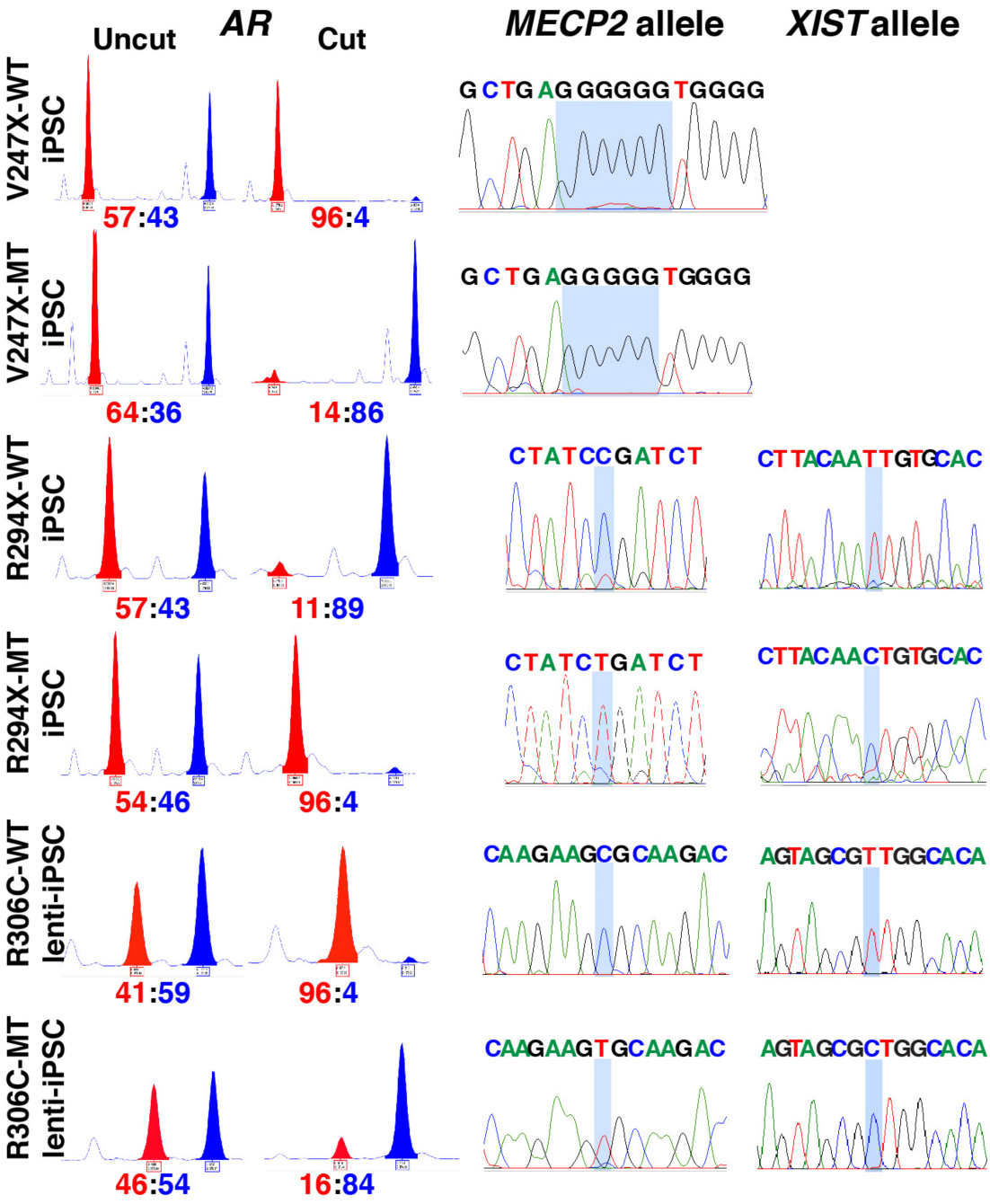

Figure 1. XCI status of isogenic RTT iPSC pairs used in this study

Results of three assays used to genotype isogenic RTT iPSC pairs. (Left) The AR assay was used to determine the XCI status of iPSC lines. Uncut traces verified the presence of

both parental AR alleles: 165 bp and 180 bp for the V247X lines, 165 bp and 171 bp for the R294X lines, 173 bp and 176 bp for the R306C lines. Cut traces of iPSCs verified the presence of only one *AR* allele due to skewed, nonrandom XCI. The source of genomic DNA is labeled to the left of each trace. The ratio between the two AR alleles is at the bottom of each trace. (Middle) Sequencing traces of regions of the *MECP2* gene that contain RTT mutations to distinguish allele-specific transcription of MECP2 in V247X-WT-iPSC, V247X-MT-iPSC, R294X-WT-iPSC, R294X-MT-iPSC, R306C-WT-iPSC, and R306C-MT-iPSC.The source of RNA is labeled in the left-most column. (Right) Sequencing traces of *XIST* SNP analysis to distinguish allele-specific transcription in R294X-WT-iPSC, R294X-MT-iPSC, R306C-WT-iPSC and R306C-MT-iPSC. SNP 1 (C or T) was examined in R294X-WT-iPSC and R294X-MT-iPSC. SNP 2 (C or T) was examined R306C-WT-iPSC and R306C-MT-iPSC. V247X-WT-iPSC and V247X-MT-iPSC are homozygous at both loci. The source of RNA is labeled in the left-most column. WT denotes expression of the wild type *MECP2* allele. MT denotes expression of the mutant *MECP2* allele. The shaded area marks the position of nucleotide that is different between WT and MT.

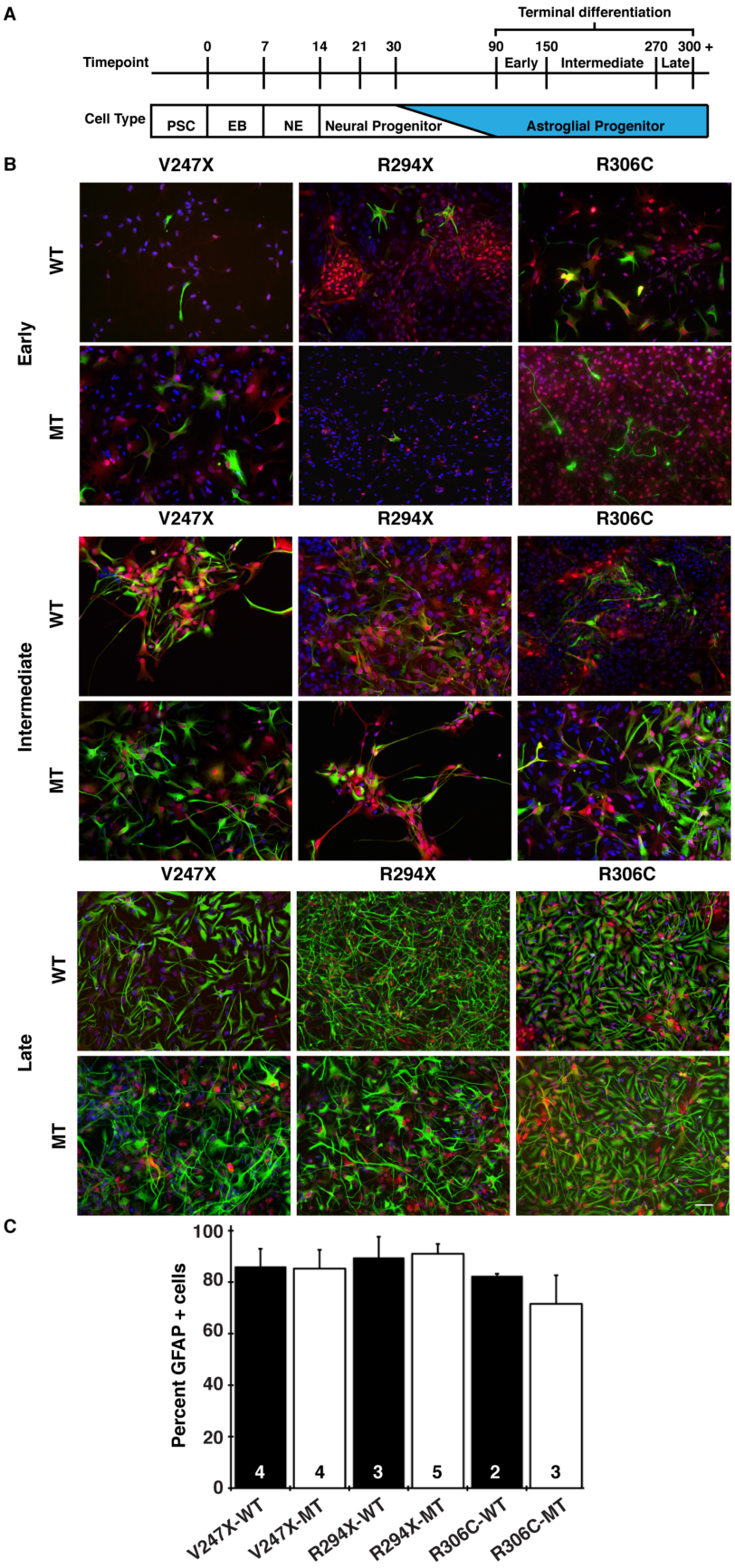
A
Terminal differentiation
Timepoint
0
7
14
21
30
90
150
270
300 +
Early
Intermediate
Late
Cell Type
PSC
EB
NE
Neural Progenitor
Astroglial Progenitor
B
V247X
R294X
R306C
Early
Intermediate
Late
WT
MT
C
Percent GFAP + cells
100
80
60
40
20
0
4
4
3
5
2
3
V247X-WT
V247X-MT
R294X-WT
R294X-MT
R306C-WT
R306C-MT

Figure 2. Differentiation of isogenic RTT iPSC lines into GFAP+ astrocytes

(A) A schematic of the differentiation timeline of pluripotent stem cells (PSCs) into astroglial progenitors. Timepoints presented in days. Day 0 represents the start of differentiation from PSCs. EB= embryoid body, NE= neuroepithelium. **(B)** Terminal differentiation of astrocytes from astroglial progenitor lines at early (90-150 days), intermediate (150-270 days) and late (270-300+ days) stages of differentiation from isogenic wild type (WT) and mutant (MT) RTT iPSC lines carrying the V247X, R294X and R306C mutations. Astroglial progenitors were labeled with S100ß (red) and definitive astrocytes were labeled with GFAP (green). Scale bar = 50μm. The scale bar at the bottom right corner of the last image applies to all images in this figure. **(C)** Stereological analysis of the purity of astrocytes differentiated from late astroglial progenitors as determined by the percentage of $GFAP^+$ cells of the total $DAPI^+$ cells. WT lines (black bars), MT lines (white bars). Error bars are standard error of the mean (SEM). The number of replicates assayed for each line is presented within its bar.

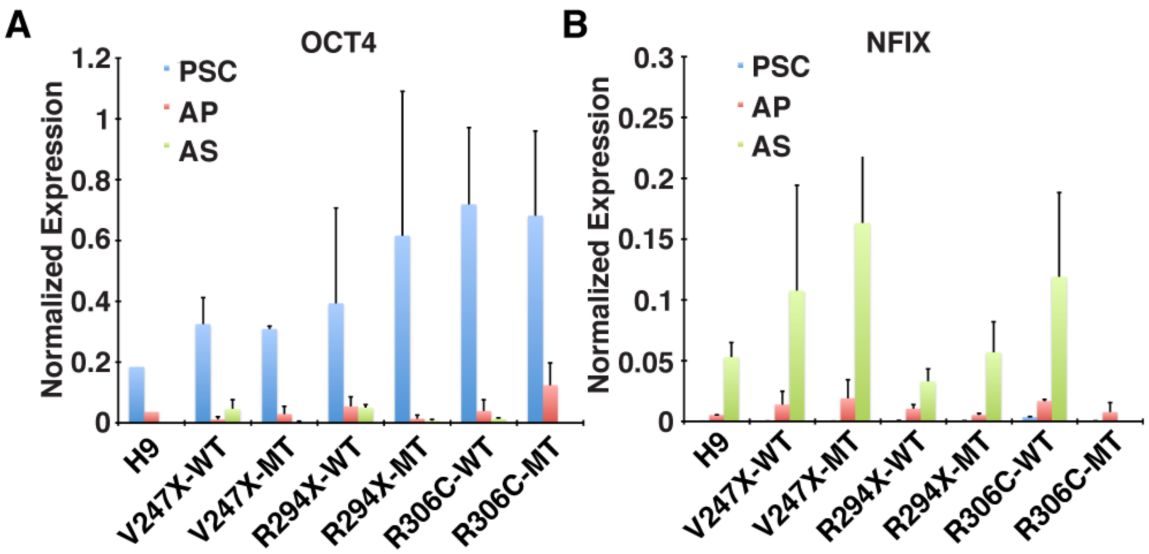

Figure 3. Expression of cell type markers in glial differentiation

(A-B) Graphs of quantitative PCR assay of cell type specific transcripts**.** The assayed gene is listed at the top of each graph. For both graphs, each iPSC line and its differentiated derivatives are arranged as follows: iPSC (blue bars), astroglial progenitor (pink bars) and terminally differentiated astrocyte (green bars). The source of RNA is listed below each bar. Values are normalized to GAPDH levels. Error bars represent standard error of the mean. Transcripts were assayed from at least two biological replicates and in the case of astrocytes, from at least two separate terminal differentiations. **(A)** Transcript levels of the pluripotency gene *OCT4* are upregulated in iPSCs while downregulated in differentiated cells. **(B)** Transcript levels of the astrocyte specific transcription factor NFIX are upregulated in terminally differentiated astrocytes compared to astroglial progenitors and PSCs.

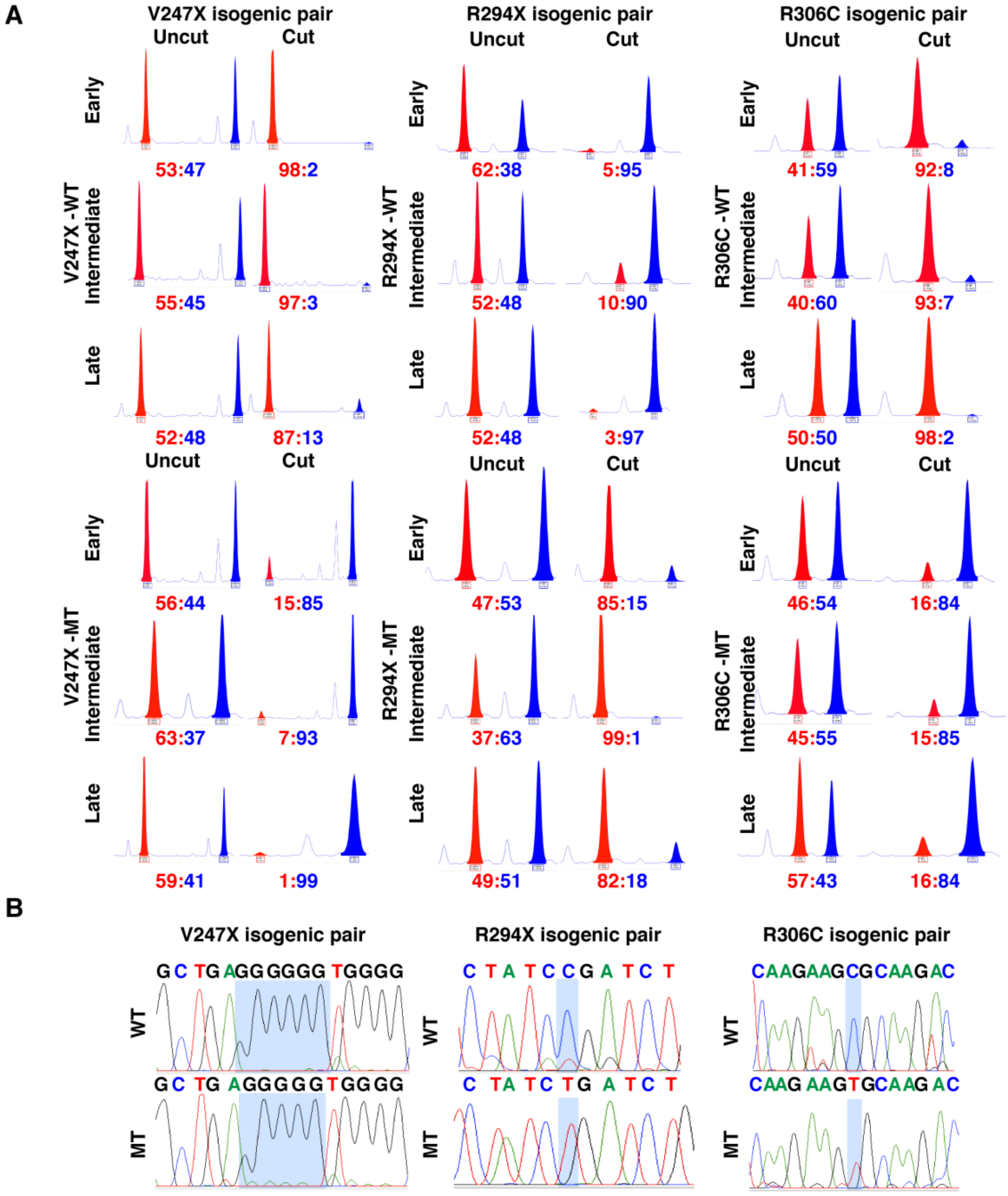

Figure 4. Maintenance of the isogenic status in astroglial progenitors differentiated from isogenic RTT iPSC lines

(A) Human androgen receptor (AR) methylation profiles for isogenic wild type (WT) and mutant (MT) RTT astroglial progenitors (AP) carrying the V247X, R294X and R306C

mutations at the early, intermediate and late stages of astroglial differentiation. Uncut traces show the presence of both parental AR alleles: 165 bp and 180 bp for the V247X lines, 165 bp and 171 bp for the R294X lines, and 173 bp and 176 bp for the R306C lines. Cut traces of astroglial progenitors verified the presence of only one *AR* allele due to skewed, nonrandom XCI, which remained constant throughout the directed differentiation. The source of genomic DNA is labeled to the left of each trace. The ratio between the two AR alleles is at the bottom of each trace. **(B)** Representative sequencing traces of allele-specific *MECP2* expression in each of the isogenic astroglial progenitor pairs. The shaded area marks the position of nucleotide that is different between WT and MT.

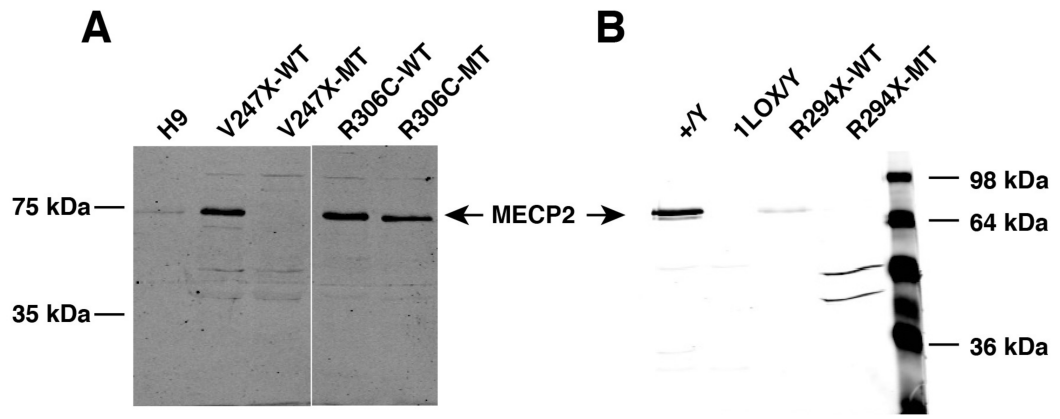

Figure 5. WT astrocytes express detectable levels of MECP2 protein

(A-B) MECP2 protein expression in astrocytes terminally differentiated from late phase RTT astroglial progenitors. **(A)** The MECP2 band was detected at ~75kDa in astrocytes differentiated from H9, V247X-WT, R306C-WT and R306C-MT astroglial progenitors but not in astrocytes differentiated from V247X-MT and R294X-MT astroglial progenitors. (**B)** MECP2 band detected in WT male (+/Y) mouse brain lysate, R294X-WT astrocytes but not MECP2-KO male mouse brain lysate (1LOX/Y) or in astrocytes differentiated from R294X-MT astroglial progenitors. The anti-MECP2 antibody used was raised against a C-terminal epitope and as such, cannot distinguish against the R306C missense mutation.

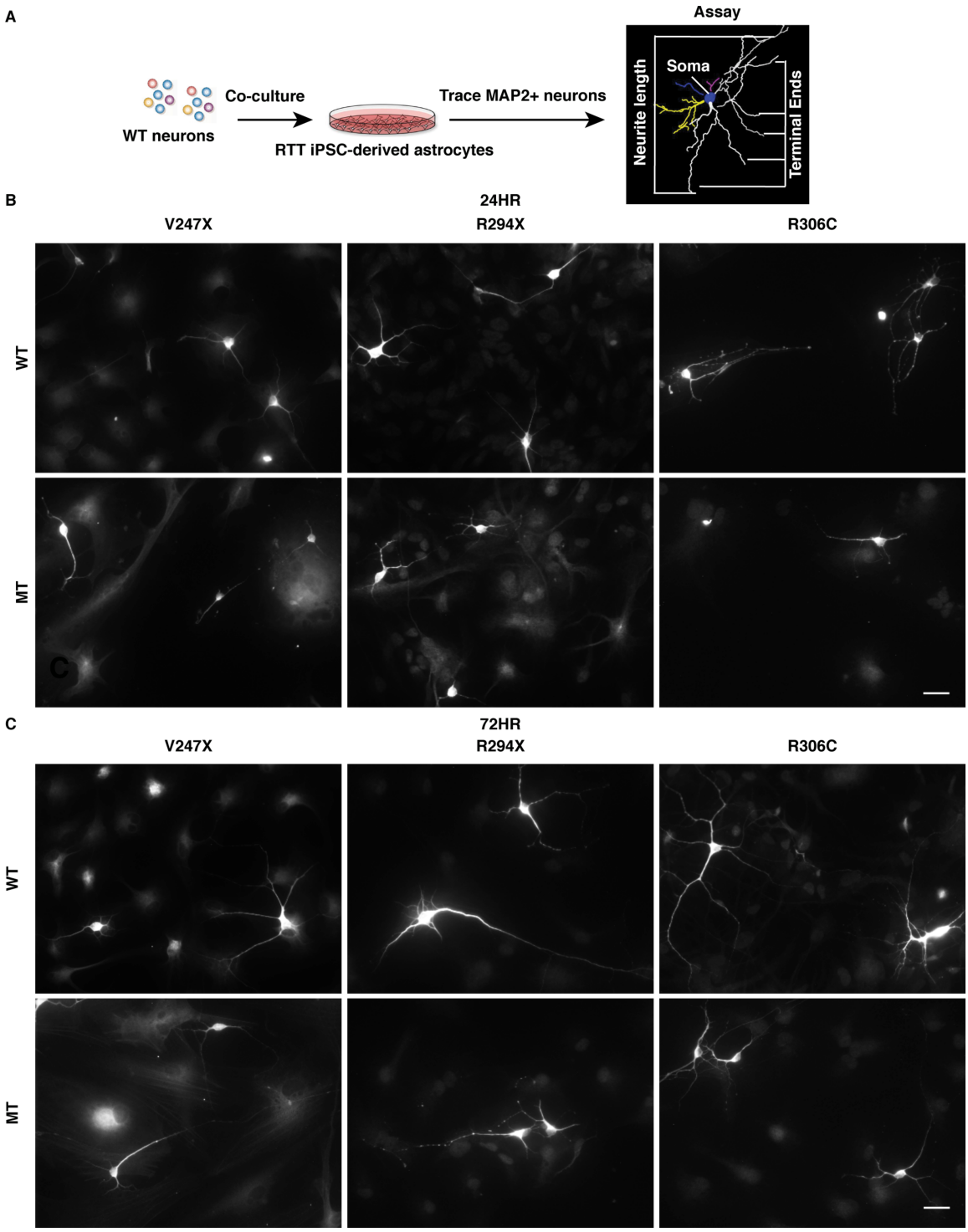

Figure 6. Schematic of experimental design and representative images of wild type mouse hippocampal neurons co-cultured on wild type and mutant RTT astrocytes

(A) A schematic of the mouse neuron/human astrocyte co-culture system and the

morphological analysis. Primary wild type mouse hippocampal neurons were co-cultured with either wild type (WT) or mutant (MT) astrocytes differentiated from each isogenic RTT pair and assayed for area of the neuronal soma, total neurite length and total number of terminal ends. **(B-C)** Representative images of MAP2 labeled neurons used to conduct morphological analysis at 24 **(B)** and 72 **(C)** hours of co-culture. Scale bar = 50μm. The scale bars apply to all images in this figure.

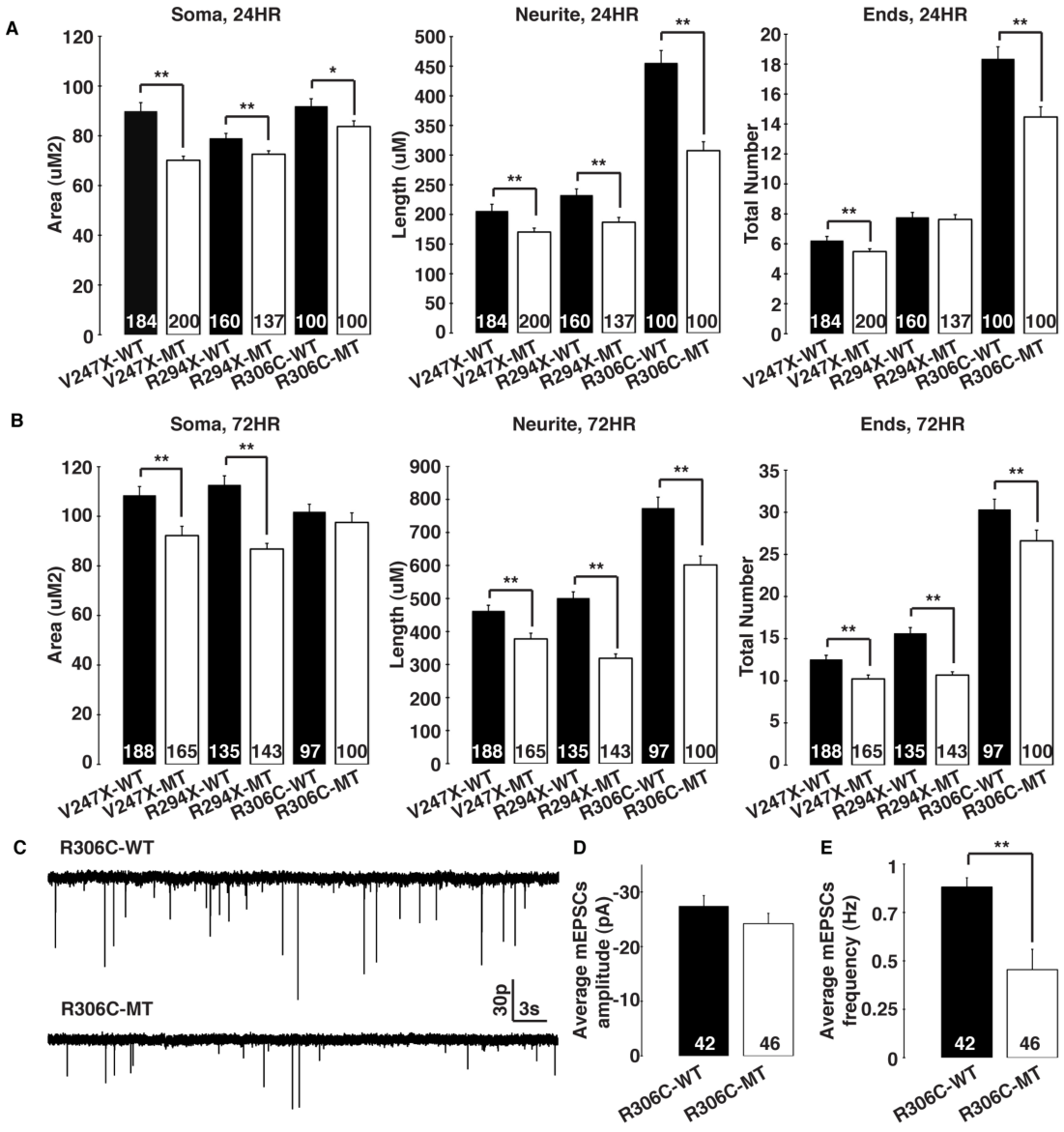

Figure 7. Morphological and functional defects of wild type mouse hippocampal neurons co-cultured on mutant RTT astrocytes

(A-B) Quantification of neuronal soma area, total neurite length and total number of terminal ends of the wild type neurons co-cultured for 24 (**A**) and 72 (**B**) hours with either WT or MT RTT astrocytes. Black bars indicate neurons co-cultured with wild type astrocytes while white bars indicate neurons co-cultured with mutant RTT astrocytes. Error bars = SEM, * = $p<0.05$, ** = $p<0.005$. The number embedded in each bar

represents the number of neurons analyzed for that condition. **(C)** Representative sample traces of mEPSCs recorded from wild type mouse hippocampal neurons (8 DIV) co-cultured on either wild type (WT) or mutant (MT) astrocytes differentiated from the R306C isogenic RTT pair. (**D-E**) Quantification of mEPSC amplitude (**D**) and frequency (**E**) recorded from the wild type neurons co-cultured with either WT (black bars) or MT (white bars) RTT astrocytes. The number embedded in each bar represents the number of neurons analyzed for that condition. Error bars = SEM, ** = $p<0.005$.

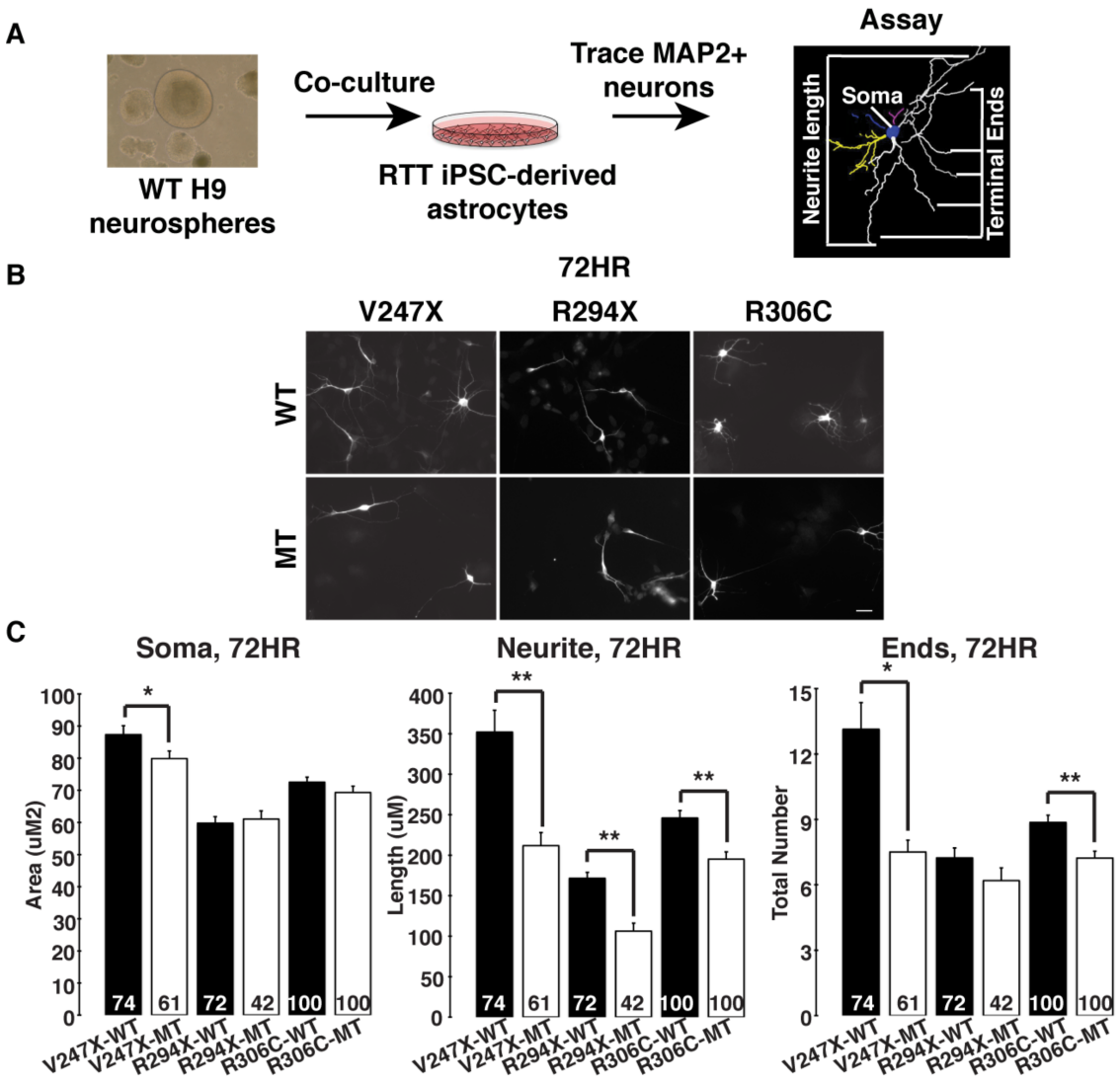

Figure 8. Schematic of experimental design, representative images and effect of wild type human forebrain neurons co-cultured on wild type and mutant RTT astrocytes

(A) A schematic of the human neuron/human astrocyte co-culture system and the subsequent morphological analysis. Wild type hESC (H9)-derived neurospheres were differentiated into post-mitotic neurons on either wild type (WT) or mutant (MT) astrocytes differentiated from each isogenic RTT pair and assayed for area of the neuronal soma, total neurite length and total number of terminal ends. **(B)** Representative images of MAP2 labeled neurons used to conduct morphological analysis at 72 hours of

co-culture. Scale bar = 50μm. The scale bar applies to all images in this figure. The number embedded in each bar represents the number of neurons analyzed for that condition. **(C)** Quantification of neuronal soma area, total neurite length and number of terminal ends of wild type human neurons after 72 hours co-culture with either WT (black bars) or MT (white bars) RTT astrocytes. * = $p<0.05$, ** = $p<0.005$.

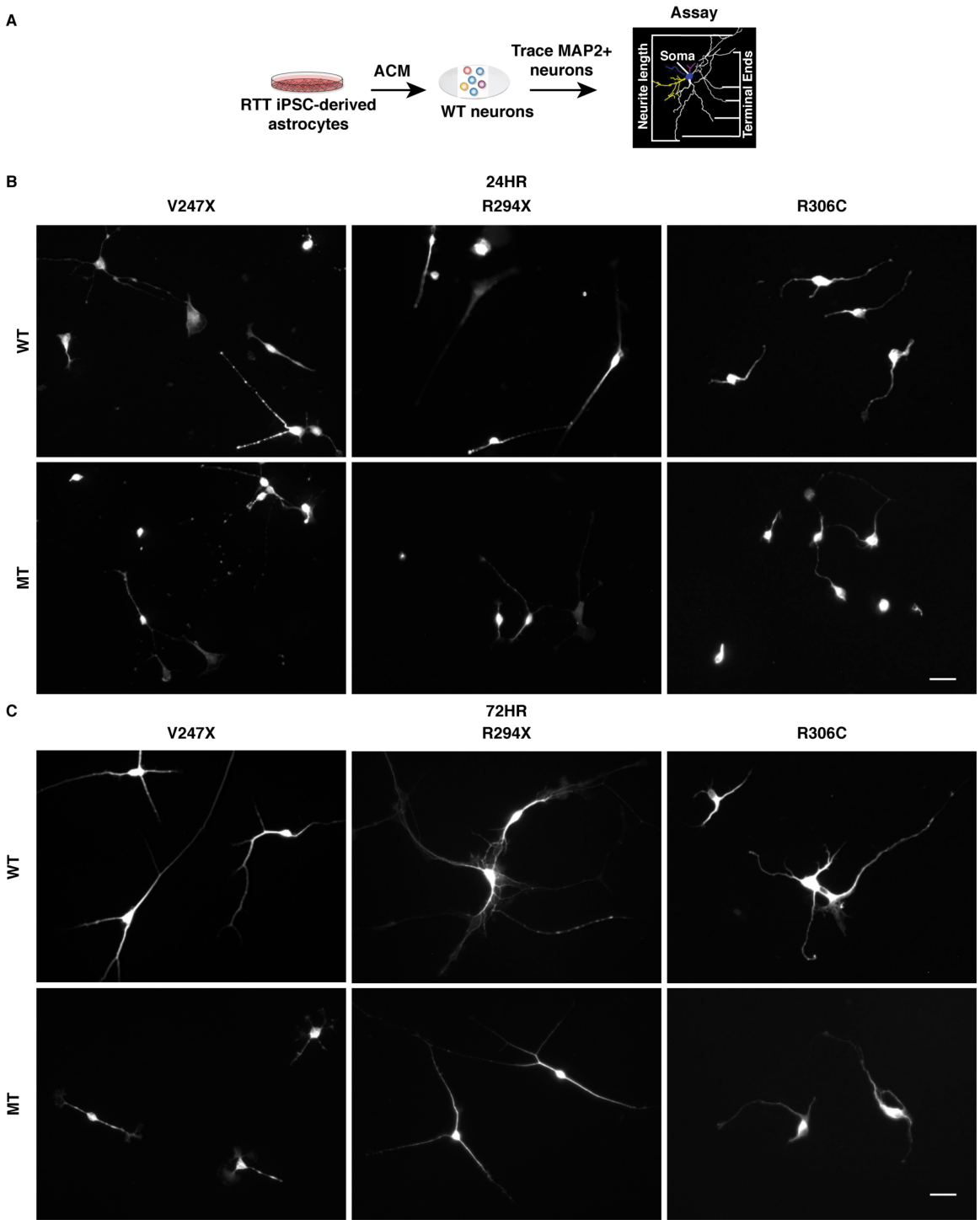

Figure 9. Schematic of experimental design and representative images of wild type mouse hippocampal neurons cultured in medium conditioned by wild type and mutant RTT astrocytes

(A) A schematic of the astrocyte conditioned media (ACM) culture system and morphological analysis. Primary wild type mouse hippocampal neurons were cultured in the ACM from either wild type (WT) or mutant (MT) astrocytes from each isogenic RTT pair and assayed for area of the neuronal soma, total neurite length and total number of terminal ends. **(B-C)** Representative images of MAP2 labeled neurons used to conduct morphological analysis after 24 **(B)** and 72 **(C)** hours of culture in ACM. Scale bar = 50μm. The scale bars apply to all images in this figure. The number embedded in each bar represents the number of neurons analyzed for that condition.

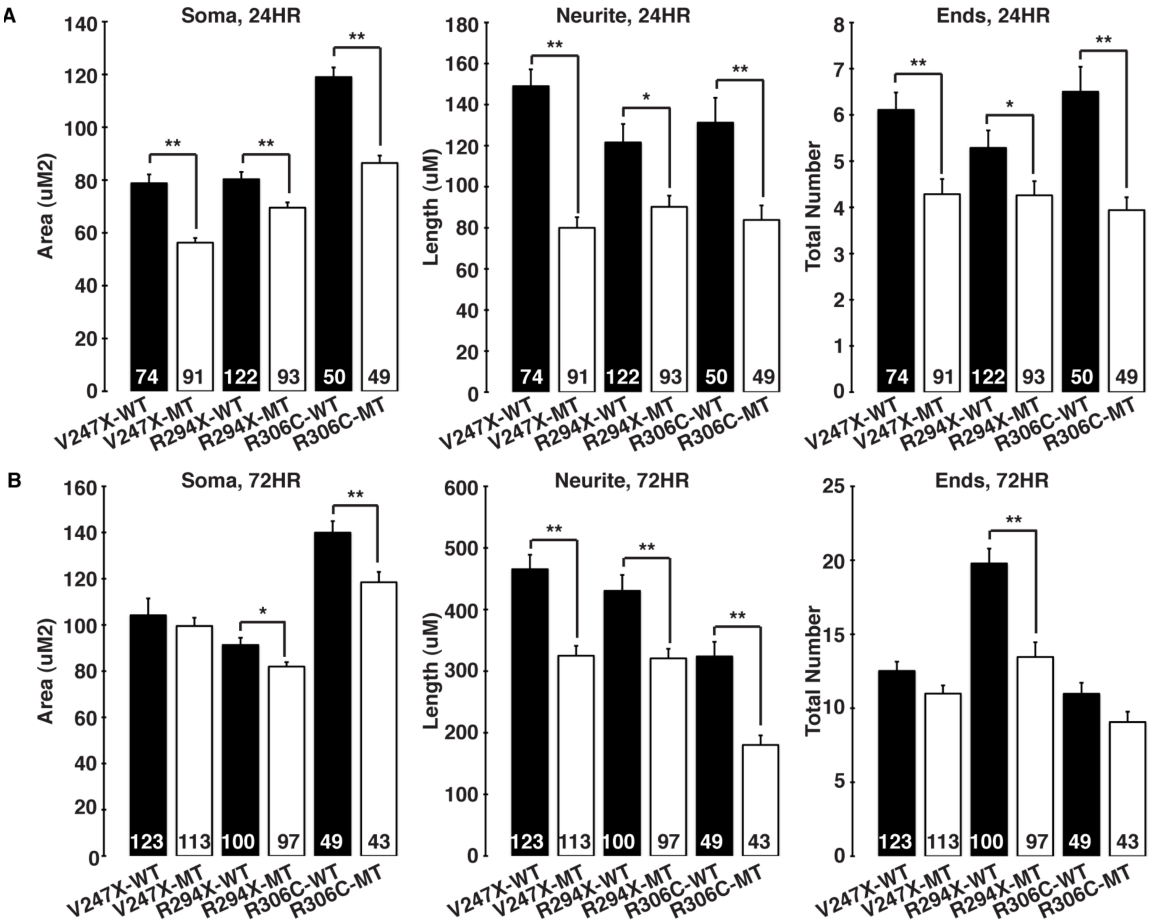

Figure 10. Morphological defects of wild type mouse hippocampal neurons cultured in medium conditioned by mutant RTT astrocytes

Quantification of neuronal soma area, total neurite length and number of terminal ends of wild type neurons after 24 (**A**) and 72 (**B**) hours of culture in either WT (black bars) or MT (white bars) ACM. Error bars = SEM, * = $p<0.05$, ** = $p<0.005$. The number embedded in each bar represents the number of neurons analyzed for that condition.

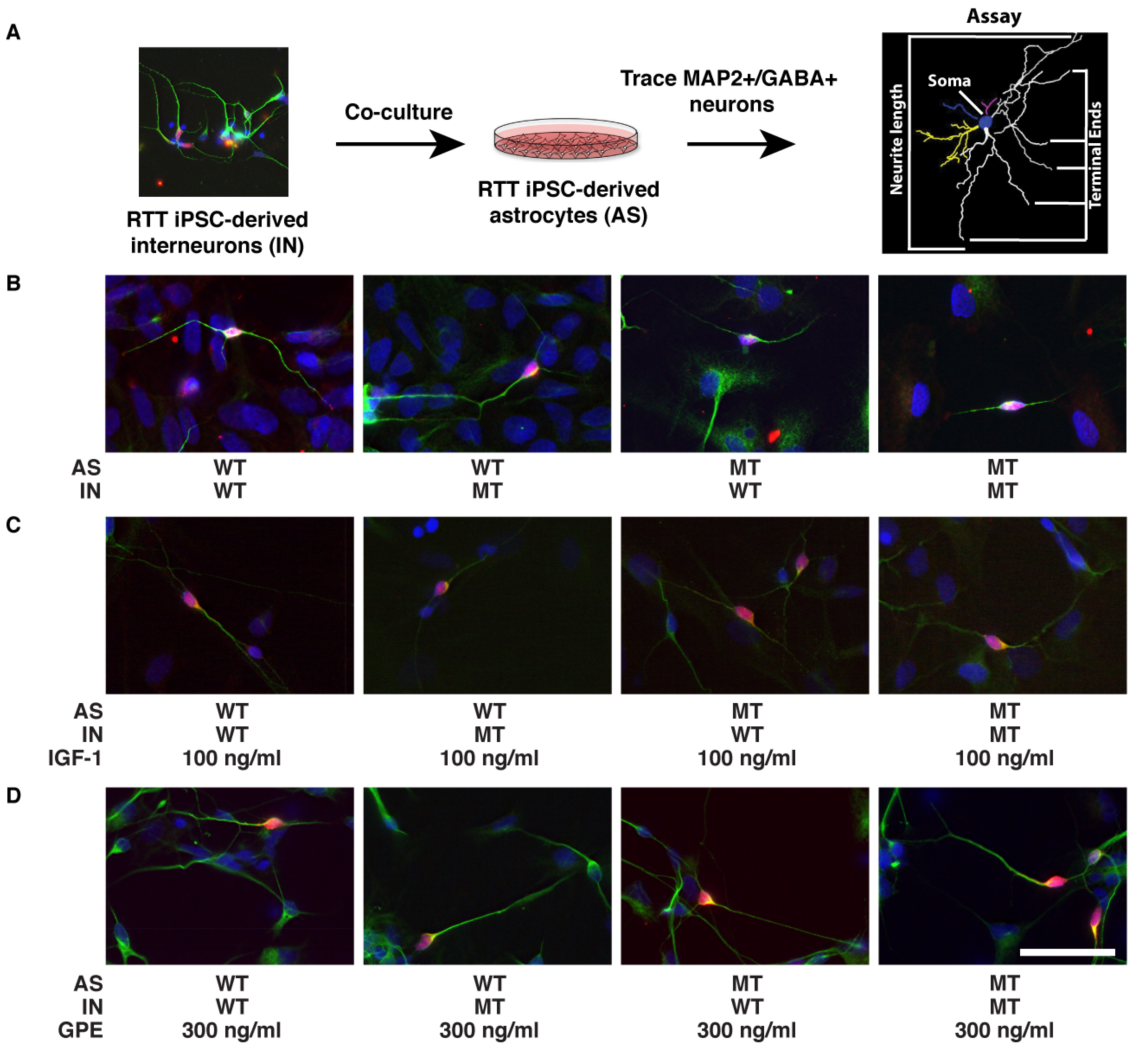

Figure 11. Schematic of experimental design and representative images of WT and MT RTT GABAergic interneurons co-cultured on WT and MT RTT astrocytes and effects of IGF-1/GPE treatment

(A) A schematic of the human interneuron(IN)/human astrocyte(AS) co-culture system with treatment and the subsequent morphological analysis. RTT MT and WT control neurospheres were differentiated into post-mitotic GABAnergic IN on either wild type (WT) or mutant (MT) R294X astrocytes and assayed for area of the neuronal soma, total neurite length and total number of terminal ends. **(B-D)** Representative images of MAP2/GABA labeled neurons used to conduct morphological analysis after co-cultures

were either untreated **(B)**, treated with 100ng/ml IGF-1 **(C)** or treated with 300ng/ml GPE **(D)** for 72 hours. Scale bar = 50μm. The scale bar applies to all images in this figure. Labels delineating the co-culture permutation and treatment conditions are listed below each image.

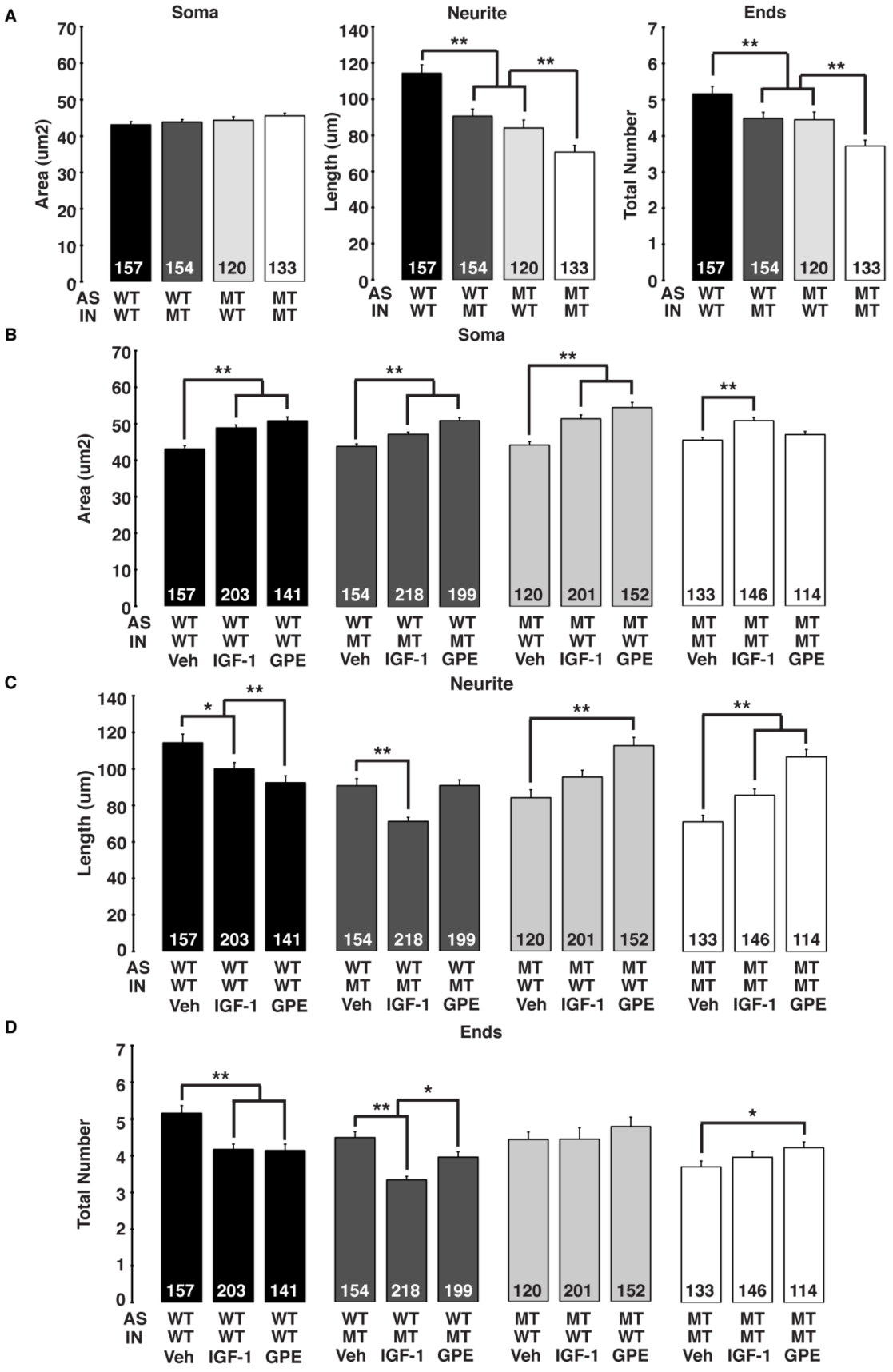
A
Soma
Area (um2)
Neurite
Length (um)
Ends
Total Number
**
157
154
120
133
AS WT WT MT MT
IN WT MT WT MT
B
Soma
Area (um2)
157 203 141 154 218 199 120 201 152 133 146 114
AS WT WT WT WT WT WT MT MT MT MT MT MT
IN WT WT WT MT MT MT WT WT WT MT MT MT
Veh IGF-1 GPE Veh IGF-1 GPE Veh IGF-1 GPE Veh IGF-1 GPE
C
Neurite
Length (um)
*
D
Ends
Total Number

Figure 12. Morphological effects of WT and MT RTT GABAergic interneurons (IN) co-cultured with WT and MT RTT astrocytes (AS) and the effects of IGF-1/GPE treatment

(A) Quantification of neuronal soma area, total neurite length and number of terminal ends of WT or MT RTT IN after 72 hours of co-culture with WT or MT RTT AS in the absence of any treatment. **(B-D)** Comparison of neuronal soma area (**B**), total neurite length (**C**), and the number of terminal ends (**D**) after 72 hours of co-culture with the addition of vehicle (Veh), 100 ng/ml IGF-1, or 300 ng/ml GPE. Black bars = WT IN co-cultured with WT astrocytes. Dark gray bars = MT IN co-cultured with WT astrocytes. Light gray bars = WT IN co-cultured with MT astrocytes. White bars = MT IN co-cultured with MT astrocytes. The number embedded in each bar represents the number of neurons analyzed for that condition. Error bars = SEM, * = $p<0.05$, ** = $p<0.005$.

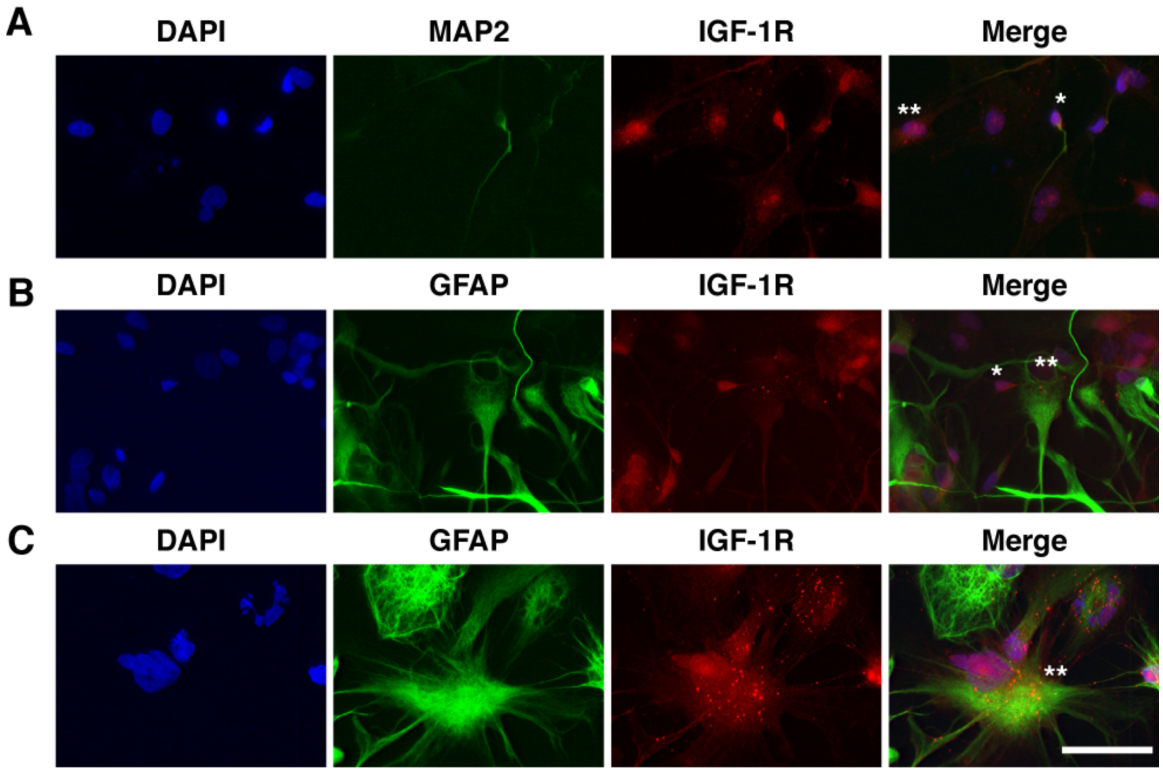

Figure 13. Neurons and astrocytes differentiated from RTT iPSCs express the IGF-1 receptor (IGF-1R)

(A-B) DAPI, MAP2 and IGF-1 Receptor (IGF-1R) immunostaining in co-cultures of R294X-WT neurons and R294X-WT AS. In the merged image (far right). * marks $MAP2^{+}/IGF\text{-}1R^{+}$ neuron; ** = $IGF\text{-}1R^{+}$ astrocyte. IGF-1R displays a diffuse cellular staining pattern in the soma of neurons and a punctate staining pattern in astrocytes. **(C)** DAPI, GFAP and IGF-1 receptor immunostaining of R294X-WT AS alone. In the merged image (far right), ** = $GFAP^{+}/IGF\text{-}1R^{+}$ astrocyte. Scale bar = 50μm. The scale bar applies to all images in this figure.

Dependent Variable: Number of ends

Source	DF	Type III SS	Mean Square	F Value	Pr > F
Model	3	148.986624	49.662208	10.19	<.0001
astrocyte	1	75.70888812	75.70888812	15.53	<.0001
neuron	1	68.29763923	68.29763923	14.01	0.0002
astrocyte*neuron	1	0.10910493	0.10910493	0.02	0.8811
Error	560	2729.899901	4.874821		
Corrected Total	563	2878.886525			

Dependent Variable: Neurite length

Source	DF	Type III SS	Mean Square	F Value	Pr > F
Model	3	145536.204	48512.068	19.51	<.0001
astrocyte	1	87375.70967	87375.70967	35.14	<.0001
neuron	1	47598.78836	47598.78836	19.14	<.0001
astrocyte*neuron	1	3821.66714	3821.66714	1.54	0.2156
Error	560	1392468.143	2486.550		
Corrected Total	563	1538004.347			

Dependent Variable: Soma size

Source	DF	Type III SS	Mean Square	F Value	Pr > F
Model	3	444.95353	148.31784	1.56	0.1978
astrocyte	1	302.3475628	302.3475628	3.18	0.0750
neuron	1	125.3502276	125.3502276	1.32	0.2512
astrocyte*neuron	1	7.8490118	7.8490118	0.08	0.7739
Error	560	53211.17263	95.01995		
Corrected Total	563	53656.12616			

Table 1. Between-subjects effects from the two-way ANOVA analysis of neuronal morphological measures in the RTT interneuron/astrocyte co-culture with no treatment (as shown in Fig. 12A)

Dependent Variable: Number of ends

Source	DF	Type III SS	Mean Square	F Value	Pr > F
Model	11	447.564780	40.687707	8.42	<.0001
astrocyte	1	2.3352186	2.3352186	0.48	0.4871
neuron	1	154.8790383	154.8790383	32.04	<.0001
trt	2	73.3114122	36.6557061	7.58	0.0005
astrocyte*neuron	1	0.0656389	0.0656389	0.01	0.9072
astrocyte*trt	2	144.2130622	72.1065311	14.92	<.0001
neuron*trt	2	9.2194067	4.6097033	0.95	0.3855
astrocyte*neuron*trt	2	11.3699529	5.6849765	1.18	0.3087
Error	1926	9309.709214	4.833702		
Corrected Total	1937	9757.273994			

Dependent Variable: Neurite length

Source	DF	Type III SS	Mean Square	F Value	Pr > F
Model	11	349812.038	31801.094	14.51	<.0001
astrocyte	1	327.7224	327.7224	0.15	0.6990
neuron	1	91051.1852	91051.1852	41.54	<.0001
trt	2	56083.8479	28041.9240	12.79	<.0001
astrocyte*neuron	1	7960.6998	7960.6998	3.63	0.0568
astrocyte*trt	2	137619.4652	68809.7326	31.39	<.0001
neuron*trt	2	22603.8350	11301.9175	5.16	0.0058
astrocyte*neuron*trt	2	11420.7833	5710.3917	2.61	0.0741
Error	1926	4221548.692	2191.874		
Corrected Total	1937	4571360.730			

Dependent Variable: Soma size

Source	DF	Type III SS	Mean Square	F Value	Pr > F
Model	11	22052.3136	2004.7558	14.64	<.0001
astrocyte	1	1103.45030	1103.45030	8.06	0.0046
neuron	1	825.38827	825.38827	6.03	0.0142
trt	2	14345.97435	7172.98718	52.39	<.0001
astrocyte*neuron	1	496.31964	496.31964	3.62	0.0571
astrocyte*trt	2	846.67103	423.33552	3.09	0.0456
neuron*trt	2	1582.56139	791.28069	5.78	0.0031
astrocyte*neuron*trt	2	1815.25965	907.62983	6.63	0.0014
Error	1926	263707.9797	136.9200		
Corrected Total	1937	285760.2933			

Table 2. Between-subjects effects from the three-way ANOVA analysis of neuronal morphological measures in the RTT interneuron/astrocyte co-culture treated with IGF-1/GPE (as shown in Fig. 12B-D). trt=treatment with IGF-1/GPE.

References

Akbarian, S. *et al*. Expression pattern of the Rett syndrome gene MeCP2 in primate prefrontal cortex. *Neurobiol Dis* **8**, 784-791 (2001).

Allen, R. C., Zoghbi, H. Y., Moseley, A. B., Rosenblatt, H. M. & Belmont, J. W. Methylation of *HpaII* and *HhaI* sites near the polymorphic CAG repeat in the human androgen-receptor gene correlates with X chromosome inactivation. *Am J Hum Genet* **51**, 1229-1239 (1992).

Amir, R. E. *et al*. Rett syndrome is caused by mutations in X-linked MECP2, encoding methyl-CpG-binding protein 2. *Nat Genet* **23**, 185-188 (1999).

Ananiev, G., Williams, E. C., Li, H. & Chang, Q. Isogenic Pairs of Wild Type and Mutant Induced Pluripotent Stem Cell (iPSC) Lines from Rett Syndrome Patients as *In Vitro* Disease Model. *PLoS ONE* **6**, e25255 (2011).

Armstrong, D., Dunn, J. K., Antalffy, B. & Trivedi, R. (1995) Selective dendritic alterations in the cortex of Rett syndrome. J Neuropathol Exp Neurol 54, 195- 201.

Ballas, N., Lioy, D. T., Grunseich, C. & Mandel, G. Non-cell autonomous influence of MeCP2-deficient glia on neuronal dendritic morphology. *Nat Neurosci* **12**, 311-317 (2009).

Belichenko, N. P., Belichenko, P. V., Li, H. H., Mobley, W. C. & Francke, U. Comparative study of brain morphology in Mecp2 mutant mouse models of Rett syndrome. *J Comp Neurol* **508**, 184-195 (2008).

Belichenko, P. V. *et al*. Widespread changes in dendritic and axonal morphology in Mecp2-mutant mouse models of Rett syndrome: evidence for disruption of neuronal networks. *J Comp Neurol* **514**, 240-258 (2009).

Chao, H. T. *et al*. Dysfunction in GABA signalling mediates autism-like stereotypies and Rett syndrome phenotypes. *Nature* **468**, 263-269 (2010).

Chen, R. Z., Akbarian, S., Tudor, M. & Jaenisch, R. Deficiency of methyl- CpG binding protein-2 in CNS neurons results in a Rett-like phenotype in mice. *Nat Genet* **27**, 327-331 (2001).

Emdad, L., D'Souza, S. L., Kothari, H. P., Qadeer, Z. A. & Germano, I. M. Efficient Differentiation of Human Embryonic and Induced Pluripotent Stem Cells into Functional Astrocytes. *Stem Cells Dev* **21**, 404-410 (2011).

Fyffe, S. L. *et al*. Deletion of Mecp2 in Sim1-expressing neurons reveals a critical role for MeCP2 in feeding behavior, aggression, and the response to stress. *Neuron* **59**, 947-958 (2008).

Hagberg, B. Rett's syndrome: prevalence and impact on progressive severe mental retardation in girls. *Acta Paediatr Scand* **74**, 405-408 (1985).

Johnson, M. A., Weick, J. P., Pearce, R. A. & Zhang, S. C. Functional neural development from human embryonic stem cells: accelerated synaptic activity via astrocyte coculture. *J Neurosci* **27**, 3069-3077 (2007).

Kishi, N. & Macklis, J. D. (2004) MECP2 is progressively expressed in postmigratory neurons and is involved in neuronal maturation rather than cell fate decisions. Mol Cell Neurosci 27, 306-321.

Krencik, R., Weick, J. P., Liu, Y., Zhang, Z. J. & Zhang, S. C. Specification of transplantable astroglial subtypes from human pluripotent stem cells. *Nat Biotechnol* **29**, 528-534 (2011).

Lioy, D. T. *et al*. A role for glia in the progression of Rett syndrome. *Nature* **475**, 497-500 (2011).

Liu Y, *et al*. Medial ganglionic eminence-like cells derived from human embryonic stem cells correct learning and memory deficits. *Nat Biotech* **31**, 440-447 (2013).

Maezawa, I., Swanberg, S., Harvey, D., LaSalle, J. M. & Jin, L. W. Rett syndrome astrocytes are abnormal and spread MeCP2 deficiency through gap junctions. *J Neurosci* **29**, 5051-5061 (2009).

Maezawa, I. & Jin, L. W. Rett syndrome microglia damage dendrites and synapses by the elevated release of glutamate. *J Neurosci* **30**, 5346-5356 (2010)

Mekhoubad, S. *et al*. Erosion of dosage compensation impacts human iPSC disease modeling. *Cell Stem Cell* **10**, 595-609 (2012).

Samaco, R. C. *et al*. Loss of MeCP2 in aminergic neurons causes cellautonomous defects in neurotransmitter synthesis and specific behavioral abnormalities. *Proc Natl Acad Sci USA* **106**, 21966-21971 (2009).

Shahbazian, M. D., Antalffy, B., Armstrong, D. L. & Zoghbi, H. Y. Insight into Rett syndrome: MeCP2 levels display tissue- and cell-specific differences and correlate with neuronal maturation. *Hum Mol Genet* **11**, 115-124 (2002).

Shahbazian, M. D., Sun, Y. & Zoghbi, H. Y. Balanced X chromosome inactivation patterns in the Rett syndrome brain. *Am J Med Genet* **111**, 164- 168 (2002).

Tropea *et al*. Partial reversal of Rett Syndrome-like symptoms in MeCP2 mutant mice. *Proc Natl Acad Sci U S A* **106**, 2029-2034 (2009).

Yuan, S. H. *et al*. Cell-surface marker signatures for the isolation of neural stem cells, glia and neurons derived from human pluripotent stem cells. *PLoS One* **6**, e17540 (2011).

Chapter III

Future Directions

Introduction

Since the initial publications describing the derivation of human iPSCs, the vast potential of patient-specific cells for disease modeling, drug screens and personalized medicine has been highly touted in mass media. However, a number of challenges exist for basic and translational research using patient-specific iPSCs. These include the complexity of polygenetic disorders, inefficient means of cell differentiation, and lack of robust phenotypic readouts for screening. In our attempt to establish the iPSC platform in our lab, we focused on modeling a monogenic disorder, which allows for the direct cause and effect relationship between genotypes and phenotypes to be clear. Additionally, taking advantage of the nonrandom pattern of X chromosome inactivation in female iPSCs, we have generated isogenic pairs of wild type and mutant iPSC lines which maintain isogenic status throughout differentiation, allowing for an internal control with which to compare disease cells. We have also utilized efficient, highly reproducible means of differentiating either astrocytes or a distinct subtype of neuron, and have shown the tractability of morphological-based assays for pathological read-out. The studies presented here demonstrate patient iPSC-derived neurons recapitulate characteristic disease phenotypes, and that RTT astrocytes have a non cell-autonomous effect upon neuronal morphology and function *in vitro*. In addition, we have demonstrated exogenous stimulation of the IGF-1 pathway is able to modulate disease phenotypes in our *in vitro* system. The number of currently ongoing clinical trials confirms the great deal of interest in targeting IGF-1 or IGF-1 signaling for the treatment of neurological disorders. Despite this interest, the mechanism by which IGF-1 and IGF-1 cleavage products lead to phenotypic improvement has not been fully characterized. Our system provides an

excellent means to characterize the suspected differential effects of IGF-1 and GPE in two distinct cell types: RTT astrocytes and RTT neurons. A thorough characterization of the IGF-1 pathway in each cell type would include the IGF-1 receptor, IGFBPs (IGF-1 binding proteins), and downstream signaling pathways. Finally, in addition to highlighting the potential role of IGF-1 and IGF-1 signaling in the RTT disease mechanism, the ability to modulate disease phenotypes in our co-culture system through exogenous application of small molecules provides feasibility for future large scale screening on this platform.

I) Characterization of non-cell autonomous astrocytic effects *in vivo*

We have demonstrated RTT patient iPSC-derived astroglial progenitors are able to differentiate into an enriched population of S100B+/GFAP+ astrocytes and have provided compelling evidence of a non cell-autonomous RTT astrocytic effect *in vitro*. The next step of our characterization of the glial contribution to RTT involves *in vivo* validation of the morphological neuronal effects elicited by RTT astrocytes in addition to behavioral effects elicited by RTT astroglia. To verify that patient iPSC-derived astroglial progenitors retain their identity *in vivo,* late-stage (8 month) astroglial progenitor clusters were transplanted directly into the adult hippocampus of SCID mouse as described in Krencik *et al*., (2011). Three months after transplantation, mice sections were immunostained for **h**uman **Nuc**lear antigen (hNuc) and GFAP (Figure 1), verifying the following: 1) patient iPSC-derived astroglial progenitors survive after transplantation and, 2) patient iPSC-derived astroglial progenitors are able to differentiate into GFAP+ astrocytes *in vivo*. These hNUC+/GFAP+ human astrocytes were found to integrate into

the existing neuronal network of the hippocampus and to migrate into surrounding regions without signs of an inflammatory response (**Figure 1)**. As in Krencik *et al*., (2011), our transplanted astroglial progenitors exhibited distinct morphology compared to mouse astrocytes (**Figure 1**). Human astrocytes were larger and extended longer processes compared to the resident mouse astrocytes. The stage of astroglial progenitors utilized in transplants correspond with those at an early stage of the developing human brain (Krencik *et al*., 2011), thus after transplantation, these human cells may acquire mature functions in response to the local cues of the *in vivo* brain. Further characterization of the transplanted human astrocytes could include expression of mature astrocyte markers such as NFIX (Wilczynska et al 2009), CHL1 (Hillenbrand et al., 1999), the excitatory amino acid transporters GLAST and GLT-1 (Swanson et al., 1997), and aquaporin 4 (Nico *et al*., 2001). Expression of these mature astrocyte markers would provide a correlative to the functionality of transplanted cells.

Past mouse-based studies have mainly relied on *Mecp2* null mice, thus the effect of astrocytes harboring specific RTT mutations remains to be characterized *in vivo*. As previously described, RTT patients display a reduction in neuron soma size, shorter dendrites and a reduction in dendrite complexity (Armstrong *et al*., 1998). Additional clinical evidence suggests that excitatory synaptic activity is affected in RTT (Johnston *et al*., 2001). *Mecp2* deficient mice have been shown to display a reduction in the proteins necessary for excitatory neurotransmission, such as VGlut (Chao *et al*., 2007), in addition to recapitulating many of the neuronal morphologies found in RTT patients (Chen *et al*., 2001; Guy *et al*., 2001). Neuronal morphology and levels of VGlut appear to be directly affected by MeCP2 dysfunction and to have a glial contribution, as selective re-

introduction of MeCP2 in astrocytes in *Mecp2 null* animals has been shown to increase the somal size of neurons, to restore normal dendritic morphology and to increase neuronal VGlut1 to wild type levels (Lioy *et al*., 2011). With our transplanted human astrocytes, we can determine if the converse is also true, verifying RTT astrocytes harboring patient-specific mutations lead to RTT-like neuronal phenotypes *in vivo*. To test the effect of patient-specific mutant astrocytes *in vivo,* the neuronal morphology from brain regions with hNuc+/GFAP+ integrated RTT astrocytes will be compared to those in wild type transplants. Specifically, effects on neuronal soma size, dendritic aborization and synaptic proteins will be assayed. Moreover, it will be interesting to test whether transplantation of wild type human astroglial progenitors may alleviate symptoms in *Mecp2* null mice. This experiment may be challenging to perform, as the *Mecp2* null allele would need to be bred into the SCID background.

To determine if integrated RTT astrocytes contribute to the behavioral phenotypes found in RTT, we will characterize the RTT astrocyte transplanted mice for two features of RTT 1) cognition 2) autistic-like behaviors. *Mecp2* deficient mice display hippocampal/ amygdala-based cognitive defects that are thought to recapitulate the intellectual disability of patients (Pelka *et al*., 2006). Due to the confirmed integration of RTT astrocytes into the hippocampus, we will utilize cognitive tests including the Morris water maze, contextual fear conditioning, and the novel object recognition paradigm. The Morris water maze is one of the most widely used tasks for studying spatial learning and memory. This task requires that mice locate and remember the location of a hidden platform, which is dependent upon the function of the hippocampus (Vorhees and Williams, 2006). In the fear-conditioning task, mice learn to associate an adverse

stimulus (a foot shock) with a particular context (a chamber different from the home cage). This task has been shown to involve both the amygdala and the hippocampus (Phillips and LeDoux, 1992). The novel objection recognition paradigm utilizes the test animal's natural preference for novel objects to evaluate recognition memory. This paradigm has been shown to involve the hippocampus (Broadbent *et al*., 2010).

In addition to cognitive deficits, RTT patients display autistic features such as anxiety and reduced social motivation. These aspects of RTT have been recapitulated in mouse models; *Mecp2* deficient mice exhibit altered anxiety-related behaviors (Chen *et al*., 2001; Guy *et al*., 2001). Additionally, there appears to be a glial influence in these particular aspects of the disorder, as post-natal re-expression of MeCP2 selectively in astrocytes was shown to improve anxiety in *Mecp2* deficient mice (Lioy *et al*., 2011). Glial effects on anxiety can be assayed by two independent tests 1) the open field test and 2) the light/dark exploration test. The open field test is a common measure of exploratory behavior. It is based on the natural balance that animals weigh between exploration of a new environment and avoidance to harm. The light/dark exploration is an additional assay utilized to measure anxiety-related behavior that is also based on natural balance between exploration of a new environment (the light chamber) and avoidance to harm (the dark chamber) (Crawley and Goodwin, 1980). Thus, these assays will also be useful for assessing the *in vivo* effects of transplanted RTT astrocytes.

II) Characterization of RTT astrocyte secreted factors

It was first shown in RTT mouse models that MeCP2-deficient astrocytes and their conditioned media have defects in supporting neurite outgrowth (Ballas *et al*.,

2009). We have also shown similar defects in patient-specific RTT astrocytes and their conditioned media. Through identifying the factors involved, we can determine what specific pathways in astrocytes are affected by MECP2 dysfunction and whether this effect is a loss-of-function whereby RTT astrocytes are not able to provide the appropriate amount of support to neurons or if this effect is a gain-of-function whereby RTT astrocytes, through MECP2 dysfunction, secrete deleterious factors. Our system is especially well suited for determining the mechanism by which astrocyte secreted factors affect the RTT phenotype of reduced neurite length. We can generate large quantities of an enriched population of astrocytes that is void of contaminating microglia (which is of hemaetopoietic orgin) and neurons, allowing for the determination of a RTT glia-specific effect. Additionally, through comparing several different RTT mutational astrocyte lines (V247X, R294X, R306C), we can determine if astrocyte-specific molecular commonalities exist between different RTT mutations. To determine the difference between wild type and RTT mutant astrocyte secreted factors, we can assay conditioned media by mass spectrometry, identify candidate factors and pathways that lead to an astrocyte-induced lack of neurite outgrowth. As mentioned previously, it is possible that the RTT astrocyte secreted factors involved in the reduction of neurite outgrowth are either downregulated or upregulated in response to MECP2 dysfunction (Chahrour *et al*., 2008). If RTT mutations are shown to cause downregulation of a necessary glial factor, rescue experiments upon RTT mutant astrocytes could be performed by chemical addition or genetic upregulation of the candidate factor followed by testing the resulting ACM for induction of neurite outgrowth. Conversely, if RTT mutation leads to detrimental upregulation of a glial factor, rescue experiments could be performed by

downregulating the factor in question through the use known inhibitors (if possible) or by genetic knockdown via shRNA (small hairpin) against the factor in question. The candidate factors may then be tested in mouse models to determine *in vivo* relevance.

III) Characterization of IGF-1 pathway in RTT astrocytes and neurons

Systemic treatment of the *Mecp2* deficient mice with the active peptide of IGF-1 (GPE) can lessen RTT-like phenotypes (Tropea *et al*., 2009). As a result of this work out of Mriganka Sur's lab, two clinical trials have been initiated to determine the safety and efficacy of full length IGF-1 and modified IGF-1 active peptides in the treatment of RTT. However, there is no efficacy data on IGF-1 in human RTT cells. Characterization of the IGF-1 pathway constituents in our patient- specific iPSC based system may shed light on each molecule's mode of action, leading to more guided RTT treatment applications. We have shown addition of IGF-1 and GPE is able to improve the RTT-like neurite outgrowth phenotype found in MT astrocyte co-cultures. Through immunostaining, we have detected the presence of the IGF-1 receptor (IGF-1R) in WT neurons and glia. This suggests astrocytes and neurons are able to respond to IGF-1 stimulation. To test if RTT neurons respond to exogenous IGF-1 and/or GPE, a simple neurite outgrowth assay could be performed on IGF-1 treated and GPE treated RTT neurons in the absence of astrocytes. Because the effect of IGF-1 and/or GPE may be non-specific, characterization of IGF-1 signaling in both neurons and glia for each of the three isogenic pairs could be performed to pinpoint potential deficits in each cell type. To determine the genotype-dependent function of the IGF-1 pathway in each cell type (astrocytes and neurons), quantification of IGF-1 pathway components transcript levels may be performed.

Specifically, the levels of IGF-1, IGFBP's, IGF-1R and the downstream IGF-1 signaling pathways including MAPK/ERK, AKT/mTOR and JAK/STAT could be compared within each isogenic pair of mutant and wild type neurons and astrocytes. It has been suggested that IGF-1 and GPE may activate different pathways in neurons and glia (Corvin *et al*., 2012). In mouse primary cortical cultures, IGF-1 was found to selectively increase activated AKT (pAKT) in neurons while GPE was found to selectively increase pAKT in glia, indicating that there may be physiological differences between IGF-1 and GPE treatments. Additionally, GPE administration was shown to increase endogenous IGF-1 levels in a positive feedback loop model. To address the actions of IGF-1 and GPE, RTT astrocytes and their isogenic wild type controls could be treated with either IGF-1 or GPE and assayed for 1) changes in transcript levels of IGF-1 components and 2) activation of IGF-1 signaling pathway components as determined by their phosphorylation states. Due to limitations in the protocols for the derivation of neurons, namely cell type heterogeneity and low yields, our astrocyte cultures would be a more ideal choice for study. Additionally, to address the issue of specificity, a less biased approach to determine the functional effects of IGF-1 or GPE treatment could be performed by expression profiling.

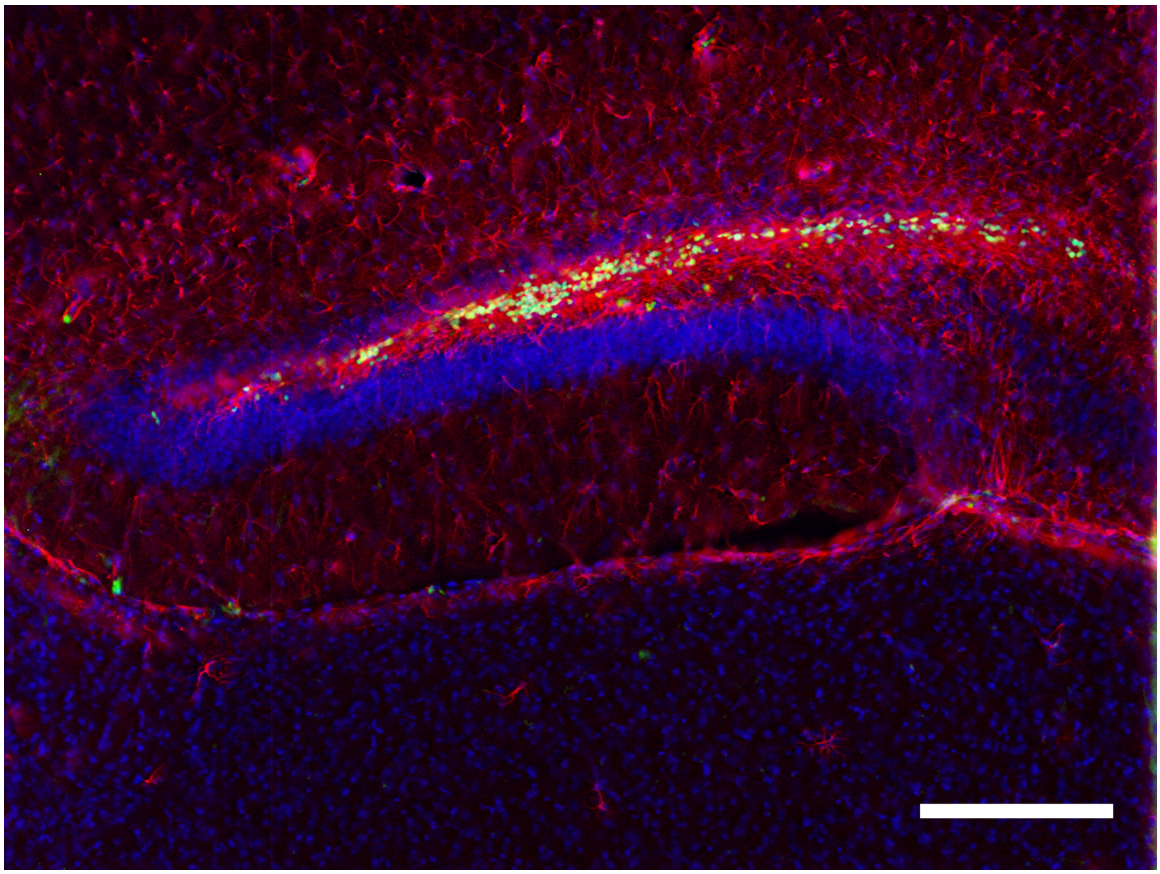

Figure 1. RTT iPSC-derived astroglial progenitors differentiate into astrocytes *in vivo*

Three months after transplantation, RTT iPSC-derived astroglial progenitors survived and differentiated into astrocytes *in vivo* as indicated by the presence of cells with co-immunoreactivity of $hNuc^{+}$/ $GFAP^{+}$ in the engrafted hippocampal region. hNuc (green), GFAP (red), DAPI (blue). Scale bar = 200μm.

References

Armstrong, D.D., Dunn, K. & Antalffy, B. Decreased dendritic branching in frontal, motor and limbic cortex in Rett syndrome compared with trisomy 21. *J Neuropathol Exp Neurol* **57**, 1013-7 (1998).

Ballas, N., Lioy, D.T., Grunseich, C. & Mandel, G. Non-cell autonomous influence of MeCP2-deficient glia on neuronal dendritic morphology. *Nat Neurosci*, **12**, 311-7 (2009).

Broadbent, N. J., Gaskin, S., Squire, L. R. & Clark, R. E. Object recognition memory and the rodent hippocampus. *Learn Mem* **17**, 5-11 (2010).

Chahrour, M. *et al*. MeCP2, a key contributor to neurological disease, activates and represses transcription. *Science* **320**, 1224-9 (2008).

Chao, H.T., Zoghbi, H.Y. & Rosenmund, C. MeCP2 controls excitatory synaptic strength by regulating glutamatergic synapse number. *Neuron* **56**, 58-65 (2007).

Chen, R.Z., Akbarian, S., Tudor, M. & Jaenisch, R. Deficiency of methyl-CpG binding protein-2 in CNS neurons results in a Rett-like phenotype in mice. *Nature Genetics* **27**, 327-331 (2001).

Corvin, A.P. *et al*. Insulin-like growth factor 1 (IGF1) and its active peptide (1-3)IGF1 enhance the expression of synaptic markers in neuronal circuits through different cellular mechanisms. *Neurosci Lett* **520**, 51-6 (2012).

Crawley, J. & Goodwin, F.K. Preliminary report of a simple animal behavior model for the anxiolytic effects of benzodiazepines. *Pharmacol Biochem Behav* **13**, 167-70 (1980).

Hillenbrand, R., Molthagen, M., Montag, D. & Schachner, M. The close homologue of the neural adhesion molecule L1 (CHL1): patterns of expression and promotion of neurite outgrowth by heterophilic interactions. *Eur J Neurosci* **11**, 813-26 (1999).

Guy, J., Hendrich, B., Holmes, M., Martin, J.E. & Bird, A. A mouse Mecp2-null mutation causes neurological symptoms that mimic Rett syndrome. *Nature Genetics* **27**, 322-326 (2001).

Krencik, R. & Zhang, S.-C. Directed differentiation of functional astroglial subtypes from human pluripotent stem cells. *Nature Protocols* **6**, 1710-1717 (2011).

Johnston, M.V., Jeon, O.H., Pevsner, J., Blue, M.E. & Naidu, S. Neurobiology of Rett syndrome: a genetic disorder of synapse development. *Brain Dev* **23 Suppl 1**, S206-13 (2001).

Lioy, D.T. *et al*. A role for glia in the progression of Rett's syndrome. *Nature* **475**, 497-500 (2011).

Nico, B. *et al*. Role of aquaporin-4 water channel in the development and integrity of the blood-brain barrier. *J Cell Sci* **114**, 1297-307 (2001).

Pelka, G.J. *et al*. Mecp2 deficiency is associated with learning and cognitive deficits and altered gene activity in the hippocampal region of mice. *Brain*, **129**, 887-98 (2006).

Phillips, R.G. & LeDoux, J.E. Differential contribution of amygdala and hippocampus to cued and contextual fear conditioning. *Behav Neurosci* **106**, 274-85 (1992).

Swanson, R.A. *et al*. Neuronal regulation of glutamate transporter subtype expression in astrocytes. *J Neurosci* **17**, 932-40 (1997).

Tropea, D. *et al*. Partial reversal of Rett Syndrome-like symptoms in MeCP2 mutant mice. *Proc Natl Acad Sci U S A* **106**, 2029-34 (2009).

Vorhees, C.V. & Williams, M.T. Morris water maze: procedures for assessing spatial and related forms of learning and memory. *Nat Protoc* **1**, 848-58 (2006).

Wilczynska, K.M. *et al*. Nuclear factor I isoforms regulate gene expression during the differentiation of human neural progenitors to astrocytes. *Stem Cells* **27**, 1173-81 (2009).